Simulation and Optimisation in Ion Chromatography

Boon Khing Ng

Bachelor of Science (Hons)

A thesis submitted in fulfilment of the requirements for the degree of

Doctor of Philosophy

Submitted on 22nd July, 2011

University of Tasmania

Declaration

To the best of my knowledge, this thesis contains no copy or paraphrase of material previously published or written by another person, except where due reference is made in the text of the thesis

Boon Khing Ng

22nd July, 2011

This thesis may be available for loan and limited copying in accordance with the Copyright Act 1968

Boon Khing Ng

22nd July, 2011

Acknowledgement

I would like to sincerely thank the following people:

A/Prof Robert Shellie, A/Prof Greg Dicinoski and Prof Paul Haddad for being awesome supervisors, especially for all your precious guidance, advice as well as financial support.

Members of ACROSS group for being great people during my candidature.

Financial support in the form of scholarships and sponsorships from Australian Research Council and Dionex Corporation are gratefully acknowledged.

And finally, to my friends and family

Statement of Co-Authorship

The following people and institutions contributed to the publication of the work undertaken as part of this thesis:

[1] Robert A. Shellie (20%), Boon K. Ng (35%), Greg W. Dicinoski (15%), Samuel D. H. Poynter (10%), John W. O'Reilly (4%), Christopher A. Pohl (1%), Paul R. Haddad (15%)

Details of the Authors roles:

Boon K. Ng executed the laboratory tasks, computational programming and simulation

Robert A. Shellie, Boon K. Ng and Paul R. Haddad wrote the draft manuscript

Robert A. Shellie, Boon K. Ng, Greg W. Dicinoski, Samuel D. H. Poynter and Paul R. Haddad contributed to the algorithm proposal and development

Robert A. Shellie, Boon K. Ng, Greg W. Dicinoski and Paul R. Haddad assisted with publication refinement and presentation

John W. O'Reilly set up the data library prior to this research study

Christopher A. Pohl established the need of study and provided valuable feedback on the work

[2] Philip Zakaria (50%), Greg W. Dicinoski (25%), Boon K. Ng (4%), Robert A. Shellie (4%), Melissa Hanna-Brown (2%), Paul R. Haddad (15%)

Details of the Authors roles:

Philip Zakaria executed the laboratory tasks, computational programming, simulation and wrote the draft manuscript

Philip Zakaria, Greg W. Dicinoski, Boon K. Ng, Robert A. Shellie and Paul R. Haddad contributed to the algorithm proposal and development

Philip Zakaria, Greg W. Dicinoski and Paul R. Haddad assisted with publication refinement and presentation

Melissa Hanna-Brown established the need of study and provided valuable feedback on the work

[3] Boon K. Ng (35%), Robert A. Shellie (20%), Greg W. Dicinoski (15%), Carrie Bloomfield (10%), Yan Liu (4%), Christopher A. Pohl (1%), Paul R. Haddad (15%)

Details of the Authors roles:

Boon K. Ng performed the method translation and simulation

Boon K. Ng and Yan Liu executed the data acquisition

Boon K. Ng and Robert A. Shellie wrote the draft manuscript

Boon K. Ng, Robert A. Shellie, Greg W. Dicinoski, Carrie Bloomfield and Paul R. Haddad contributed to the method translation and development

Boon K. Ng, Robert A. Shellie, Greg W. Dicinoski and Paul R. Haddad assisted with publication refinement and presentation

Christopher A. Pohl established the need of study and provided valuable feedback on the work

[4] Viktor Drgan (20%), Boon K. Ng (20%), Marjana Novič (10%), Greg W. Dicinoski (10%), Milko Novič (10%), Robert A. Shellie (10%), Paul R. Haddad (15%)

Details of the Authors roles:

Viktor Drgan performed the computational programming and simulation

Boon K. Ng and Viktor Drgan executed the data acquisition

Viktor Drgan, Paul R. Haddad and Boon K. Ng wrote the draft manuscript

Viktor Drgan, Boon K. Ng, Marjana Novič, Greg W. Dicinoski, Milko Novič, Robert A. Shellie, Paul R. Haddad contributed to the proposal of algorithm and development

Viktor Drgan, Boon K. Ng, Marjana Novič, Greg W. Dicinoski, Milko Novič, Robert A. Shellie, Paul R. Haddad assisted with publication refinement and presentation

We the undersigned agree with the above stated "proportion of work undertaken" for each of the above published (or submitted) peer-reviewed manuscripts contributing to this thesis:

Signed: _____ _____

A/Prof Greg W. Dicinoski
Supervisor
School of Chemistry
University of Tasmania

Prof Emily F. Hilder
Graduate Research Coordinator
School of Chemistry
University of Tasmania

Date: 22nd July 2011

List of Publications

Description	Number of Publications	National	International
Research Papers	4		
Oral Presentations		1	3
Poster Presentations		2	3

Refereed Journal Articles

[1] Robert A. Shellie, Boon K. Ng, Greg W. Dicinoski, Samuel D. H. Poynter, John W. O'Reilly, Christopher A. Pohl, Paul R. Haddad. Prediction of analyte retention for ion chromatography separations performed using elution profiles comprising multiple isocratic and gradient steps. Anal. Chem. (2008), 80(7), 2474-82. (Chapter 4)

[2] Philip Zakaria, Greg W. Dicinoski, Boon K. Ng, Robert A. Shellie, Melissa Hanna-Brown, Paul R. Haddad. Application of retention modelling to the simulation of separation of organic anions in suppressed ion chromatography. J. Chromatogr. A (2009), 1216(38), 6600-10. (Chapter 4)

[3] Boon K. Ng, Robert A. Shellie, Greg W. Dicinoski, Carrie Bloomfield, Yan Liu, Christopher A. Pohl, Paul R. Haddad. Methodology for porting retention prediction data from conventional-scale to miniaturised ion chromatography systems. J. Chromatogr. A (2011), 1218, 5512-19 (Chapter 6)

[4] Viktor Drgan, Boon K. Ng, Marjana Novič, Greg W. Dicinoski, Milko Novič, Robert A. Shellie, Paul R. Haddad. Prediction of retention time and peak width for complex elution profiles in ion chromatography based on analyte velocities determined using isocratic data. Submitted to Anal. Chem. on 30th May 2011 (Chapter 5)

Conference Presentations

[1] Boon K. Ng, Greg W. Dicinoski, Robert A. Shellie, Samuel D. H. Poynter, John W. O'Reilly, Christopher A. Pohl, Paul R. Haddad. Ion chromatography *in-silico*. Poster presented by Boon K. Ng at the Royal Australian Chemical Institute 14th Research and Development Topics Conference 2006 (RACI 14th R&D Topics Conference 2006), Wollongong, Australia, 5 – 9 December 2006

[2] Boon K. Ng, Greg W. Dicinoski, Robert A. Shellie, Christopher A. Pohl, Paul R. Haddad. *in-silico* Simulation of Retention in Ion Chromatography Using Multi-Step Gradient Eluent Profiles. Poster presented by Boon K. Ng at the ACROSS Symposium on Advances in Separation Science 2008 (ASASS 2008), Hobart, Australia, 8 – 10 December 2008

[3] Boon K. Ng, Robert A. Shellie, Greg W. Dicinoski, Christopher A. Pohl, Paul R. Haddad. Porting Retention Data from Conventional to Microbore Ion Chromatographic Systems. Lecture presented by Boon K. Ng at the RACI 17th R&D Topics Conference 2009, Gold Coast, Australia, 6 – 9 December 2009

[4] Boon K. Ng, Robert A. Shellie, Greg W. Dicinoski, Christopher A. Pohl, Paul R. Haddad. Porting Retention Data from Conventional to Microbore Ion Chromatographic Systems. Lecture presented by Boon K. Ng at the Pittcon Conference and Exposition 2010 (Pittcon 2010), Orlando, Florida, USA, 28 Feb – 5 March 2010

[5] Boon K. Ng, Greg W. Dicinoski, Robert A. Shellie, Christopher A. Pohl, Paul R. Haddad. Real Time *in-silico* Simulation of Retention under Multi-step Gradient Elution Conditions in Ion Chromatography. Poster presented by Boon K. Ng at the Pittcon 2010, Orlando, Florida, USA, 28 Feb – 5 March 2010

[6] Greg W. Dicinoski, Philip J. Zakaria, Paul R. Haddad, Boon K. Ng, Robert A. Shellie, Melissa Hanna-Brown, Roman Szucs. Computer-based Simulation and Optimisation of Ion Chromatographic Separations of Pharmaceutically Related Compounds. Poster presented by Greg W. Dicinoski at the Pittcon 2010, Orlando, Florida, USA, 28 Feb – 5 March 2010

[7] Boon K. Ng, Greg W. Dicinoski, Robert A. Shellie, Christopher A. Pohl, Paul R. Haddad. Real Time *in-silico* Simulation of Retention under Complex Elution Methods in Ion Chromatography. Poster presented by Boon K. Ng at the RACI 18th R&D Topics Conference 2010, Hobart, Australia, 5 – 8 December 2010

Invited Conference Presentation

[1] Paul R. Haddad, Greg W. Dicinoski, Robert A. Shellie, Boon K. Ng, Samuel D. H. Poynter, Computer Simulation and Optimisation of Separations in Suppressed Ion Chromatography Using Combined Isocratic and Gradient Elution Profiles. Lecture presented by Paul R Haddad at the Pittcon 2008, New Orleans, Louisiana, USA, 2 – 7 March 2008

[2] Paul R. Haddad, Greg W. Dicinoski, Robert A. Shellie, Boon K. Ng. Transferring Ion Chromatographic Methods from 4 mm Columns to Capillary Format. Lecture presented by Paul R Haddad at the Pittcon 2011, Atlanta, Georgia, USA, 13 – 18 March 2011

List of Important Terms, Constants and Abbreviations

a	degree of interaction between the analyte and stationary phase
A_m	amount of analyte present in mobile phase
A_s	amount of analyte present in stationary phase
b	effective charge of the analyte relative to competing ion
B	gradient ramp (mM/min)
D_A	distribution coefficient of the analyte between mobile and stationary phases
E^-	competing ion
E^{y-}	competing ion carries charge of y
E_m^{y-}	competing ion carries charge of y in mobile phase
$E_E^{v,z}$	total amount of eluent in the column segment z after v movement of mobile phase through the column
$E_{A_i}^{v,z}$	total amount of the analyte i in the column segment z after v movement of the mobile phase through the column
$f\left({}^{eq}\left[E^{y-}\right]^{v,z}\right)$	function f dependent on the eluent concentration in mobile phase of the column segment z after m movements of the mobile phase
G	compression factor in gradient condition
H	plate height of the analyte
IC	ion chromatography
i.d.	internal diameter
k	retention factor of the analyte
k_f	retention factor of the analyte at the elution concentration
$K_{A,E}$	ion-exchange selectivity coefficient between the analyte and the eluent competing ion
L	column length (cm)
L_{final}	total distance travelled of the analyte in the step (cm)
LSSM	linear solvent strength model
L_{moved}	displacement of the analyte after step time (cm)
L_R	distance remaining of the analyte to reach the end of the column (cm)

m	cubic coefficient of the numerical incremental isocratic steps model
m	parameter obtained from linear regression for Drgan *et al.* peak width model[1]
M^+	insoluble matrix material comprising a fixed positive charge
min R_s	minimum resolution
n	quadratic coefficient of the numerical incremental isocratic steps model
n	parameter obtained from linear regression for Drgan *et al.* peak width model[1]
N	number of plates of the analyte during isocratic elution
o	linear coefficient of the numerical incremental isocratic steps model
Q	effective ion-exchange capacity of the stationary phase
r	normalised resolution product
R	gradient ramp (mM/mL)
R_s	resolution
t	Students t-test
t_{app}	total apparent time available for movement in the step
t_f	final fraction of retention which will be less than or equal to 0.05 min
t_{lag}	time taken of the new step to reach the analyte (min)
t_m	void time of the mobile phase to fully fill the column (min)
$t_{m(step)}$	void time of the mobile phase in relation to the step time
t_{new}	updated void time based on the length remaining of the analyte
t_{step}	step time (min)
t_R	retention time of the analyte (min)
t'_R	adjusted retention time of the analyte (min)
t_{Ri}	isocratic retention time observed under isocratic conditions at gradient initial concentration (min)
u	flow-rate of the eluent (mL/min)
$v_{initial}$	initial velocity of the analyte in gradient elution (cm/min)
v_{final}	final velocity of the analyte in gradient elution (cm/min)
v	velocity of the analyte in isocratic elution (cm/min)

V_m	void volume of the mobile phase inside the column (mL)
V_R	retention volume of the analyte (mL)
V'_R	adjusted retention volume of the analyte (mL)
V_z	volume of the connecting tubing between the outlet of the gradient-generating device and the top of the column
w	peak width of the analyte
w_{ave}	average width of the two adjacent peaks
x	charge of the analyte
y	charge of competing ion
σ	variance of the peak width
ΠR_s	product of resolution
ΣR_s	sum of resolution

List of Equations

Mathematical Equation	Equation	Page Number
$A_m \rightleftharpoons A_s$	1.1	1
$D_A = \frac{[A_S]}{[A_m]}$	1.2	1
$k = D_A\left(\frac{w}{V_m}\right)$	1.3	2
$M^+E^- + A^- \rightleftharpoons M^+A^- + E^-$	1.4	2
$y\ A_m^{x-} + x\ E_s^{y-} \rightleftharpoons y\ A_s^{x-} + x\ E_m^{y-}$	1.5	2
$K_{A,E} = \frac{\left[A_s^{x-}\right]^y\left[E_m^{y-}\right]^x}{\left[A_m^{x-}\right]^y\left[E_s^{y-}\right]^x}$	1.6	2
$R_s = 2\frac{t_{R1} - t_{R2}}{w_1 + w_2}$	1.7	11
$y = a_1LV_1 + a_2LV_2 + ...+ a_mLV_m$	1.8	12
$LV_i = \alpha x_1 + \beta x_2 + \delta x_3 + ... + \upsilon x_n$	1.9	12
$\log k = \frac{1}{y}\log\left(K_{A,E}\right) + \frac{x}{y}\log\left(\frac{Q}{y}\right) + \log\left(\frac{w}{V_m}\right) - \frac{x}{y}\left[E^{y-}\right]$	1.10	14
$\log k = a - b\ \log\left[E^{y-}\right]$	1.11	14
$\log k = \left(f_1 + f_2\left[E_T\right]\right) + \left(f_3 + f_4\left[E_T\right]\right)\log\left[E^{2-}\right]$	1.12	14

Mathematical Equation	Equation	Page Number
$$\log k = \log C_g - \frac{x}{x+y} \log R$$	1.13	16
$$t_R = \left(\frac{1}{u}\right)\left\{\left(\frac{1}{B}\right)\left[(xb+1)\left(Bat_m u+\left[E^{y-}\right]_i^{(xb+1)}\right)\right]^{\frac{1}{xb+1}} - \frac{\left[E^{y-}\right]_i^{\frac{1}{x}}}{B}\right\} + t_m$$	1.14	16
$$t_R = \frac{t_m}{B} \log\left(2.3k_i B+1\right) + t_m$$	1.15	17
$$f\left({}^{eq}\left[E^{y-}\right]^{v,z}\right) = E_E^{v,z} - \frac{Q}{y \cdot V_m} - {}^{eq}\left[E^{y-}\right]^{v,z} - \sum_{i=1}^{n} E_{A_i}^{v,z} b_i a_i \frac{\left(\phi\,{}^{eq}\left[E^{y-}\right]^{v,z}\right)^{b_i}}{\left(E_E^{v,z} - {}^{eq}\left[E^{y-}\right]^{v,z}\right)^{b_i} + a_i\left(\phi\,{}^{eq}\left[E^{y-}\right]^{v,z}\right)^{b_i}}$$	1.16	18
$$w = \frac{4t_R}{\sqrt{N}}$$	1.17	20
$$\log k = a_0 + a_1 \log\left[E_m^{y-}\right] + a_2\left[E_m^{y-}\right]^2$$	1.18	20
$$\log k_{Front\,\frac{1}{2}H} = a_0 + a_1 \log\left[E_m^{y-}\right] + a_2\left[E_m^{y-}\right]^2$$	1.19	20
$$\log k_{Trailing\,\frac{1}{2}H} = a_0 + a_1 \log\left[E_m^{y-}\right] + a_2\left[E_m^{y-}\right]^2$$	1.20	20
$$w = \frac{4V_R}{\sqrt{N}}\left\{1+a\left[E^{y-}\right]_i^{-b}\left[\left[E^{y-}\right]_i^{\frac{1}{x}} + Bu\left(V_R^{'} - V_z\right)\right]^{-xb}\right\}$$	1.21	21
$$w = \frac{(2.3B+1)Gt_m}{2.3B\sqrt{N}}$$	1.22	21

Mathematical Equation	Equation	Page Number
$\sum R_s = \sum_{i=1}^{n-1} R_{s_{i,j+1}}$	1.23	22
$\prod R_s = \prod_{i=1}^{n-1} R_{s_{i,j+1}}$	1.24	24
$r = \prod_{i=1}^{n-1} \frac{R_{s_{i,j+1}}}{\frac{1}{n-1}\sum_{i=1}^{n-1} R_{s_{i,j+1}}}$	1.25	24
$R_s = \min_{1 \to n-1} R_s$	1.26	25
$t = \frac{\lvert \bar{x} - \mu \rvert}{\sigma} \sqrt{n}$	3.1	43
$\log k = a - b \log R$	4.1	57
$H = \frac{\sigma^2}{L}$	4.2	63
$H = \frac{2D_A}{u}$	4.3	64
$\left(\frac{w}{4}\right)^2 = \sigma^2 = 2D_A t_R = HL$	4.4	64
$w = \frac{4t_R}{\sqrt{N}} \sqrt{\frac{t_R}{t_{R_i}}}$	4.5	64
$t_R = t_{R_n} + \sum_{i=1}^{n-1} t_{step\ i}$	4.6	68

Mathematical Equation	Equation	Page Number
$t_R = t_{R_n} + t_{step\ 1} + t_{step\ 2}$	4.7	68
$t_R'\left(\left[E^-\right]\right) = a\left[E^-\right]^b$	4.8	73
$\left[E^-\right](t) = \left[E^-\right]_i + Bt$	4.9	74
$t_R'\left(\left[E^-\right]\right) = a\left(\left[E^-\right]_i + Bt\right)^b$	4.10	74
$v(t) = \dfrac{L}{a\left(\left[E^-\right]_i + Bt\right)^b}$	4.11	74
$L(t) = \int_0^{t_R - t_m} v(t)\,dt = \int_0^{t_R - t_m} \dfrac{L}{a\left(\left[E^-\right]_i + Bt\right)^b}\,dt$	4.12	74
$L(t) = \dfrac{L}{aB(1-b)}\left(\left\{\left[E^-\right]_i + B\left(t_R - t_m\right)\right\}^{1-b} - \left[E^-\right]_i^{1-b}\right)$	4.13	74
$t_R = \dfrac{1}{B}\left\{\left[\dfrac{laB(1-b)}{L} + \left[E^-\right]_i^{1-b}\right]^{\frac{1}{1-b}} - \left[E^-\right]_i\right\} + t_m$	4.14	75
$t_{lag} = \dfrac{L_{moved}}{L} t_m$	4.15	75
$t_R = a\left[E^-\right]_n^b + t_m + \sum_{i=1}^{n-1} t_{step\ i}$	4.16	75
$t_R = \dfrac{1}{B}\left\{\left[\dfrac{laB(1-b)}{L} + \left[E^-\right]_i^{1-b}\right]^{\frac{1}{1-b}} - \left[E^-\right]_i\right\} + t_m + \sum_{i=1}^{n-1} t_{step\ i}$	4.17	76

Mathematical Equation	Equation	Page Number
$w = \frac{4t_R}{\sqrt{N}} \sqrt{\sum_{i=1}^{n} \frac{t_R}{t_{R_i}} \times \left(\frac{L_{moved(stepi)}}{L} \right)^2}$	4.18	76
$v(t) = m\left[E^-\right]_i^3 + n\left[E^-\right]_i^2 + o\left[E^-\right]_i$	5.1	89
$t_R = \frac{L}{v(t)}$	5.2	89
$\left[E^-\right]_j = \left[E^-\right]_i + Bt_j$	5.3	94
$L_j = vt_j$	5.4	94
$t_f = \frac{L_R}{v}$	5.5	94
$t_R = t_f + t_m + \sum_{j=1}^{n-1} t_j$	5.6	96
$w = m + nk_f$	5.7	102

Abstract

Ion chromatography (IC) is the premier technique for the separation of inorganic and organic ions. Two fundamental elution regimes, namely isocratic and gradient elution, are available for separation but both are often inadequate for the separation of complex mixtures. Hence, complex elution profiles involving multiple isocratic and linear gradient steps have become the most attractive solution to accomplish the desired separations. However, the number of parameters requiring trial-and-error optimisation of such elution profiles demands a huge investment in time. This problem can be solved through the development of *in-silico* (computerised) simulation, and ultimately optimisation, methods.

The Virtual Column Separation Simulator (Dionex Corporation, Sunnyvale, CA, USA) is an efficient commercial software package for simulating and optimising IC separations. However, it has a number of limitations. The objective of this study was to address the limitations of the Virtual Column Separation Simulator and improve its prediction and optimisation abilities. This project focussed on improving the algorithms used for simulation and modelling of retention and peak width.

This study commenced with an evaluation of the maximum tolerable prediction error thresholds for retention time and peak width needed for an accurate *in-silico* optimisation. A sample mixture is normally designed to be separated within a time window of less than 30 minutes. So the acceptable maximum prediction error evaluation was analysed based on a 30-min separation. This analysis indicated that retention time had a much greater influence than peak width on the accuracy of *in-silico* optimisation. It was found that the acceptable average error limits for representative prediction were 2.5% and 35% for retention time and peak width respectively.

Three retention time algorithms and two peak width models were proposed in this study for modelling IC separations. Prediction of analyte

retention times under complex eluent profiles using these methods relied on monitoring the analyte displacement through the chromatographic column. The three devised algorithms mapped the position of the analyte in different ways where the position mapping methods of the three algorithms relied on mathematical iteration (which this algorithm was entitled the "*linear analyte displacement model"*), integrated displacement equations and numerical segmented isocratic steps. The three algorithms were found to be highly similar in their predictive errors, which were all 4% on average. Peak width modelling was much more difficult due to well known peak broadening processes. Two empirical peak width models were found to be viable for peak width simulation of analyte under complex eluent profiles. The first peak width model measured the compression exerted from each individual step using a weighting function with a compression term calculation. The second peak width model simulated the peak width using only the eluting retention factor under isocratic conditions. Both models were found to deliver predictive errors of 17% on average.

In summary, this study indicated that the retention time simulation of analytes using the newly derived models can be predicted with an average error of ≤ 4%, which is very close to the target acceptable average error limit of 2.5% required for reliable prediction. The second aspect of the modelling process investigated the broadening of the chromatographic during a separation. It was found that the width of an analyte peak could be simulated reliably using both of the derived models with an average error of ≤ 17%. This can be compared to the error threshold of up to 35% that was determined to be manageable for reliable peak width simulation. Hence, two peak width models investigated were deemed to achieve this target.

Retention prediction in the Virtual Column Separation Simulator requires the input of analyte information. This information is stored inside the pre-existing data library and is known as embedded data. This data has been collected over a period of 5 years, and to use this embedded data to predict analyte retention on newer columns could be problematic due to the variability in column manufacture and tubing configuration. This incompatibility issue was more

obvious when this older embedded data, collected on 4 mm i.d columns, was used to predict separations on the new micro-bore (2 mm) and capillary (0.4 mm) IC columns as a result of the changes in column internal diameter that results in changes related to wall effects, phase ratios and total ion-exchange capacities. These changes will somewhat alter the overall separation selectivity. A method, which was coined "*porting*", has been used to calibrate the pre-existing data library with minimal experimental input. This process allowed the data to be "refreshed" for newer columns, along with those of different internal dimensions, and allowed retention time simulation to be reliably performed. By incorporation of this porting methodology for calibration and the *linear analyte displacement model* for retention prediction, a predictive error of 3% was achieved for these newer column formats while employing data collected on older column formats.

Table of Contents

Chapter 1

Introduction and Literature Review

1.1 Ion Chromatography

Ion chromatography (IC) is a powerful analytical technique for the separation and determination of inorganic solutes. IC falls into the general classification of liquid-solid chromatographic methods in which a liquid (called the mobile phase or eluent) is passed over a solid stationary phase and then through a suppression device before entering a flow-through detector (typically a conductivity type). The sample to be separated is introduced into the flowing eluent stream by means of an injection device inserted into the flow-path prior to the column[2].

When a sample is introduced into an IC system, equilibrium is established for each sample component between the mobile and stationary phases. Thus, for a component, A, this can be written as[2]:

$$A_m \rightleftharpoons A_s \qquad \text{Equation 1.1}$$

where the subscript m refers to the mobile phase (eluent) and s refers to the stationary phase.

The distribution of component A between the two phases is given by the distribution coefficient, D_A, where[2]:

$$D_A = \frac{[A_S]}{[A_m]} \qquad \text{Equation 1.2}$$

The value of D_A is dependent on the population of component A in the stationary and eluent phases[2]. Since the equilibrium shown is dynamic, there is a continual, rapid interchange of component A between the two phases.

Sample components will only progress towards the end of column when they are in the mobile phase. If component A has a large value of D_A, it will retained longer in the stationary phase so takes a longer period of time to

reach the end of the column. Hence it has a large retention time. Retention can also be expressed in terms of retention factor, k:

$$k = D_A\left(\frac{w}{V_m}\right) \qquad \text{Equation 1.3}$$

where V_m is the volume of the mobile phase and w is the weight of the stationary phase.

The stationary phase for anion analysis usually comprises secondary, tertiary or quaternary ammonium functional groups as anion ion-exchange moieties, whilst sulfonate or carboxylate functional groups are usually employed for cation separations[2].

An anion-exchange material can be expressed as M^+E^-, where M^+ denotes the insoluble matrix material comprising a fixed (positive) charge and E^- represents the competing ion. When a solution containing an analyte anion, A^-, is injected into the separation column, equilibrium is established between the two mobile ions E^- and A^- as follows[2]:

$$M^+E^- + A^- \rightleftharpoons M^+A^- + E^- \qquad \text{Equation 1.4}$$

A single univalent anion A^- displaces a single univalent counter-ion E^-. Thus the equation can be expressed for y moles of A^{x-} exchanging with x moles of E^{y-} to give[2]:

$$y\,A_m^{x-} + x\,E_s^{y-} \rightleftharpoons y\,A_s^{x-} + x\,E_m^{y-} \qquad \text{Equation 1.5}$$

where the subscript m denotes the mobile phase and s denotes the stationary phase.

Therefore, the equilibrium constant of the reaction is given by[2]:

$$K_{A,E} = \frac{\left[A_s^{x-}\right]^y\left[E_m^{y-}\right]^x}{\left[A_m^{x-}\right]^y\left[E_s^{y-}\right]^x} \qquad \text{Equation 1.6}$$

where the brackets indicate molar or molal concentrations, or equivalent fraction units.

When a mixture of analytes is injected into an IC system, the analytes will begin interacting with the stationary phase to different degrees depending on their $K_{A,E}$ values, which leads to different rates of progression through the column. The movement of the analyte relies on the physio-chemical properties, including its size, polarisability, hydrophobicity and charge, the concentration of the mobile phase (MP), the temperature of operating condition, the flow-rate of the system and the morphology of the stationary phase (SP)[2].

The eluent concentration and the stationary phase possess the greatest influence on the retention of a separation. The empirical refinement of chromatographic conditions to accomplish an efficient separation is known as method development and can be very time-consuming.

Method development involves two stages, namely column selection followed by intelligent manipulation of the eluent profile. Column selection is a rapid, but crucial process. Incorrect selection of a column could lead to incorrect selectivity, poor resolution, and unnecessarily long separation times. Eluent profile manipulation is then used to fine-tune the separation of any co-eluting analytes in a separation. Fine-tuning of a separation is a usually iterative process which means that it is often the rate-determining step in method development. This review focuses on manipulation of the elution profile.

1.2 Elution Modes

1.2.1 Isocratic Elution

The first fundamental elution regime is isocratic elution, whereby the eluent composition remains constant throughout the entire separation. The constant eluent strength typically leads to several general elution problems in separating mixtures containing analytes with widely differing distribution coefficients (D_A). On one hand, low eluent concentrations can easily separate those solutes in the mixture that have smallest D_A and they appear as sharp peaks. Analytes with intermediate D_A will be eluted with increased peak width and reduced peak height, whilst analytes with high D_A will have long elution times as well as poor peak shape. On the other hand, high eluent

concentrations result in analytes with high D_A emerging in a reasonable time as sharp peaks, however, analytes with small and medium distribution coefficients have insufficient time for separation and thus will be co-eluted with poor resolution[3]. In summary, co-elution, insufficient peak capacity and excessive separation time of the later eluting peaks are the typical problems observed in isocratic separations (**Figure 1.1**).

1.2.2 Gradient Elution

The second elution mode involves the application of a gradient whereby the mobile phase changes with time either physically or compositionally. Physical gradient elution can be introduced by the altering the temperature, whilst compositional gradient elution is accomplished by varying the concentration of the eluent.

1.2.2.1 Linear Concentration Gradient Elution

Linear concentration gradient elution is performed by varying the eluent concentration linearly over time. This mode is an ideal solution for simple mixtures consisting of a small number of analytes[4].

Figure 1.2 shows an illustration of a gradient separation. The separation commences at low eluent concentration enabling time for the first peaks to separate, while the increasing solvent strength shortens the separation time and compresses the peak widths of later eluting analytes, which ultimately offers much greater peak capacity[5]. Figure 1.2 shows a more evenly spaced and better-resolved separation compared to the isocratic separation illustrated in Figure 1.1. Early eluters are well resolved and the separation is complete in 33 min compared to 35 min for the isocratic separation. Notwithstanding these improvements, insufficient resolution and excessive space are still observed.

1.2.2.2 Multi-step Concentration Gradient Elution

Complex eluent profiles generally comprise a number of isocratic and linear gradient steps[5, 6]. Multi-step concentration gradient elution usually commences with a short isocratic step followed by implementation of a mild gradient ramp to address the co-elution for early eluters. Medium eluters in the mixture can then separated using a combination of isocratic and gradient

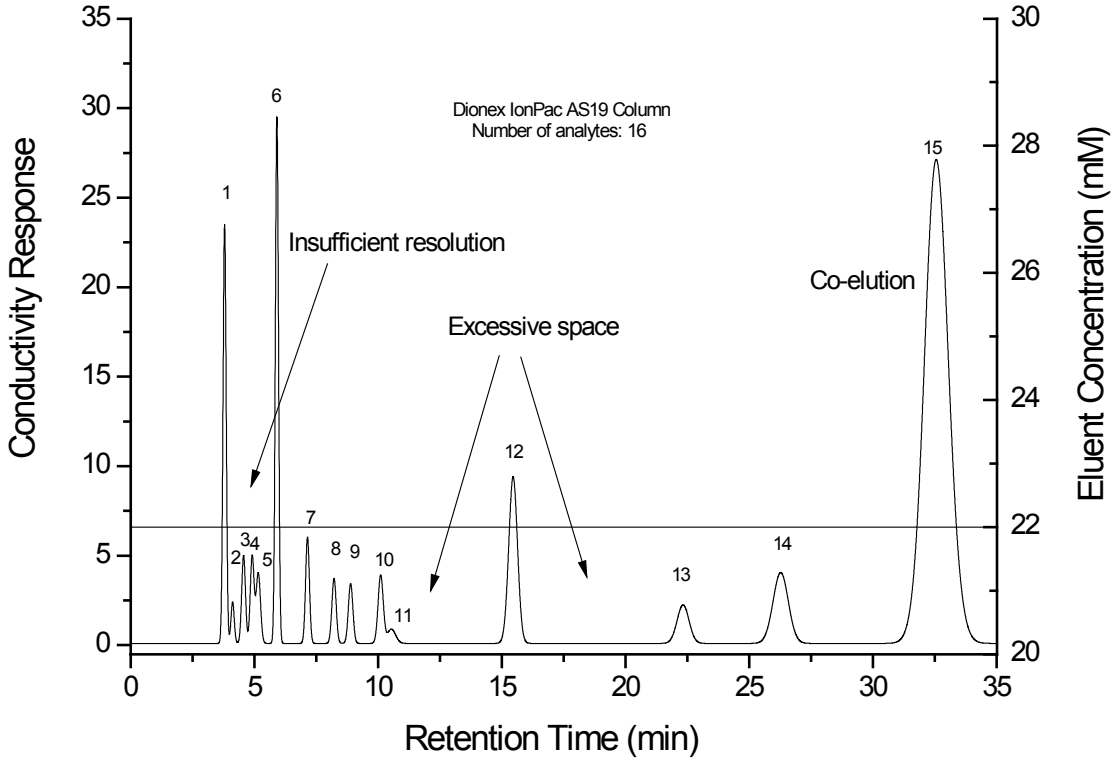

Figure 1.1 Illustration of general problems observed in isocratic separation. The separation consists of 16 analytes eluting in the order of 1-fluoride, 2-propionate, 3-methanesulfonate, 4-chlorite, 5-bromate, 6-chloride, 7-nitrite, 8-chlorate, 9-bromide, 10-nitrate, 11-carbonate, 12-oxalate, 13-iodide, 14-thiosulfate, 15-thiocyanate and phosphate.

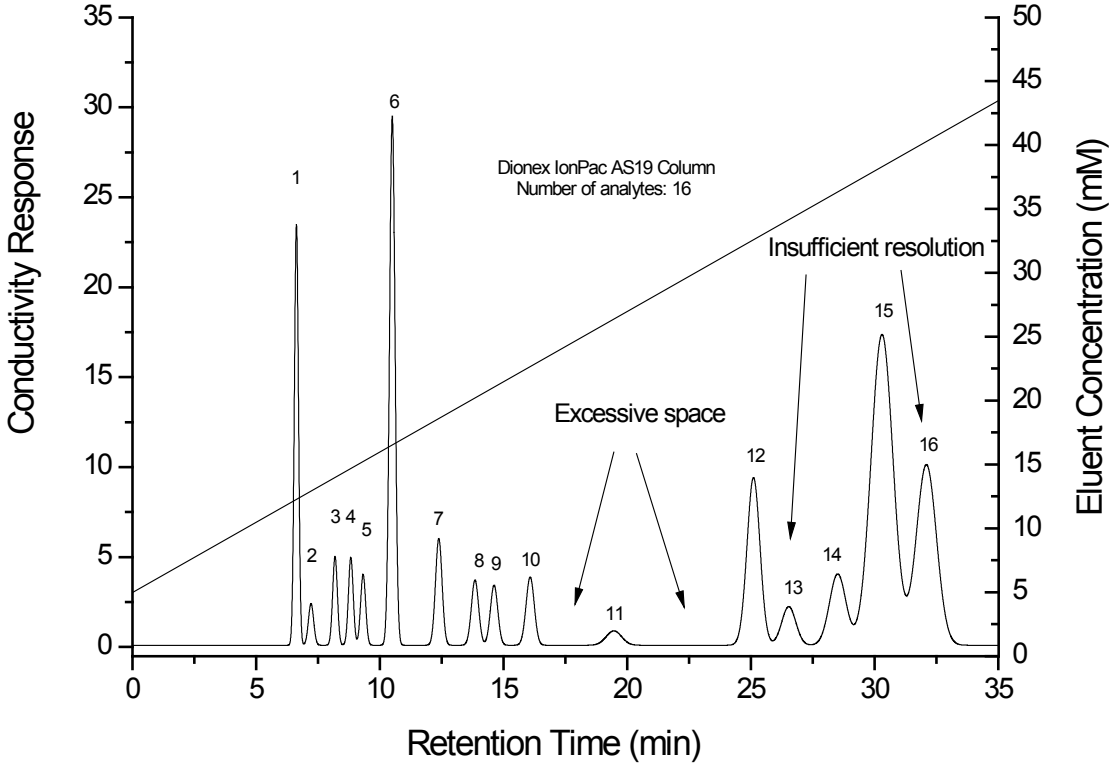

Figure 1.2 Illustration of general problems observed in gradient separation. The separation consists of 16 analytes eluting in the order of 1-fluoride, 2-propionate, 3-methanesulfonate, 4-chlorite, 5-bromate, 6-chloride, 7-nitrite, 8-chlorate, 9-bromide, 10-nitrate, 11-carbonate, 12-oxalate, 13-iodide, 14-thiosulfate, 15-thiocyanate and 16-phosphate.

steps. A steep ramp is often introduced at the end to speed up the later eluting peaks and remove the unnecessary space of the separation. An illustration of a separation comprising isocratic and gradient steps is shown in **Figure 1.3**. Typical problems of co-elution, insufficient separation and unnecessary space encountered in isocratic (Figure 1.1) and linear gradient (Figure 1.2) separations are better addressed in this elution mode.

One of the major advantages to IC is the routine use of electrolytic eluent generator in which water used as mobile phase feed is converted via an electrolysis step into the desired eluent[7]. An electrolytic eluent generator is typically configured between a pump and separation column. **Figure 1.4** shows the configuration of a modern reagent-free ion chromatograph (RFIC^{TM}). Eluent generation for isocratic, linear and non-linear gradient, and complex elution profiles comprising sequential multiple isocratic and gradient steps is therefore an easy practice. Due to the invention of electrolytic eluent generation module and the applicability of complex eluent profiles on separating the problematic mixtures, this method has now become the most widely used approach in IC and LC. This is one of the applications where multi-step gradient elution was employed for separation of peptides[4].

1.2.2.3 Non-Linear Concentration Gradient Elution

Non-linear concentration gradient elution utilises a non-linear increase in the eluent concentration, which is a relatively easy exercise to achieve with an electrolytic eluent generator. Non-linear gradients can be defined as either convex or concave[8, 9]. One of the applications employing concave gradient elution is nucleotide analysis[10]. Concave gradient elution is particularly useful in separating a problematic mixture, since it introduces a shallow ramp at the start allowing molecules with low retention to separate with the ramp getting steeper at the end providing strong eluent strength for molecules with large retention.

1.2.2.4 Temperature Gradient Elution

Temperature gradient elution involves varying the temperature of the mobile phase during the elution process. Temperature gradient is an attractive alternative to compositional gradient elution, as they do not require a gradient

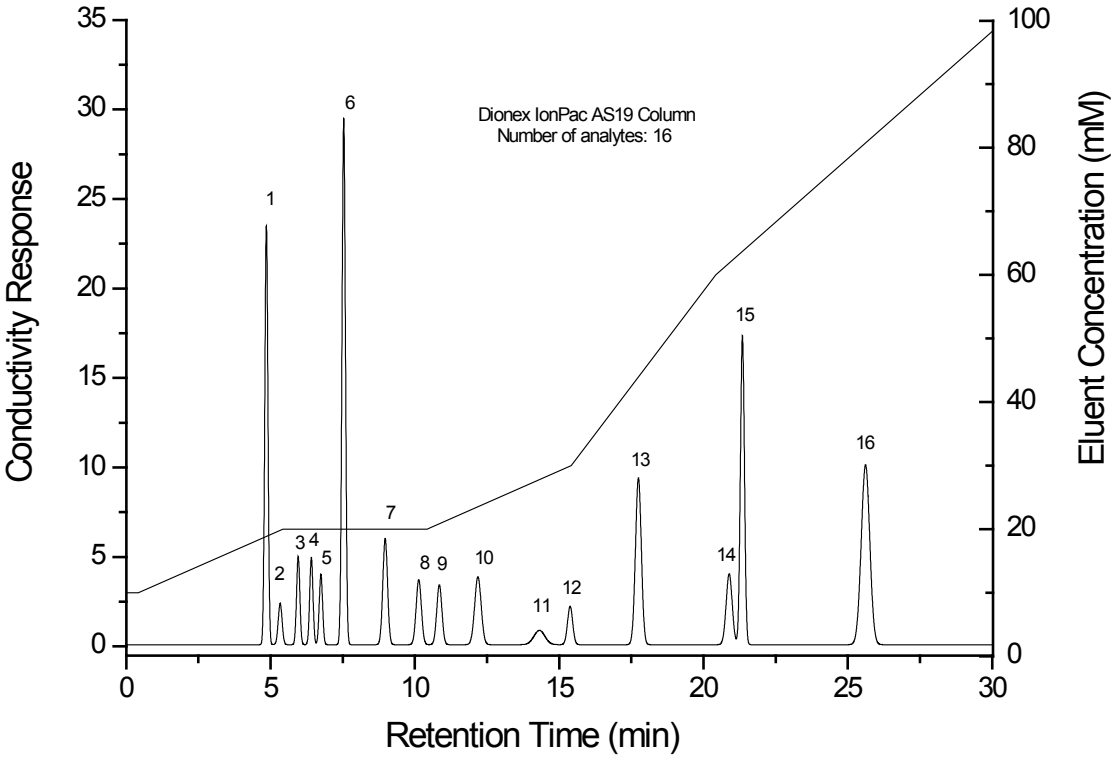

Figure 1.3 Illustration of a separation consisting of gradient and isocratic steps. The separation consists of 16 analytes eluting in the order of 1-fluoride, 2-propionate, 3-methanesulfonate, 4-chlorite, 5-bromate, 6-chloride, 7-nitrite, 8-chlorate, 9-bromide, 10-nitrate, 11-carbonate, 12-iodide, 13-oxalate, 14-thiosulfate, 15-phosphate and 16-thiocyante.

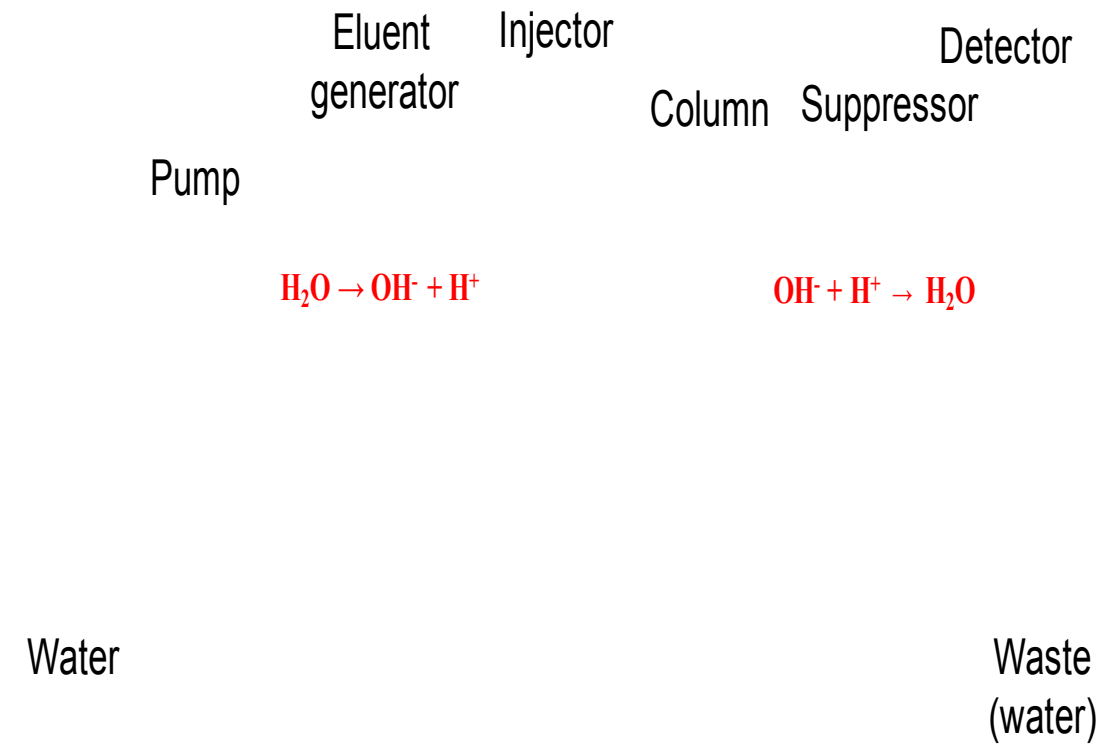

Figure 1.4 A schematic of a typical reagent-free ion chromatographic system

pump and shorter equilibration periods between sequences can be accommodated. Temperature gradients however have a weaker effect on analyte retention compared to concentration gradients. In addition, a special thermal compartment is required to provide rapid heat transfer to the column and to stabilise the column at elevated temperatures[11]. There are few applications[12-14] employing this technique in either IC or reversed-phase liquid chromatography (LC).

1.2.2.5 Dual-Mode Gradient Elution

Dual-mode gradient elution involves varying the chemical composition and physical characteristics of the eluent simultaneously. Typically, dual-mode gradient elution employs the temperature variations as the physical gradient portion and a concentration multi-step gradient ramp as the chemical component. This combination offers the best capability in terms of both physical and chemical aspects[15-18]. Dual-mode gradient elution is much more powerful than the application of complex eluent profiles, but its complexity makes optimisation considerably more difficult. This is a new application and only a few research papers[19, 20] have been published in this area.

In summary, a series of elution modes can be used for fine-tuning the separation, however regardless of the type of elution mode, the development of the conditions required must be determined through an optimisation process. Trial-and-error is the conventional optimisation approach. Typically, a set of designed experiments will be firstly performed, followed by running a further set of experiments to determine the most feasible conditions. More experiments will be carried out as necessary to achieve the desired separation. This method is an iterative optimisation approach and it requires a large investment of time. Computerised optimisation, (optimisation *in-silico*) therefore becomes an attractive solution as it is a much more efficient tool for method development.

1.3 Retention Time Modelling

Resolution is an indicator of the quality of a separation. To perform optimisation *in-silico*, the main factors that are responsible for manipulating

the resolution in a chromatographic separation need to be modelled mathematically. Resolution is given by[21]:

$$R_s = 2\frac{t_{R1} - t_{R2}}{w_1 + w_2} \qquad \text{Equation 1.7}$$

where t_{R1} and t_{R2} are the retention times of the adjacent peaks and w_1 and w_2 are the base widths of both peaks. It is important to note that the peak widths at half height can also be used to calculate the resolution of a peak pair.

From Equation 1.7, it is obvious that both retention times and peak widths are crucial for optimisation and therefore both need to be modelled accurately. These two parameters can be predicted using both soft and hard models. Soft models are derived independently of any theoretical explanations. In contrast, hard models are derived from fundamental theory and invariably require knowledge of parameters relating to the characteristics of analytes, stationary phases and eluent profiles for accurate predictions[22].

1.3.1 Soft Retention Time Modelling

Soft models typically aim to fit the best mathematical relationship between the controlled and the measured parameters. Artificial Neural Networks (ANN)[22-30] and genetic algorithms (GA)[31-34] are typically the most popular approaches, and are often referred to as a form of machine learning.

1.3.1.1 Artificial Neural Networks

An ANN is a network consisting of an array of units activated by weighting functions. The basic processing unit in an ANN is a node, which is a simulated neuron. Multiple nodes can be built into different layers where each node of a present layer is a connection of each node for a previous and future layer. The entire group of nodes constitutes a complete ANN.

Artificial Neural Networks have been extensively employed by Bolanca *et al.* [22-28] in IC simulation and optimisation. These authors use a multi-layer perception, feed-forward neural network with Delta-bar-Delta variation of the back propagation as the connecting weighting function for the regular training scheme. A multi-layer network is strongly interconnected by

nodes and consists of one input layer, one output layer and at least one hidden layer. The complexity of the nodes and layers remains chaotic and fully dependent on the variables and their relationships [22-28]. During the modelling process, the hidden layer nodes and iteration steps of neural network were optimised in order to derive the most accurate retention model. This approach has been applied to limited set of analytes consisting of eight anions and eight cations for predicting the analyte retentions under various isocratic, linear concentration and temperature gradient conditions. The validation was conducted using potassium hydroxide for anion analysis and methanesulfonic acid for cation separations. Bolanca *et al.* has found that the retention prediction using ANN to be less than ± 2% error on average [22-28].

1.3.1.2 Genetic Algorithm (GA)

Deriving a soft model using a genetic algorithm involves a number of phases. Initially, this approach uses the genetic algorithm selection routine to determine the subsequent parameters for the training set, followed by implementing a cross-validated model based on a “leave one out” technique [31-34].

The partial least squares algorithm is an example of a genetic algorithm and it employs the latent variables from a larger set of correlated descriptors in a manner similar to that used in principal component analysis. The algorithm is expressed as follows:

$$y = a_1 LV_1 + a_2 LV_2 + ...+ a_m LV_m \qquad \text{Equation 1.8}$$

where y is the dependent variable (such as retention factor), LV_i is the i^{th} latent variable and a_i is the i^{th} regression coefficient corresponding to LV_i.

Each latent variable LV_i can be expressed as a linear combination of the independent variables x_i:

$$LV_i = \alpha x_1 + \beta x_2 + \delta x_3 + ... + \upsilon x_n \qquad \text{Equation 1.9}$$

where x_i is the independent molecular descriptor.

The latent variables are orthogonal to each other, and the first latent variable usually accounts for the most weight in the data[31]. There has been

relatively few research works reported in the literature using this approach[31-34].

This approach requires high cost in future maintenance due to lack of theoretical explanations and requirements of large training sets[24, 27]. For instance, an ANN trained for isocratic elution is not compatible for gradient separations. This means that additional data acquisition is required for gradient separations as a new data set must be collected for the training process.

1.3.2 Hard Retention Time Modelling

Hard models are much more informative compared to soft models, but model derivation is a long process. There are a number of mathematical models that have been derived for IC, gas chromatography (GC)[35-39], reversed-phase liquid chromatography (RPLC)[16-18], and other separation science technologies[40-46].

1.3.2.1 Isocratic Retention Time Models

Retention models for chromatography are derived from factors affecting the elution of analytes, such as their interactions with stationary phase, analyte charge, flow-rate and characteristics of the competing ion.

Madden *et al.* published two important reviews[47, 48] critically comparing the predictive abilities of a range of isocratic retention models [49-55] suitable for IC. The performance of retention models for isocratic chromatography were comprehensively reviewed over different suppressed[48] and non-suppressed[47] conditions using single and dual species eluent on different columns. Of the numerous existing models, two approaches, namely the linear solvent strength model, and linear solvent strength model – empirical approach, were found to have the best predictive ability for single (for example, hydroxide) and dual (for example, carbonate/bicarbonate) species eluents.

The linear solvent strength model (LSSM)[49] is an isocratic retention model capable of predicting the separations consisting of single species eluents and is given by:

$$\log k = \frac{1}{y}\log\left(K_{A,E}\right) + \frac{x}{y}\log\left(\frac{Q}{y}\right) + \log\left(\frac{w}{V_m}\right) - \frac{x}{y}\left[E^{y-}\right] \quad \text{Equation 1.10}$$

where k is the retention factor, $K_{A,E}$ is ion-exchange selectivity coefficient between the analyte and the eluent competing ion, x is the charge of the analyte, y is the charge on the eluent, Q is the effective ion-exchange capacity of the stationary phase, w is the mass of the stationary phase, V_m is the volume of the eluent species and $\left[E^{y-}\right]$ is the concentration of the eluent.

If this model is employed for isocratic separations consisting of a single competing ion, $K_{A,E}$, Q, w and V_m can be treated as constants and thus the model can be simplified to:

$$\log k = a - b \log\left[E^{y-}\right] \quad \text{Equation 1.11}$$

where a and b are both constants.

A plot of log k *versus* log $\left[E^{y-}\right]$ will give rise to a linear relationship with the effective charge of the analyte relative to the competing ion as the slope, b, and the intercept, a, indicating the degree of interaction between analyte and stationary phase. The LSSM has been verified for its high accuracy for isocratic separations employing a single eluent species[49].

The linear solvent strength model – empirical approach (LSSSM – EA) is an extension of the LSSM. It is capable of predicting the separations consisting of dual species eluent, such as carbonate/bicarbonate. The model is given by following[56]:

$$\log k = \left(f_1 + f_2\left[E_T\right]\right) + \left(f_3 + f_4\left[E_T\right]\right)\log\left[E^{2-}\right] \quad \text{Equation 1.12}$$

where f_1, f_2, f_3 and f_4 are isocratic constants and can be determined experimentally, $[E_T]$ is the total eluent concentration of both singly and doubly charged competing ions and $[E^{2-}]$ is the eluent concentration of the higher

charged species. The first portion ($f_1 + f_2 [E_T]$) of Equation 1.12 accounts for the solvent strength exerted from singly charged species whilst the second part ($f_3 + f_4 [E_T] \log [E^{2-}]$) integrates the effect from the higher charged competing ion. Four experimental data points were required to solve for this model. Note that for retention prediction of single species eluent, $[E^{2-}]$ is 0 and Equation 1.12 reverts to Equation 1.11.

These two models (the LSSM and LSSM-EA) and a range of isocratic retention models [49-55] were initially applied to simulate the retention of limited set of anions using Dionex IonPac columns[47, 48] under IC suppressed and non-suppressed conditions. It was found that the LSSM and LSSM-EA are the best isocratic models for predicting IC separations consisting of single and dual species eluents respectively. These two models delivered an error of ≤ 5% on average compared to experimental results for retention prediction where only positive errors were observed in the prediction. It was also found that these two models were more reliable on predicting the IC suppressed separations. The validity of these two models were expanded to extensive sets of analytes, columns and eluents under suppressed conditions in 2002[56] and they are currently employed in the commercial IC optimisation tool, Virtual Column Separation Simulator (Sunnyvale, CA, USA) [56].

1.3.2.2 Gradient Retention Models

Compared to isocratic elution, there are fewer gradient retention models reported in the literature as the gradient elution mode is more complicated than isocratic elution. Existing models have been typically derived from the chemical and physical interactions occurring inside the column, as well as the effect of the change of the eluent strength. All the existing IC models are derivatives of the LSSM.

Rocklin *et al.* [57]proposed a gradient elution model that has a very good predictive ability and is expressed as[57]:

$$\log k = \log C_g - \frac{x}{x+y} \log R$$ Equation 1.13

where R is the gradient ramp in mM/min, C_g is a gradient constant and normally determined from a limited set of experiments, y is the charge of the eluent and x is the charge of the analyte.

This model is valid for single eluent species and a plot of log k *versus* log R will give rise to a straight line with a slope of $\frac{x}{x+y}$[57].

However, the important variables such as flow-rate of the eluent and the initial eluent concentration are not incorporated in this model. As a result, the predictions are limited to gradient separations at fixed flow-rate and starting concentration[57]. This model is currently employed in the commercial IC optimisation tool, Virtual Column Separation Simulator (Sunnyvale, CA, USA)[56].

A highly useful gradient model was proposed in 1974 by Jandera *et al.*[9, 58] and is expressed as follows:

$$t_R = \left(\frac{1}{u}\right)\left\{\left(\frac{1}{B}\right)\left[(xb+1)\left(Bat_m u + \left[E^{y-}\right]_i^{(xb+1)}\right)\right]^{\frac{1}{xb+1}} - \frac{\left[E^{y-}\right]_i^{\frac{1}{x}}}{B}\right\} + t_m$$

Equation 1.14

where a is the value of the interaction between stationary phase and the analyte, b is the effective charge of the analyte, B is the gradient ramp in mM/min, t_m is the void time, u is the flow-rate, $[E^{y-}]_i$ is the initial concentration, x is the characteristic shape of the ramp and t_R is the retention time. This model was originally derived for RPLC.

Jandera *et al.* successfully utilised this model for the simulation of retention behaviour of analytes in gradient elution of reversed phase liquid chromatography involving dual eluent species where one species exerted a much higher eluent strength than the other. This model was also applied by Baba *et al.* in simulating the retention of polyphosphates in IC[8, 59, 60].

To predict the retention behaviour of analytes, the constants a and b, along with the void time of the column need to be obtained either from isocratic or gradient experimental data.

In 1979, Snyder *et al.* proposed a gradient model [3, 61] for liquid-solid chromatography and is given by:

$$t_R = \frac{t_m}{B} \log\left(2.3k_i B+1\right) + t_m \qquad \text{Equation 1.15}$$

where k_i is the isocratic retention factor observed under isocratic conditions at gradient initial concentration.

This model has been successfully applied to predict the retention of five benzene derivatives for reversed-phase gradient separations where high correlation was found between the prediction and actual retention data (average error of 0.6%). This gradient model has been incorporated into the commercial optimisation software, DryLab (LC Resources Inc., Walnut Creek, CA, USA)[3, 61]. It is important to note that no research work has been conducted in proving the validity of this model for IC separations.

An important parameter, namely the flow-rate of the system, is not found in the expression. As a result, the validity of this model is limited at a fixed flow-rate.

No critical review is yet to be found in the literature to compare the predictive ability of gradient models for IC separations. Therefore, an evaluation of existing gradient models for IC separations is in the scope of this study.

1.3.2.3 Retention Algorithm for Complex Eluent Profiles

The use of complex eluent profiles provides superior separation ability than using either the isocratic or gradient elution mode. However, the simulation of retention behaviour for a combination of isocratic and gradient steps is exponentially more complicated due to the number of isocratic and gradient steps involved. One algorithm was found in the literature for simulating the retention of complex eluent profiles for IC separations.

In 2009, Drgan *et al.* proposed a discontinuous plate model[62]. The underlying concept of this discontinuous plate model remains identical to the LSSM. In this model the separation column was divided into numerous column segments and the analyte movement is closely monitored in each column segment. This model monitors the analyte movement using the LSSM to understand the distribution of the analyte between the mobile and stationary phases in each column segment and is expressed as follows:

$$f\left({}^{eq}\left[E^{y-}\right]^{v,z}\right) = E_E^{v,z} - \frac{Q}{y \cdot V_m} - {}^{eq}\left[E^{y-}\right]^{v,z} - \sum_{i=1}^{n} E_{A_i}^{v,z} b_i a_i \frac{\left(\phi\,{}^{eq}\left[E^{y-}\right]^{v,z}\right)^{b_i}}{\left(E_E^{v,z} - {}^{eq}\left[E^{y-}\right]^{v,z}\right)^{b_i} + a_i\left(\phi\,{}^{eq}\left[E^{y-}\right]^{v,z}\right)^{b_i}} \qquad \text{Equation 1.16}$$

where $f\left({}^{eq}\left[E^{y-}\right]^{v,z}\right)$ is the function f dependent on the eluent concentration in the mobile phase of the column segment z after m movements of the mobile phase, $E_E^{v,z}$ is total amount of eluent in the column segment z after v movement of mobile phase through the column, $E_{A_i}^{v,z}$ denotes the total amount of the analyte in the column segment z after v movement of the mobile phase through the column and ϕ is the ratio between volumes of stationary phase and mobile phase. This algorithm relies on the Newton method to calculate the distribution of the analyte between the mobile and stationary phases in each segment[62]. When the analyte reaches the end of column after m movement, the segment z can be transposed into retention time.

This highly complex discontinuous plate model delivered an average error of ± 4% for the simulation of retention behaviour of 8 anions on the Dionex AS17 column. However, the time required for predicting a chromatogram could be sizeable depending on the complexity of the profiles. Due to the sizeable processing time, this approach is not very useful for *in-silico* optimisation. Therefore, a better retention algorithm is required.

There are other retention models in the literature, such as those derived for proteins[63-67] and other modes of chromatography [6, 16-18, 68-70] however these models will not be discussed in this present scope.

1.3.3 Soft Models *versus* Hard Models

There are a number of existing soft and hard models proposed for prediction of retention behaviour in IC separations. Bolanca *et al.*[24-27] commented that the retention predictions using soft models or ANNs had excellent predictive ability with an average error of 2%. ANNs rely solely on fitting of mathematical expressions empirically with the nodes and hidden layers using large training sets. These models do not provide any theoretical explanations for the separations achieved, and this will be potentially problematic in further maintenance as data re-acquisition and ANN retraining will be required for new systems. In terms of predictive ability, this method is an excellent option for retention time simulation.

As for hard models, these were proposed mainly based on the key factors responsible for manipulating separations. The derivation process for the model can be very time-consuming, while the accuracy is no better than soft models. However, hard models can provide useful chemical relationships and represent elution properties[47, 48, 56]. The main advantages of hard models are that there is no need for a retraining process for new columns as well as they require a minimal set of training sets in comparison to soft models.

In summary, both models offer different strengths and weaknesses for *in-silico* optimisation. Hard models provide unique fundamental theory for researchers in detailed analysis and justification while soft models can be employed as simulation tools in order to offer a potentially superior predictive ability. Overall, both models should be used to support each other.

1.4 Peak Width Modelling

In isocratic elution mode, peak width is affected by well-known peak broadening processes. These processes cause the band of analyte molecules to spread as it migrates down the column[71, 72]. Peak width of

an analyte eluted under isocratic conditions can be easily predicted using the rearranged theoretical plate count expression:

$$w = \frac{4 t_R}{\sqrt{N}} \qquad \text{Equation 1.17}$$

where N is the theoretical plate number of the analyte.

Peak width in gradient separation is governed by two major factors, namely peak broadening and band-compression. Increasing solvent strength in a gradient elution tends to speed up the trailing edge of the analyte band relative to the leading edge, which results in the compression phenomenon. The broadening of a peak is partially counteracted by this compression effect, which generally results in a narrower peak width across the entire chromatogram in gradient elution compared to isocratic elution. These two effects have been investigated in order to enable peak width modelling.

1.4.1 Soft Peak Width Modelling

There is only one peak width model reported in the literature for gradient IC separations, which was published by Bolanca *et al.* in 2009[73]. This empirical model was derived using an ANN approach. The model measures the peak broadening at three points on the peak; the peak maximum, at half height of the front end of the peak, and at half height of the trailing end of the peak using the following equations:

$$\log k = a_0 + a_1 \log\left[E_m^{y-}\right] + a_2\left[E_m^{y-}\right]^2 \qquad \text{Equation 1.18}$$

$$\log k_{\text{Front}\frac{1}{2}H} = a_0 + a_1 \log\left[E_m^{y-}\right] + a_2\left[E_m^{y-}\right]^2 \qquad \text{Equation 1.19}$$

$$\log k_{\text{Trailing}\frac{1}{2}H} = a_0 + a_1 \log\left[E_m^{y-}\right] + a_2\left[E_m^{y-}\right]^2 \qquad \text{Equation 1.20}$$

where a_i are regression coefficients with characteristic values for a given IC system, which were determined by using the common regression method. This model was reported to deliver a very good predictive ability for peak width[73], however no indication of the accuracy was quoted.

1.4.2 Hard Peak Width Modelling

Due to the complex nature of gradient peak width modelling, the predictive ability of existing peak width hard models found in the literature are typically no better than in accuracy compared to the retention models.

In 1974, Jandera *et al.*[9] proposed a peak width model for predictions in LC and this is based on the column plate number under isocratic conditions and the instantaneous isocratic retention factor of the solute at the time the peak maximum leaves the column. The model is expressed by:

$$w = \frac{4V_R}{\sqrt{N}}\left\{1+a\left[E^{y-}\right]_i^{-b}\left[\left[E^{y-}\right]_i^{\frac{1}{x}}+Bu\left(V_R^{'}-V_z\right)\right]^{-xb}\right\} \qquad \text{Equation 1.21}$$

where w is the width of the analyte peak, V_R is the retention volume, N is the isocratic theoretical plate number, $V_R^{'}$ is the adjusted retention volume and V_z is the volume of the connecting tubing between the outlet of the gradient-generating device and the top of the column.

Jandera *et al.* successfully applied this equation to predict the peak widths of organic analytes in RPLC and the results deviated from experimental data by ± 25%[9, 58, 74]. This model was further evaluated in a review by Baba *et al.*[8] for predicting the peak widths of separated oligonucleotides in IC.

In 1979, Snyder *et al.* derived a peak width model for liquid-solid chromatography where the relationship is detailed as follows[3].

$$w = \frac{(2.3B+1)Gt_m}{2.3B\sqrt{N}} \qquad \text{Equation 1.22}$$

where G is the compression factor which can be calculated from numerical integration.

This model was based on the normal chromatographic broadening process and the compression mechanism in gradient elution. This equation was successfully applied in RPLC for the prediction of peak widths of five benzene derivatives with an accuracy of ±12%[3].

1.5 Optimisation

Retention time and peak width modelling enables *in-silico* optimisation of IC separations to be accomplished. *in-silico* optimisation is a two-step procedure. First, a search area (minimum and maximum boundaries) for each parameter (such as initial concentration and gradient slope) that manipulates the separations needs to be defined. A condition within the defined search area is then systematically/randomly generated, followed by assessing the quality of the potential separation. This process will be repeated until the potential separation meets the defined target. There are a number of strategies that are applicable for optimum searching in the defined area. Each method relies on assigning a numerical quality indicator to predicted chromatograms. The numerical quality indicators are commonly referred to as criterion functions.

A criterion function assigns a numerical rating to each potential simulated chromatogram. The criterion function typically assesses each peak pair in the chromatogram, or the overall chromatogram. The degree of separation of two components only is commonly known as elemental criterion. Separation factor, resolution factor, peak-to-valley ratios and area of overlap are all examples of elemental criteria. Elemental criteria for each adjacent peak pair are integrated to give a "*composite criterion*" that reflects the quality of the entire chromatogram. There are several composite criteria defined in the literature.

A common composite criterion is the sum of resolution criterion function. The equation is given by:

$$\sum R_S = \sum_{i=1}^{n-1} R_{S_{i,j+1}} \qquad \text{Equation 1.23}$$

where subscript i refers to a specified peak and subscript j denotes its adjacent peak[75]. The most well resolved peak pair in a chromatogram dominates the resolution sum so co-elution could be observed for an optimal condition determined from this criterion[75]. A large resolution sum normally corresponds to the peaks in the separation being well resolved. For example, the resolution sum for the separation shown in **Figure 1.5** is 36. This separation has a large resolution sum due to the presence of excessive

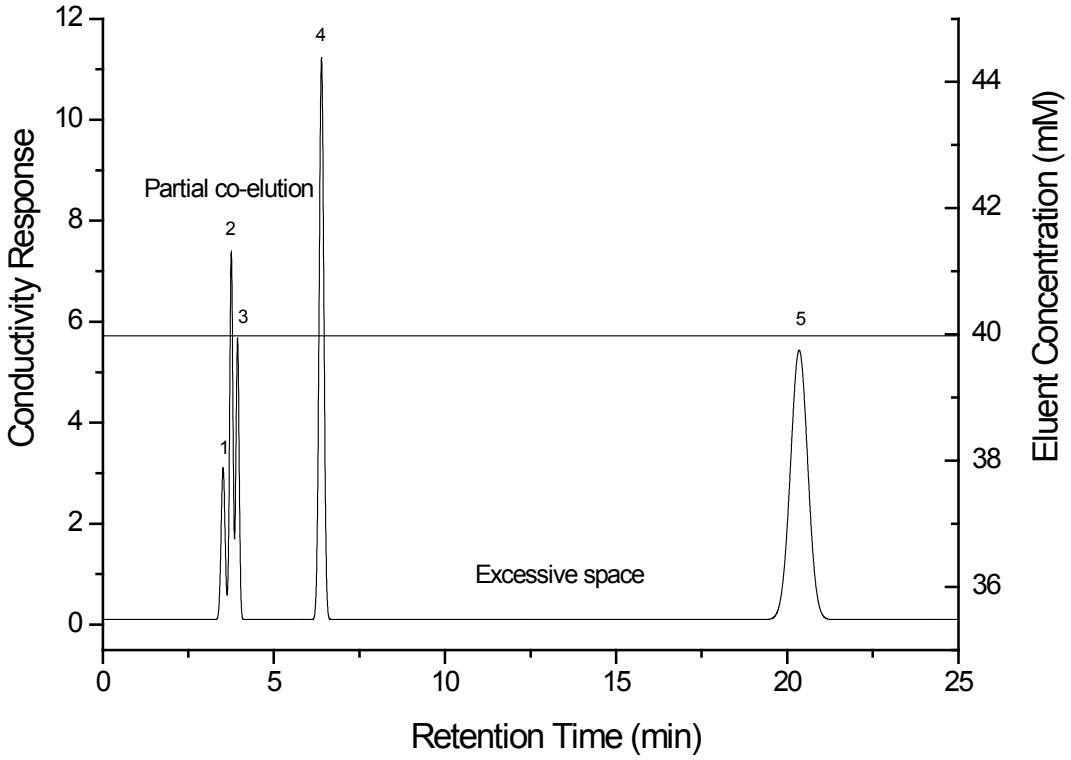

Figure 1.5 Illustration of a 5-component (1-propionate, 2-formate, 3-bromate, 4-bromide and 5-thiocyanate) separation consisting of two general elution problems, namely co-elution and excessive space.

space between peaks 4 and 5 however it does not accurately reflect the partial co-elution between peaks 1, 2 and 3. So this criterion is not useful for the separations consisting of co-elution.

The product of resolution is also a commonly used criterion function. The equation is detailed as[75]:

$$\prod R_s = \prod_{i=1}^{n-1} R_{s_{i,j+1}} \qquad \text{Equation 1.24}$$

The least resolved peak pair in a chromatogram dominates the resolution product. The simulated optimum using this criterion function might end up having excessive space between peak pairs while overlooking other conditions where peaks are more evenly spaced[75]. A small resolution product typically corresponds to the co-elution observed in the separation. For example, the resolution product of this separation (Figure 1.5) is 471. A typical resolution product value is considerably large however the resolution product of this separation (Figure 1.5) is relatively small due to the partial co-elution of peaks 1, 2 and 3. Therefore these two peak pairs dominate the resolution product with a small value without indicating the excessive space between peaks 4 and 5.

Normalised resolution product evaluates all peak pairs equally. The equation is expressed as:

$$r = \prod_{i=1}^{n-1} \frac{R_{s_{i,j+1}}}{\frac{1}{n-1}\sum_{i=1}^{n-1} R_{s_{i,j+1}}} \qquad \text{Equation 1.25}$$

This criterion equals zero due to the appearance of co-elution and one is the “perfect optimal condition” when all peaks are evenly resolved in a chromatogram[75]. For example, the r value for this separation (Figure 1.5) is 1.1×10^{-9}. This small value of r corresponds to the co-elution and uneven space between the peaks. The small value of r indicates that more input is required to optimise this mixture. As this criterion measures the co-elution and evenly spaced distribution for a separation, hence it is useful indicator for most IC separations[75].

Minimum resolution is designed to evaluate the least resolved peak pair in the separation. The equation is given by[5]:

$$R_s = \min_{1 \to n-1} R_s \qquad \text{Equation 1.26}$$

Baseline resolution of 1.5 is typically employed for an optimum search[5]. It does not measure the excessive space between peak pairs in the separation. For example, the minimum resolution for this separation (Figure 1.5) is 1.2 which corresponds to the least resolved peak pair of peaks 1 and 2. It is less than baseline resolution of 1.5 so this represents more input is required for this mixture. However the minimum resolution does not indicate the excessive space observed in the separation. Therefore this criterion function is not as useful as the normalised resolution product.

Other criteria can also be found in the literature[22, 76, 77] and are useful for other purposes. These criteria are applicable when factors other than resolution need to be evaluated, such as observed number of components, maximum allowed retention time, retention times of first and final peaks. These factors are implemented to provide more efficient optimisation for separation. The research interest of this study is to focus on the modelling of retention time and peak width and the criterion functions relying on resolution are found to be providing more information for optimisation. As a result, other existing criteria will not be discussed further here.

Following selection of a suitable criterion function, the quality of each potential chromatogram can be assessed in a systematic or random way until the best chromatogram is found. Full factorial experimental designs are an extremely useful approach for systematic multivariate optimisation. Each parameter (variable) is examined at a number of levels. For instance, to analyse two parameters at 3 levels, an evenly spaced 3 x 3 grid is drawn. Each intersection describes a combination of the two parameters at different levels, a total of 9 (3 × 3) combinations are therefore defined. An illustrative example of a 3-level factorial design for two parameters (initial concentration and gradient slope) is presented in **Figure 1.6** where the dotted points define the potential condition does not meet the criterion, a new condition will be

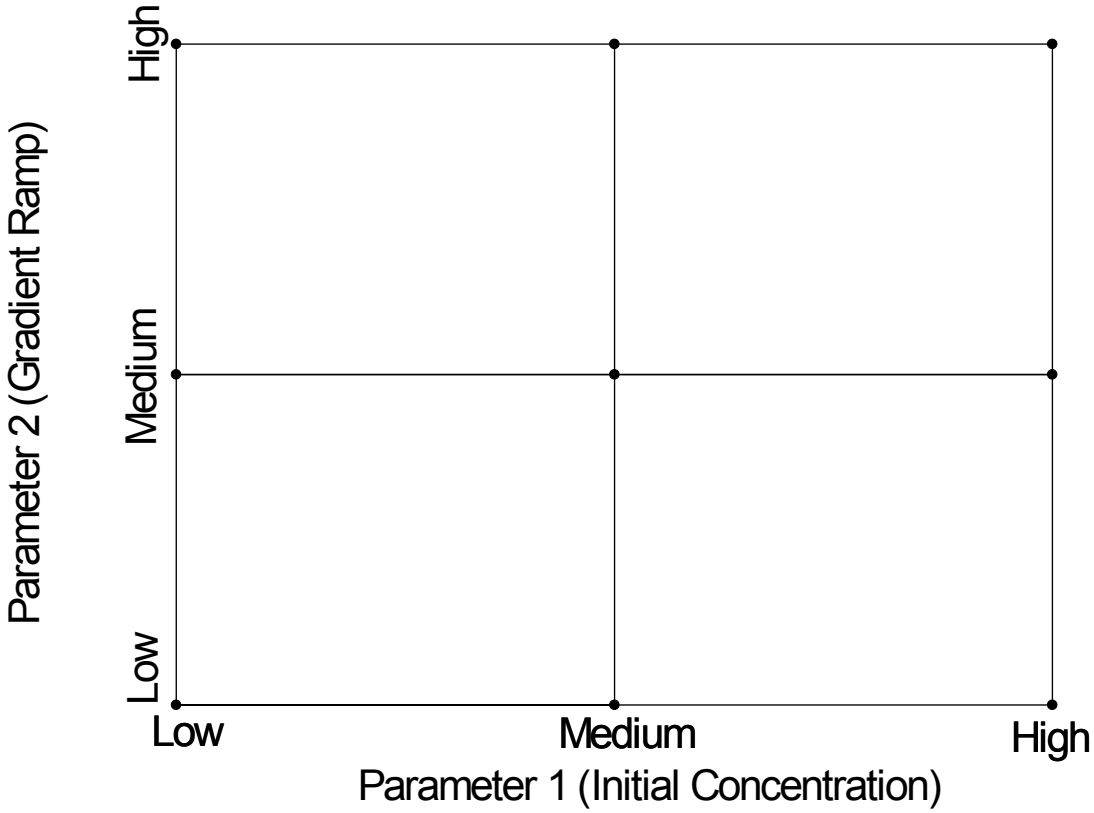

Figure 1.6 A typical example of a 3-level factorial design for two variables

the conditions. The retention time and peak width will then be predicted for all conditions followed by searching for the optimal condition.

It is also possible to employ an iterative tool for the optimum search. Two potential iterative programs, namely Goalseek and Solver, which are both available in Microsoft Excel, can be used for this purpose. Goalseek varies only one parameter sequentially, while Solver can manage multiple parameters simultaneously. After setting the initial conditions and parameters, the retention time and peak width of this input condition will be simulated. If automatically generated and entered into the search system. This process will be repeated until the optimum is found. However, this method has difficulty managing multiple parameters, especially when there are a number of local minima within the defined region. Therefore, different inputs are highly recommended if numerous variables are involved[5]. Overall, this strategy is much more efficient than full factorial design.

Alternatively, computational algorithms such as the Monte Carlo method, which rely on repeated random sampling to compute the results can be employed for optimisation. The Monte Carlo is the most efficient method in the search for a global optimum for multiple variables using a deterministic algorithm. It is often used for simulating physical and mathematical systems by automated repetition of the mathematical system using pseudo-randomly generated numbers as inputs/conditions. The retention time and peak width will be simulated for all potential conditions and the Monte Carlo algorithm will then identify the global optimum. This method requires no set up time however it is not a commonly used approach in IC method development[78].

The prerequisites of *in-silico* optimisation are to select appropriate retention time and peak width models, criterion function and strategy for the optimum search. A package consisting of all these tools is an attractive solution. A number of commercial software packages including DryLab^{TM} [3, 61, 78] and ChromSword^{TM} [78-80] are available for LC optimisation. However, they are not the focus of this review and so will not be discussed further. Of relevance is an IC optimisation tool named Virtual Column Separation Simulator which has been published in the literature and this tool will be reviewed for its strengths and weaknesses.

1.6 Simulation and Optimisation Software

Virtual Column Separation Simulator is marketed by the Dionex Corporation (Sunnyvale, CA, USA) and it is currently the only commercial simulation and optimisation tool for IC method development. It was originally developed in the Australian Centre of Research on Separation Science (ACROSS) in collaboration with the Dionex Corporation[56].

Virtual Column Separation Simulator provides rapid optimisation as well as a simulation for IC separations on two different column diameters (4 mm and 2 mm) where the prediction on 4 mm separations is available for a variety of columns but the software is not widely available on predicting the 2 mm IC columns. It is capable of predicting separations on single (potassium hydroxide for anion analysis and methanesulfonic acid for cation separations) and dual species (carbonate/bicarbonate) eluents. Retention prediction on dual species eluent is only available for isocratic separations whilst simulation of retention on single species eluent is available for isocratic and gradient conditions but its predictive ability is limited to a defined range of initial concentration and gradient slope for gradient separations[57]. It employs a total of three existing models for retention time simulation. The linear solvent strength model (LSSM)[49] discussed earlier is employed for predicting an isocratic condition containing single competing ion, while the prediction for an isocratic condition comprising dual eluent species relies on the linear solvent strength model – empirical approach (LSSM – EA)[56], and the model proposed by Rocklin *et al.*[57] is implemented for predicting gradient separations. Retention prediction of three models relies heavily on the pre-existing data library embedded in the program and it provides the unique characteristics of each analyte inside the column. The data library which stores all the embedded information is capable to provide rapid and accurate prediction for over 150 ion species and 3 different eluents on 20 different columns at 3 different temperatures[7].

There are several important features not found in this software package. For example, the prediction for gradient separation is limited to only three different start concentrations with a defined range of gradient ramps at that flow-rate and temperature. This is because some important parameters

such as flow-rate of the system and initial eluent concentration are not found in the model of Rocklin *et al.* This indicates retention prediction is not feasible for any other flow-rates and starting concentrations. As a result, the Virtual Column Separation Simulator is incapable of simulating any gradient separations outside the defined range (initial concentrations and gradient slopes). In addition, there is no gradient peak width model incorporated in the simulator. All gradient separation is assumed to have the constant theoretical plate count for analyte.

A large range of 4 mm IC column is available for retention prediction in Virtual Column Separation Simulator but the selection of column is very limited for microbore 2 mm IC columns. In addition, there is no prediction available for capillary (0.4 mm) columns which is growing in popularity.

The key limitation of the Virtual Column Separation Simulator is its inability to simulate a complex eluent profile. This method is currently the most widely used approach for separation of problematic samples. This means that the Virtual Column Separation Simulator requires a crucial upgrade.

1.7 Summary

The discussion of all elution modes available in IC suggests that complex elution profiles are currently the most widely employed strategy for trial-and-error optimisation. However, trial-and-error optimisation is losing popularity due largely to time considerations. Computer assisted optimisation is now leading the trend.

Modelling of both retention time and peak width modelling is required for *in-silico* optimisation.

Scope of the Thesis

The overarching objective of this project was to develop new prediction and optimisation abilities for IC.

The first aim was to define the retention time and peak width accuracy thresholds required for predicting a chromatogram accurately. Understanding

the accuracy is important because it permits an informed comparison of the predictive ability of the newly developed models.

The second aim was to devise a real time simulator for complex elution profiles. This simulator was to include both retention time and peak width modelling. This part of the research program involved the incorporation of the existing models as well as formulating new algorithms. The simulators were used to predict the retention times for an extensive set of ions, columns and conditions to validate its applicability.

IC columns exist in different scale of diameters (4 mm, 2 mm and 0.4 mm). The embedded data acquired from a 4 mm separation is not compatible for retention prediction of a 2 mm separation. It is because the changes in column internal diameter represent changes in wall effects, phase ratios and total ion-exchange capacities. A method was therefore required to calibrate the embedded retention data to account for the change in phase ratio, ion-exchange capacity and column differences in miniaturised systems.

Chapter 2

Experimental

2.1 Instrumentation

The research detailed herein was performed using three different Dionex ion chromatographs, (Dionex Corporation, Sunnyvale, CA, USA) that were configured according to the specifications listed in **Table 2.1**. Each IC instrument utilised a configuration established according to the user manual for the instrument. Data acquisition was performed using Chromeleon™ version 6.80 software.

Table 2.1 Details of three ion chromatograph configurations

Model Number	Gradient Pump (GP)	Eluent Generation Module (EGM)	Thermal Compartment	Conductivity Detector (CD)	Auto-sampler (AS)
DX600	GP50	EG40	AS50	CD25A	AS50
ICS3000	ICS3000 Dual GP	ICS3000 EGM	ICS3000 detector/chromatography module		AS
ICS5000	ICS5000 Dual GP	ICS5000 EGM	ICS5000 detector/chromatography module		AS

2.2 Reagents

All reagents used in this project are listed in **Table 2.2**.

Table 2.2 List of Chemicals

Chemical Name	Grade	Supplier
Sodium Acetate	AR	May & Baker (Dagenham, England)
Sodium Bromide	LR	BDH (Kilsyth, VIC, Australia)
Potassium Chloride	AR	Ajax (Sydney, Australia)
Sodium Fluoride	AR	Prolabo (Paris, France)
Sodium Formate	AR	Ajax (Sydney, Australia)
Sodium Iodide	GPR	Aldrich (St. Louis, MO, USA)
Sodium Nitrite	UNK	Ajax (Sydney, Australia)
Potassium Nitrate	AR	Griffin (Loughborough, Leistershire, UK)

Table 2.2 continues

Chemical Name	Grade	Supplier
Sodium Oxalate	UNK	Mallinckrodt (Hazelwood, MO, USA)
Sodium Phosphate	AR	Fluka (Buchs, Switzerland)
Potassium Hydrogen Phthalate	AR	Ajax (Sydney, Australia)
Sodium Sulfate	AR	Prolabo (Paris, France)
Sodium Thiocyanate	GPR	Aldrich (St. Louis, MO, USA)
Sodium Thiosulfate	AR	BDH (Kilsyth, VIC, Australia)
Sodium Tungstate	AR	BDH (Kilsyth, VIC, Australia)
Sodium Molybdate	AR	Ajax (Sydney, Australia)
Sodium Perchlorate	LR	Ajax (Sydney, Australia)
Sodium Pyruvate	LR	Sigma (St. Louis, MO, USA)
Sodium Methacrylate	LR	Aldrich (St. Louis, MO, USA)
Sodium Benzoate	AR	Aldrich (St. Louis, MO, USA)
Sodium Chlorite	80%	Aldrich (St. Louis, MO, USA)
Sodium Chlorate	LR	BDH (Kilsyth, VIC, Australia)
Potassium Bromate	GPR	Hopkins & Williams (Essex, England)
Sodium Carbonate	AR	Ajax (Sydney, Australia)
Sodium Methanesulfonate	AR	Aldrich (St. Louis, MO, USA)
Sodium Chromate	AR	Aldrich (St. Louis, MO, USA)
Sodium Propionate	AR	Aldrich (St. Louis, MO, USA)
Potassium Hydroxide	AR	Dionex (Sunnyvale, CA, USA)
Methanesulfonic Acid	AR	Dionex (Sunnyvale, CA, USA)
Ammonium Nitrate	AR	Univar (Sydney, Australia)
Barium Chloride	LR	Ajax (Sydney, Australia)
Calcium Chloride	LR	Ajax (Sydney, Australia)
Cesium Nitrate	LR	Hopkins & Williams (Essex, England)
Lithium Chloride	LR	Ajax (Sydney, Australia)
Rubidium Chloride	LR	KOCH (Houston, TX, USA)
Methylammonium Chloride	LR	Sigma (St. Louis, MO, USA)
Ethylammonium Chloride	LR	BDH (Kilsyth, VIC, Australia)

2.3 Preparation of Standard Solutions

Standard solutions were prepared by weighing the appropriate amount of the salts listed in Table 2.2 and transferring these to a 200.00 mL volumetric flask and diluting with Milli-Q water (Millipore, MA, USA, 25 ^{o}C, 18.2 MΩ,). Stock solutions were made up to a concentration of 1000 mg/L of the respective ion. Working standard solutions were prepared by diluting the stock solutions with Milli-Q water to concentrations in the range 5 - 30 mg/L. Various mixtures of analytes were prepared based upon their retention times, separation conditions, columns and temperatures chosen.

2.4 Properties of IonPac Columns

There were eight stationary phases (SP) selected for this study, including five anion-exchange SP columns and three cation-exchange SP columns. Full details of the column properties are listed in **Table 2.3**.

Table 2.3 Properties of IonPac Exchange Columns Used for Suppressed IC

Exchange Column	Column Length (mm)	Column Diameter (mm)	Particle Diameter (μm)	Column Capacity (μequiv)	Hydrophobicity
AS11 HC	250	4	9	290	Medium-Low
AS16	250	4	9	170	Ultra-Low
AS19	250	4	7.5	240	Low
AS19	250	2	7.5	60	Low
AS19	250	0.4	7.5	2.4	Low
CS12A	250	4	8	2800	Medium-Low
CS16	250	5	5.5	8400	Medium
CS16	250	3	5.5	3000	Medium

All columns were equilibrated overnight by flushing with the starting eluent concentration. Detection was achieved using conductivity detection after suppression of the eluent using a self-regenerating micromembrane suppressor (SRS ULTRA-II or SRS300, Dionex Corporation, Sunnyvale, CA, USA).

2.5 General Chromatographic Conditions

The general conditions used for anionic analysis in the study were:

Analytical Columns: AS11 HC, AS16 and AS19

Guard Columns: AG11HC, AG16 and AG19

Eluent Concentration: will be discussed in subsequent chapters

Eluent Source: Eluent Generator Cartridge (EGC) II Potassium Hydroxide (KOH) with a Continuously Regenerated Anion Trap Column (CR-ATC)

Temperature: 30 ^{o}C

The general conditions used for cationic analysis in the study were:

Analytical Columns: CS12A and CS16

Guard Columns: CG12A and CG16

Eluent Concentration: will be discussed in corresponding chapters

Eluent Source: EGC II Methanesulfonic Acid (MSA) with a Continuously Regenerated Cation Trap Column (CR-CTC)

Temperature: 40 ^{o}C

Flow-rates, injection loop sizes and types of suppression used for all analyses are summarised in **Table 2.4**.

Table 2.4 List of operating parameters where ASRS: Anion Self-Regenerating Suppressor operated in AutoSuppresion recycle mode, ACES: Anion Capillary Electrolytic Suppressor, CSRS: Cation Self-Regenerating Suppressor operated in AutoSuppresion recycle mode

Column Diameter (mm)	Flow-rate (mL/min)	Injection Loop Size (µL)	Suppression
4.0	1.00	25.0	ASRS 4mm
2.0	0.25	10.0	ASRS 2mm
0.40	0.01	0.40	ACES
5.0	1.00	25.0	CSRS 4mm
3.0	0.36	10.0	CSRS 2mm

2.6 Random Number Generation for Retention Time Error Threshold Analysis

The random number generation for predictive retention time error threshold analysis was performed as follows:

Step 1: A matrix consisting of numbers centred at 0 with a standard deviation of 0.75 of its reported average error (x%) was generated using a normal distribution in Microsoft Excel. For example, random number generation for an average error of x% required the inputs of mean (0%) and standard deviation (0.75x %)

Step 2: Each reading in the matrix generated from the random number generator was then randomly allocated a positive/negative sign using the function of RAND() > 0.5 in Microsoft Excel, followed by incorporating the reported average error (x%). **Table 2.5** shows an example of two sets of target average and maximum errors, the inputs for steps 1 and 2 required to generate the matrix for each set of target average and maximum errors and the outputs obtained from the generated matrix

This sequence was employed for the random number generation detailed in Chapter 3.2.

Table 2.5 An example of two sets of target average and maximum errors for retention time prediction, inputs for steps 1 and 2 required generating the matrix for each set of target average and maximum errors and the outputs of average and maximum errors obtained from the matrix

Target		Input			Output	
		Step 1				
Average Error (%)	Maximum Error (%)	Mean	Standard Deviation	**Step 2**	Average Error (%)	Maximum Error (%)
0.01	0.04	0	0.0075	0.01	0.0109	0.0388
x_{target}	y_{target}	0	0.75x	x	x_{output}	y_{output}
10.0	40.0	0	7.5	10.0	10.83	38.06

2.7 Random Number Generation for Peak Width Error Threshold Analysis

The random number generation for predictive peak width error threshold analysis was performed as follows. A matrix consisting of numbers centred at the reported average error with a standard deviation of 0.75 of its reported average error was generated using the Random Number Generator in Microsoft Excel. For example, random number generation for an average error of x% required the inputs of mean and standard deviation (0.75x %). **Table 2.6** shows an example of two sets of target average and maximum errors, the inputs required to generate the matrix for each set of desired average and maximum errors and the outputs obtained from the generated matrix.

Table 2.6 An example of two sets of target average and maximum errors peak width prediction, inputs for steps 1 and 2 required generating the matrix for each target average and maximum errors and the outputs of average and maximum errors obtained from the matrix

Target		Input		Output	
Average Error (%)	Maximum Error (%)	Mean	Standard Deviation	Average Error (%)	Maximum Error (%)
0.01	0.04	0.01	0.0075	0.0101	0.0415
x_{target}	y_{target}	x	0.75x	x_{output}	y_{output}
50.0	200.0	50.0	37.5	50.12	201.17

This sequence was employed for random number generation in Chapter 3.3.

Chapter 3

Error Thresholds for Accurate Modelling of Retention Time and Peak Width

3.1 Introduction

A quality separation requires an appropriate elution method to accomplish the separation in the shortest time frame. Development of a suitable method for a separation however often requires a large investment in time. This indicates that method development involves a large operating cost to the organisation. The operating costs include staff salary, consumables, chemicals and water usage, waste disposal, etc. Computer-assisted optimisation hence becomes an attractive solution to reduce these costs.

Resolution is a universal indicator for a separation and so it is commonly utilised as a crucial tool for assessing the quality of a chromatogram generated either experimentally or via computer-assisted optimisation. The definition of a quality separation is usually to accomplish a baseline resolution for all adjacent peaks in the shortest time. As a result, it is essential to predict the overall resolution as accurately as possible.

A range of hard and soft models [8, 9, 27, 56-58, 81] for retention time and peak width prediction are described in the literature. All the existing models deliver different predictive abilities and therefore carry different potential prediction errors. However, several crucial points are yet to be discussed in the literature. First, what are the maximum tolerances on errors associated with predicted retention time and peak width that permit an accurate reflection of a real chromatogram of a complex mixture? Second, are these existing models able to predict a satisfactory chromatogram? Therefore, a series of random number generations were employed to produce the error-imposed chromatograms followed by comparing the generated chromatograms with the experimental separation to understand the impact of the predictive error. The objective of this study was to quantify the accuracy required for retention time and peak width modelling in order to accomplish an acceptable *in-silico* optimisation.

3.2 Evaluation of Retention Time Error Threshold

Fifteen test chromatograms comprising isocratic, gradient and multi-step complex eluent profiles were compiled for this statistical analysis. In order for the retention time and peak width data to be realistic examples, all chromatograms were randomly selected from AS11 HC, AS16, AS19, CS12A and CS16 Dionex user manuals[7]. Each chromatogram consisted of between 6 and 20 analytes with differing retention and total separation times. A detailed summary of all chromatograms is shown in **Table 3.1.**

This study proceeded by first selecting an average error limit for retention time. Average errors were in the range of 0.01 to 10.0%. For each specified average error (using 0.01% increments in the range of 0.01 to 10.0%), retention times for each peak in the chromatogram were simultaneously varied (using both positive and negative deviations), up to the average error limit. The retention time for each peak was randomly varied 200 times, so that for a chromatogram with 20 components (for example, **Figure 3.1**), 200 of error-imposed 20-component chromatograms could be generated at each specified average error. Each specified retention average error typically has minimum and maximum errors. The minimum error is very close to 0 whilst maximum error could be up to 10 times the average error. These maximum errors could be problematic for *in-silico* optimisation. For example, if the simulated separation for retention times incurs an average error of 1.0%, the prediction would be considered as highly accurate. However, if one retention time prediction has an error of 10% and this causes a change of elution order for a pair of peaks, this would lead to poor prediction for the entire separation despite the retention average error being only 1%. Therefore, it is crucial to evaluate both the average error as well as the maximum error for retention time. A plot of maximum errors *versus* average errors of retention time is illustrated in **Figure 3.2**. All retention time error data were based on the difference between observation and simulation of each condition, obtained from Chapters 4, 5 and 6. From Figure 3.2, the average of $\frac{|\text{maximum error observed}|}{|\text{average error observed}|}$ for retention time was calculated

Table 3.1 Important details of 15 chromatograms including type of analysis, analytical column, type of eluent, column diameter, flow-rate, temperature, number of components, elution mode and separation time

Chromatogram	Analysis	Column	Eluent	Column Diameter (mm)	Flow-rate (mL/min)	Temperature (^{o}C)	Number of Components	Elution Mode	Separation Time (min)
1	Anionic	AS19	KOH	4	1.0	30	20	Gradient	30
2	Anionic	AS19	KOH	4	1.0	30	11	Complex	30
3	Cationic	CS16	MSA	3	0.36	40	6	Isocratic	20
4	Cationic	CS16	MSA	5	1.0	40	6	Isocratic	10
5	Anionic	AS16	KOH	4	1.0	30	7	Isocratic	20
6	Anionic	AS16	KOH	4	1.5	30	9	Complex	10
7	Cationic	CS16	MSA	3	0.5	60	12	Complex	30
8	Cationic	CS16	MSA	3	0.43	40	8	Complex	35
9	Cationic	CS16	MSA	3	0.5	60	9	Complex	30
10	Anionic	AS19	KOH	4	1.0	30	11	Complex	20
11	Cationic	CS16	MSA	5	1.0	40	9	Complex	20
12	Anionic	AS11 HC	KOH	4	1.0	30	8	Gradient	25
13	Anionic	AS11 HC	KOH	4	1.0	30	9	Gradient	25
14	Anionic	AS16	KOH	4	1.0	30	9	Gradient	20
15	Anionic	AS11 HC	KOH	2	0.38	30	7	Isocratic	10

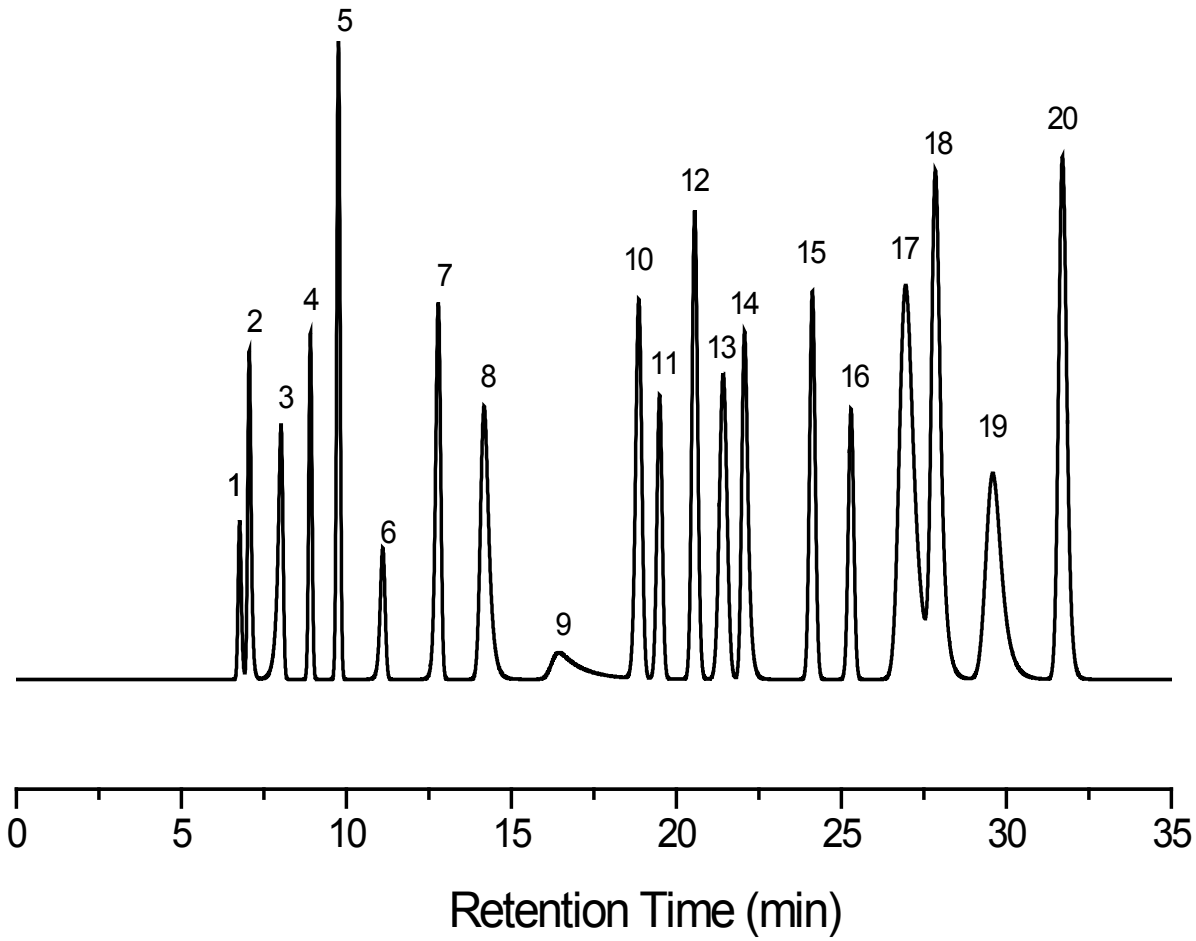

Figure 3.1 An AS19 test chromatogram consisting of 20 components in the elution order of 1-quintate, 2-lactate, 3-pyruvate, 4-bromate, 5-chloride, 6-trifluoroacetate, 7-bromide, 8-azide, 9-octanesulfonate, 10-phthalate, 11-tungstate, 12-chromate, 13-iodide, 14-arsenate, 15-citrate, 16-cis-aconitrate, 17-thiocyanate, 18-tran-aconitrate, 19-perchlorate, 20-trimetaphosphate where details of the separation can be found on chromatogram 1 in Table 3.1.

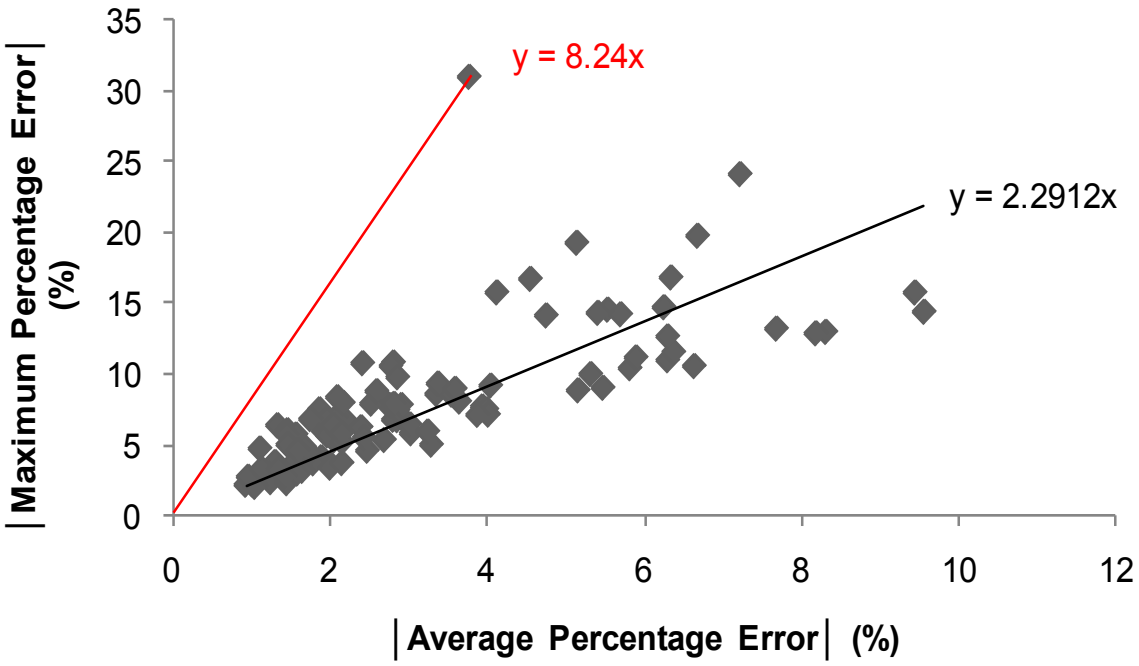

Figure 3.2 Maximum percentage errors against average absolute percentage errors for 24 anions and 13 cations on AS11 HC, AS16, AS19, CS12A and CS16 columns over 5 linear and 4 5-step gradient conditions

using a line of best fit and was found to be 2.29. In Figure 3.2, the largest value (8.24) of $\frac{|\text{maximum error observed}|}{|\text{average error observed}|}$ was manually found based on the retention predictive error data from Chapters 4, 5 and 6 and this value (8.24) was defined as the maximum of $\frac{|\text{maximum error observed}|}{|\text{average error observed}|}$. These two values (2.29 and 8.24) have a strong connection to the standard deviation in the random number generation process. The magnitude of the standard deviation has a direct correlation to the average and maximum of $\frac{|\text{maximum error observed}|}{|\text{average error observed}|}$. After manually adjusting the input (standard deviation) and monitoring the output (so that average and maximum of $\frac{|\text{maximum error observed}|}{|\text{average error observed}|}$ for retention time equate 2.29 and 8.24) iteratively, standard deviation was determined to be 0.75 of its reported average error. For example, random number generation for 5% retention average error requires setting the standard deviation to be 3.75%. All retention errors were generated using the Random Number Generation in Microsoft Excel described in Chapter 2.6.

Each of 200 generated chromatograms (Figure 3.1) was analysed in the following sequence. Resolution of each adjacent pair in the chromatogram was calculated. There are 20 peaks in each chromatogram so 19 adjacent pairs are present. The resolutions of these 19 peak pairs were then assessed by three criterion functions, namely product of resolution (Equation 1.24), normalised product of resolution (Equation 1.25) and minimum resolution (Equation 1.26). Each of the chromatograms has one response value for each criterion function. A total of 200 chromatograms therefore yields 200 responses for each criterion function at each specified average error. The mean, $\overline{X}$, and standard deviation, σ, for each set of criterion function responses at the specified average error were therefore calculated. A Students t-test was then employed to distinguish if each generated chromatograms at the specified average error were significantly different from the starting chromatogram. (i.e. a condition with the specified

average error where the predicted chromatograms do not accurately reflect the observed chromatogram). The value of Student's t, t, is given by[21]:

$$t = \frac{|\bar{x} - \mu|}{\sigma} \sqrt{n} \qquad \text{Equation 3.1}$$

where μ is the response of the criterion function for the observed chromatogram, $\bar{x}$ is the average response of the criterion function, as determined above (from 0.01 to 10.0%), σ is the standard deviation of the response of the criterion function (as determined above) and n is the number of randomly generated chromatograms (n = 200).

At each specified average error, the evaluation involves 200 chromatograms so it has 199 degrees of freedom. 200 chromatograms were statistically evaluated as follows. The null hypothesis states that the two means (response of the criterion function for the observed chromatogram and the average response of the criterion function for 200 chromatograms) are significantly different if the t-value of the criterion function at the average error is greater than 1.96[21]. Therefore, if the t-value of 200 generated chromatograms at the specified average error is below 1.96, they are deemed to accurately reflect the original chromatogram.

This full sequence was carried out over a range of 0.01% to 10.0% average error using 0.01% increments. Once all the t-values at each average error ranging from 0.01 to 10.0% for each criterion were generated, the maximum average error tolerance for retention time based on the criterion was identified as follows. There were a number of t-values at different average errors for each criterion function below 1.96. The asterisked t-value corresponds to the largest average error found with the t-value being less than 1.96, and is therefore the maximum acceptable error for accurately predicting the retention times of this chromatogram.

As the increment of this retention average error analysis is very small, only the t-values within the critical region using the corresponding criterion functions for the chromatogram (Figure 3.1) were tabulated in **Table 3.2**.

Table 3.2 t-test values from 0.07 to 0.10% with 0.01% increment for three criterion functions ($\prod R_s$, r, and min R_s) where asterisked t-values correspond to the maximum error tolerances for this 20-component chromatogram with respect to the criterion functions

Criterion Function \ % error	0.07	0.08	0.09	0.10
$\prod R_s$	0.598	1.40*	2.21	2.63
R	0.698	1.88*	2.58	2.84
min R_s	0.0442	0.989	1.66*	2.49

In Table 3.2, each asterisked value corresponds to the maximum retention average error tolerance for the criterion function. It was found that the maximum average error tolerances for retention time were 0.09%, 0.08% and 0.08% for min R_s, $\prod R_s$ and r respectively. An average of 0.08% was found for retention time based on three criteria.

Likewise, the sequence was extended to determine the retention error threshold for the other chromatograms. The summary of retention average errors required for all 15 chromatograms is shown in **Table 3.3**. It is important to note that the total separation time window, the resolution of the critical adjacent pair, complexity and the numbers of components in a chromatogram usually all play a role in this error threshold evaluation. From Table 3.3, the *ultimate* average percentage error threshold of retention time was determined to be 0.7%.

3.3 Evaluation of Peak Width Error Threshold

The peak width threshold evaluation was also based on the 15 test chromatograms. Peak width is more difficult in terms of simulation as it involves both broadening and compression processes (see Chapter 1.4) and the average percentage error observed for peak width simulations is therefore considerably larger than for retention times. Based on the observations from Chapters 4 and 5, peak width predictions display systematic errors which are either positive (broader peaks predicted) or negative (narrower peaks predicted). In this section, a peak width error

Table 3.3 List of maximum error tolerances for retention time based on three criterion functions (ΠR_s, r, and min R_s) with respect to the 15 chromatograms consisting of different number of peaks, complexity/saturation and min R_s The *ultimate* average maximum tolerances of 15 chromatograms is shown in the last row.

Chromatogram	Number of Peaks	Complexity /Saturation	min R_s	Average Maximum Error Tolerance (%)
1	20	0.27	1.67	0.08
2	11	0.20	1.46	0.67
3	6	0.28	3.01	0.97
4	6	0.44	1.83	0.77
5	7	0.22	2.24	1.60
6	9	0.39	0.89	0.40
7	12	0.37	1.71	0.13
8	8	0.25	1.14	0.77
9	9	0.26	0.27	0.90
10	11	0.28	1.27	0.10
11	9	0.28	1.97	0.53
12	8	0.13	1.72	0.90
13	9	0.13	2.00	0.77
14	9	0.17	5.15	0.27
15	7	0.34	1.02	1.67
Ultimate Average Error				0.70

threshold will therefore be evaluated in terms of systematic positive and negative errors. Selecting an average error limit for peak width was in the range of 0.01 to 50.0%. Again, average and maximum errors of peak width are crucial in this evaluation. The maximum errors were compared with the average errors and are shown in **Figure 3.3**. All the peak width error data were based on the difference between observation and simulation of each condition, obtained from Chapters 4 and 5. In Figure 3.3, the average and maximum of $\frac{|\text{maximum error observed}|}{|\text{average error observed}|}$ of peak width were determined to be 3.13 and 5.32 using the same method as discussed in the previous section. The standard deviation was again determined to be 0.75 of its

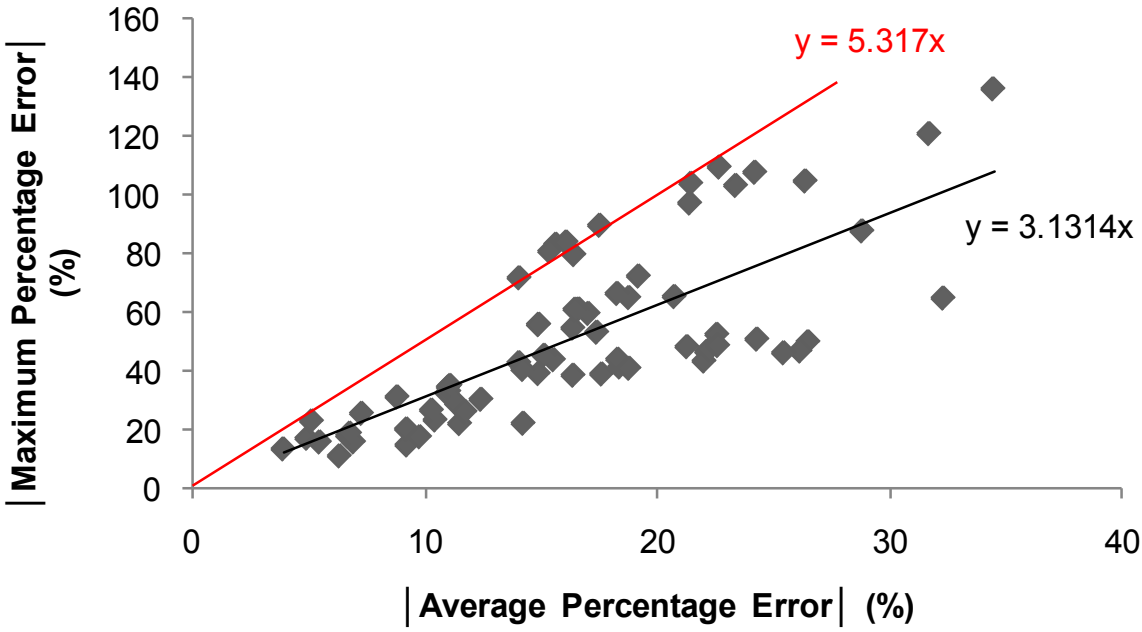

Figure 3.3 Maximum percentage errors against average absolute percentage errors for 24 anions and 13 cations on AS11 HC, AS16, AS19, CS12A and CS16 columns over 5 linear and 4 5-step gradient conditions

reported average error using a trial-and-error approach. All the errors were again generated using the Random Number Generation in Microsoft Excel described in Chapter 2.7.

The peak width of each peak in a chromatogram was again varied 200 times for each specified average error. So a total of 200 error-imposed chromatograms were generated at each specified average error. Resolution of each peak pair in each generated chromatogram was then calculated. All peak pairs in each chromatogram were again assessed by three criterion functions. 200 generated chromatograms gave rise to a set of mean and standard deviation for each criterion function response. Therefore a total of three means and standard deviations were obtained for corresponding criterion functions at each specified average peak width error analysis. The Students t-test was again employed to distinguish if the generated chromatograms at each specified average error were significantly different from the starting chromatogram.

For instance, to search for the peak width error threshold based on systematic negative error format of the 20-component chromatogram illustrated in Figure 3.2, the sequence was implemented followed by using the Students t-test to differentiate if the generated chromatograms have any significant difference from the starting chromatogram. This sequence was repeated in the same manner as discussed in Section 3.2 over a range of 0.01% to 50.0% in 0.01% increments. The maximum peak width average error tolerance for each criterion was identified based on the t-value where the t-value was below 1.96 and associated with the highest permissible average error. The t-test values of three criterion functions between 0.05 to 20% with differing increment levels are shown in **Table 3.4**.

A similar pattern is expected for t-test values of three criterion functions as indicated in the previous section. From Table 3.4, the three criterion functions exhibit totally different t-test values with only normalised resolution, r, giving rise to values below 1.96. Two criterion functions ($\prod R_s$ and min R_s) indicate that a minor difference compared to actual peak width is statistically significant, even at 0.05% error. However, it was observed that all three criterion functions show a pattern where t-test values of each criterion

Table 3.4 t-test values from 0.05 to 20% with differing increment based on three criterion functions (ΠR_s, r, and min R_s) for this 20-component chromatogram (Figure 3.1)

Criterion Function \ % error	0.05	0.1	1	5	10	20
ΠR_s	70.3	84.4	69.1	57.9	32.6	23.4
r	0.513	1.30	0.508	1.42	1.83	6.61
min R_s	24.4	25.4	25.0	23.5	24.7	25.1

are similar for peak width average errors from 0.05% to 20.0%. Thus the threshold error remains unspecified. In conclusion none of the criterion functions provide a suitable metric for determination of the peak width error threshold. Further consideration is discussed in Section 3.4.

This evaluation was repeated using systematic negative error for the other chromatograms. Identical findings were observed where the t-test values for the three criterion functions were inconsistent as well as the t-test values at different percentage errors for each respective criterion function showing little change as the error was varied. This analysis was further extended to systematic positive error and the same observations were found. In conclusion, the use of three criterion functions for retention time successfully determined the error threshold to be 0.7%, but these functions were unsuitable when applied to peak width. Further investigation was therefore needed.

3.4 Further Investigation

As shown above, high accuracy is required for retention time prediction whilst the error threshold for peak width remains ambiguous. To better understand the requirements for width prediction, further investigation using 2 two-component separations was attempted. Here the peak pair of the first separation had short retention times and narrow peak widths while the peak pair of the second separation had long retention times and broader peak

widths. First and final peaks of typical IC separations have retention times of around 4 min and 30 min, respectively, so these two separations will be evaluated using this information.

The first hypothetical separation consisted of two peaks (R_s = 2.0) where the first peak (A) is defined by t_R = 4.0 min and base width = 0.2 min. The second peak (B) is defined by t_R = 4.4 min and base width = 0.2 min (**Figure 3.4**(a)). Based on this peak pair, the influence of predictive error of retention time and peak width will be emphasised independently.

Suppose the peak widths are free of predictive error (Figure 3.4(a)). If peak A at 4.0 min now has a predicted retention time error of 2.5%, this would move peak A to 4.1 min and give rise to a resolution of 1.5. (Figure 3.4(b)).

Now suppose the retention times are free of predictive error. For the same resolution of 1.5, the average simulated width of this peak pair is given by:

$$R_s = \frac{t_{R1} - t_{R2}}{\frac{w_1 + w_2}{2}}$$

$$1.5 = \frac{4.4 - 4.0}{\frac{w_1 + w_2}{2}}$$

$$w_{ave} = 0.27 \text{min}$$

That is, peaks A and B would need to have a predicted width of 0.27 min as illustrated in Figure 3.4(c). This equates to 35.0% difference between predicted and actual peak widths, indicating that the peak width error threshold is substantially more forgiving than that for retention time.

An additional hypothetical separation was investigated in the same manner. This separation consisted of two peaks (R_s = 2.0), where the first peak (A) is defined by t_R = 30.0 min and base width = 0.7 min. The second peak (B) is defined by t_R = 31.4 min and base width = 0.7 min (**Figure 3.5**(a)).

It was found that 3.5% movement of peak A at 30.0 min towards peak B stationed at 31.4 min will result in a resolution of 1.5, as shown in

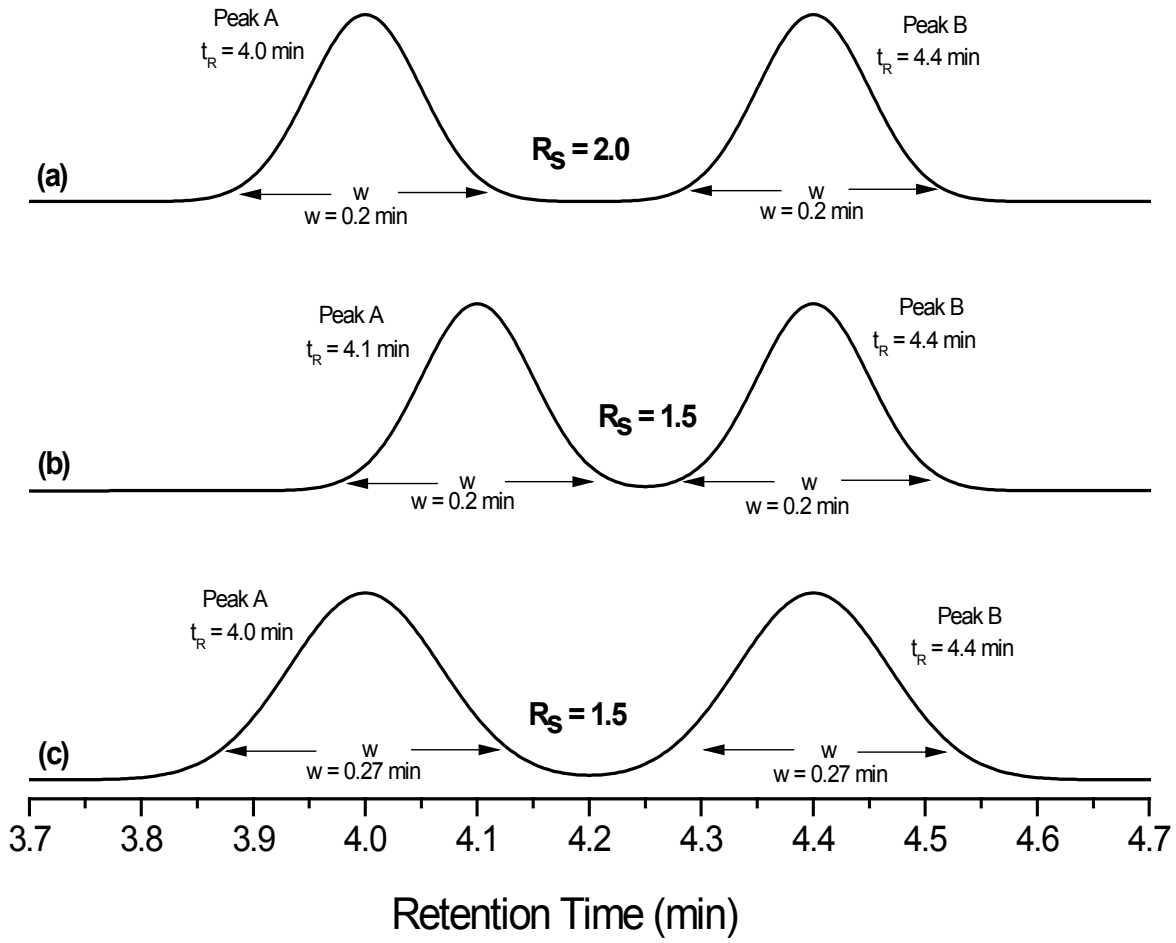

Figure 3.4 A two-component separation where (a) the first peak is noted at 4.0 min with a base width of 0.2 min and the second peak is detected at 4.4 min with a base width of 0.2 min, (b) the first peak is noted at 4.1 min with a base width of 0.2 min and the second peak is detected at 4.4 min with a base width of 0.2 min, (c) the first peak is noted at 4.0 min with a base width of 0.27 min and the second peak is detected at 4.4 min with a base width of 0.27 min

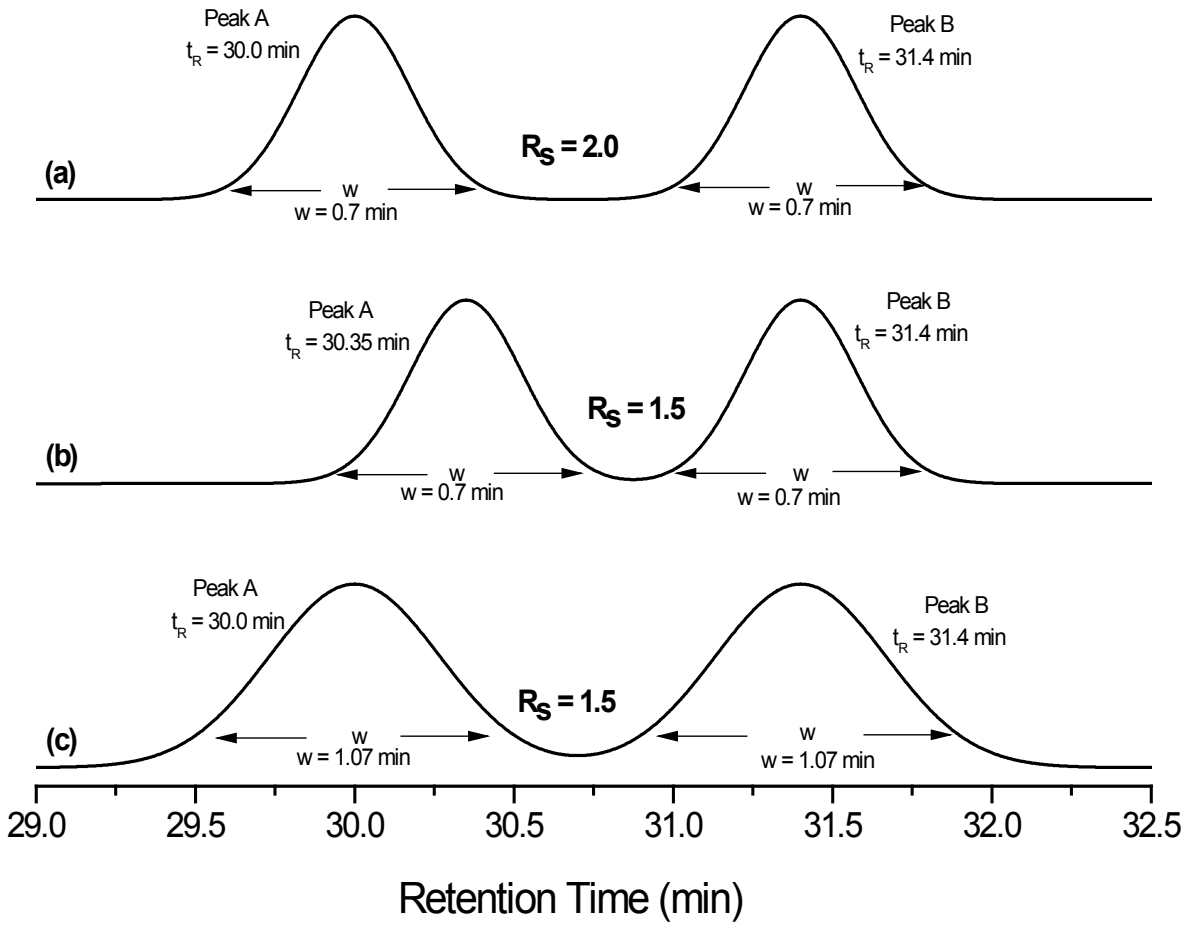

Figure 3.5 A two-component separation where (a) the first peak is noted at 30.0 min with a base width of 0.7 min and the second peak is detected at 31.4 min with a base width of 0.7 min, (b) the first peak is noted at 30.35 min with a base width of 0.7 min and the second peak is detected at 31.4 min with a base width of 0.7 min, (c) the first peak is noted at 30.0 min with a base width of 1.07 min and the second peak is detected at 31.4 min with a base width of 1.07 min

Figure 3.5(b). The same reduction of resolution caused by peak width would require an error of 52.9%. (Figure 3.5(c))

In summary, both separations illustrate that retention time prediction has an enormous influence (i.e. an error of 2.5% is permissible for a 30-min separation window) on *in-silico* optimisation, whereas peak width is relatively unimportant (a percentage error of 35.0% is manageable for a 30-min separation window). Based on the thresholds found for retention time and peak width, it is obvious that accuracy of prediction of retention time is at least 10 times more important than for peak width.

3.5 Chapter Conclusions

A set of 15 test chromatograms was selected to investigate error thresholds in retention time and peak width simulation. These chromatograms consisted of isocratic, gradient and complex elution conditions containing between 6 and 20 analytes with a separation time between 10 and 35 minutes. Random number generation was employed to create the matrix needed for the investigation. Students t-tests were used throughout this study to search for the error thresholds required for retention times and peak widths. This statistical method determined the error threshold for the retention time to be 0.7% while the maximum error tolerance for peak width remained unclear using this approach. Therefore this approach was abandoned. Further investigation was undertaken based on 2 two-component separations where the first separation displayed short retention times and narrow peak widths while the second displayed a peak pair of long retention times and broader peak widths. It is apparent that the error threshold for peak width may be of the order of 10 times the error threshold for retention time where error thresholds of retention time and peak width were determined to be 2.5% and 35.0%, respectively, based on a 30-min separation window. These error thresholds for retention time (2.5%) and peak width (35.0%) were used as the targets required for an accurate retention time and peak width modelling in Chapters 4 and 5.

Chapter 4

Prediction of Analyte Retention for the Elution Profiles Comprising Multiple Isocratic and Gradient Steps

4.1 Introduction

Gradient elution is now the preferred separation mode in IC for several reasons[5]. Some of these reasons are generic in nature in that they are applicable to most forms of liquid chromatography, while other reasons are unique to IC. The prime generic reason is the enhanced peak capacity obtainable in gradient elution, which leads to the ability to separate complex mixtures containing analytes having diverse ion-exchange selectivity coefficients. Under isocratic elution conditions, such samples will often exhibit poor separation of weakly retained analytes and excessively long separation times for strongly retained analytes[61].

In IC there are two further major advantages to the use of gradient elution, which are unique to this form of chromatography. The first is the routine use of electrolytic eluent generators in which water used as mobile phase feed is converted via an electrolysis step into the desired eluent[7]. Moreover, complex elution profiles comprising multiple isocratic and gradient steps performed sequentially can also be generated easily. Gradient elution and complex elution profiles are therefore employed widely in IC. The second unique reason why gradients are commonplace in IC is the routine use of a suppressor which converts the eluent back to water prior to the detection step which typically employs conductivity. This greatly simplifies detection by eliminating the unstable baselines that often result from gradient elution in other forms of liquid chromatography.

Together, these generic and unique advantages provide powerful incentives to employ gradient elution in IC and to also utilise complex elution profiles to fine-tune a separation. However, the routine use of complex eluent profiles makes the task of selection of the optimal elution conditions much

more difficult. For this reason, there is intense interest in the development of tools that enable reliable simulation and optimisation of IC separations that use combinations of isocratic and gradient steps.

The aim of this chapter was to devise an efficient simulator for IC separations consisting of various isocratic and/or gradient steps. It is important to note that the research in this chapter is a continuation and extension of preceding research. Major data acquisition for the isocratic and gradient data library in this present study has been completed prior to the start of this study. The range of anionic and cationic analytes and columns used of isocratic retention data was previously collected according to the experimental design described in this reference[56]. The analytes and conditions are summarised in **Table 4.1**. Retention data for linear gradients (starting from time zero) were then obtained for the same set of analytes and columns. Each analyte has a total of 9 retention data, consisting of three initial concentrations and each starting concentration has three different gradient ramps. All the isocratic and gradient data were acquired at different times using different instruments and columns from different manufacturing batches. Any comparisons of data made between the isocratic and gradient measurements will therefore include variability between instruments and column batches.

4.2 Prediction of Retention Times in Isocratic Elution

There are a number of retention models found in the literature for isocratic separations. The best model was found to be the linear solvent strength model (LSSM)[47, 48]. The retention factor, k, of an analyte anion in IC under isocratic conditions is described by Equations 1.10 and 1.11[2]:

For a given analyte and a fixed eluent composition and stationary phase, x, y, $K_{A,E}$, Q, w and V_m are constant. Equation 1.11 shows that a plot of log k *versus* log $[E^{y-}]$ is therefore linear for isocratic separations, with the intercept, a, and the slope, b, being determined only by the parameters x, y, $K_{A,E}$, Q, w and V_m. However, these parameters are often difficult to quantify and the retention behaviour of an analyte anion therefore cannot be predicted reliably from theory alone. In practice, a and b are normally

Table 4.1 List of anions, cations, columns and eluents used for isocratic and gradient retention databases used in this study (For gradient retention data, each separation started at the initial concentration listed as follows followed by ramping up to the maximum eluent concentration of 100 mM using the respective gradient slopes)

Anions	Column	Isocratic retention data			Gradient retention data					
		Concentration (mM)			Initial Concentration (mM)			Gradient Ramp (mM/min)		
acetate, acrylate, arsenate, azide, benzenesulfonate, **benzoate, bromate, bromide,** bromoacetate, butanesulfonate, butyrate, **carbonate, chlorate, chloride, chlorite,** chloroacetate, chromate, cis-aconitate, citrate, dibromoacetate, dichloroacetate, difluoroacetate, ethanesulfonate, **fluoride,** fluoroacetate, **formate,** fumarate, glutarate, glycolate, heptanesulfonate, hexafluorophosphate, hexanesulfonate, iodate, **iodide,** iso-citrate, lactate, malate, maleate, malonate, **methacrylate,** methanesulfonate, **molybdate,** monofluorophosphate, n-butyrate, **nitrate, nitrite,** n-valerate, octanesulfonate, **oxalate,** p-chlorobenzenesulfonate, pentanesulfonate, **perchlorate,** perrhenate, **phosphate, phthalate,** propanesulfonate, propionate, pyrophosphate, **pyruvate,** quinate, selenate, selenite, selenocyanate, sorbate, succinate, **sulfate,** sulfite, tartrate, tetrafluoroborate, **thiocyanate, thiosulfate,** trans-aconitate, tribromoacetate, trichloroacetate, trifluoroacetate, trimetaphosphate, tripolyphosphate, **tungstate**	AS4A-SC	2	4	6	-	-	-	-	-	-
	AS9-HC	6	11	20	-	-	-	-	-	-
	AS10	60	80	100	-	-	-	-	-	-
	AS11	-	-	-	0.5	2.0	5.0	0.4	4.0	8.0
	AS11-HC	16	30	45	1	6	12	0.3	1.5	3.0
	AS12A	2	4	6	-	-	-	-	-	-
	AS14	2.5	4.5	6.5	-	-	-	-	-	-
	AS14A	4	9	15	-	-	-	-	-	-
	AS15	-	-	-	2	11	20	0.3	1.5	3.0
	AS16	10	20	35	1	6	12	0.3	3.0	6.0
	AS17	-	-	-	-	-	10.0	0.4	2.5	5.0
	AS18	16	30	42	2	10	18	0.3	1.0	4.0
	AS19	14	25	40	1	9	17	0.4	2.5	4.5
	AS20	20	35	65	2	5	10	0.6	2.0	4.0

Table 4.1 continues

Cations	Column	Isocratic retention data			Gradient retention data					
		Concentration (mM)			Initial Concentration (mM)			Gradient Ramp (mM/min)		
1-amino-2-propanol, 1-dimethylamino-2-propanol, 2-(2-aminoethoxy)ethanol, 2-amino-1-propanol, 3-(dimethylamino)-1,2-propanediol, 3-methoxypropylamine, 5-amino-1-pentanol, aminoethylethanolamine, **ammonium, barium(II), calcium(II)**, **cesium,** cobalt(II), copper(II), diethanolamine, diethylamine, diethylaminoethanol, dimethylamine, dimethylaminoethanol, dipropylamine, ethanolamine, **ethylamine,** ethylaminoethanol, ethylenediamine, hydrazine, iron (II), iso-butylamine, **lithium, magnesium(II), manganese(II), methylamine,** methylaminoethanol, methyldiethanolamine, morpholine, n,n-dimethylethylamine, nickel(II), **potassium,** propylamine, **rubidium, sodium, strontium(II)**, triethanolamine, triethylamine, trimethylamine	CS12A	15	20	40	-	-	-	-	-	-
	CS16	25	40	62	6	15	24	0.4	1.5	4.0

estimated on the basis of experiments in which the retention factor is measured at a limited number of isocratic eluent compositions and the resultant data are fitted to Equation 1.11[2].

4.3 Prediction of Retention Times in Gradient Elution

When an analyte is eluted in IC using a linear gradient ramp starting from the time that the analyte first reaches the separation column, the retention factor observed under gradient conditions k can be described by Equation 1.13[57]. Equation 1.13 can be simplified to:

$$\log k = a - b \log R \qquad \text{Equation 4.1}$$

A plot of log k *versus* log R is therefore linear and can be used to model retention behaviour under gradient conditions. However, it is important to note that a different set of constants will be required for each initial eluent concentration used to start the gradient.

An alternative gradient elution retention model is shown in Equation 1.14. This was proposed by Jandera and Churăček[9] for reversed-phase high performance liquid chromatography and was later applied by Baba *et al.*[60, 82, 83] to ion-exchange chromatography of polyphosphates. The coefficients, a and b, have the same meaning as in Equation 1.11.

Data from the gradient database can be used to solve Equation 4.1 for a and b using three values of k and R (at a given starting concentration) for each eluent/column combination, and the equation can then be applied to prediction of retention factors under different gradient conditions commencing at the same value of start concentration. **Figure 4.1** illustrates the use of Equation 4.1 to predict gradient retention factors using this approach and shows that there is reasonable agreement between the predicted and experimental retention times under the action of a simple linear gradient eluent profile. Equation 4.1 can therefore be used for gradient prediction provided that the void volumes of the chromatographic systems used for data collection and verification are similar. However, it is important to note that at least three gradient experiments need to be performed to provide the necessary input data, and that new values of a_g and b_g need to be derived for

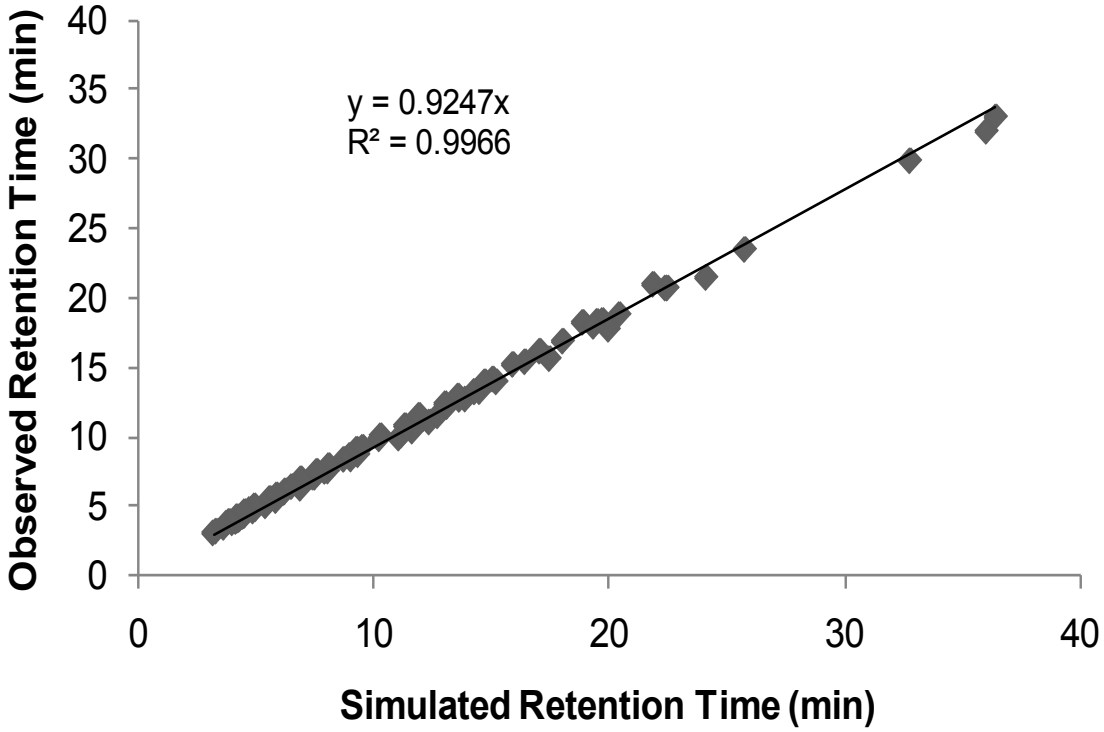

Figure 4.1 Correlation plot showing the use of Equation 4.1 to predict linear gradient retention times using the gradient database for input on the AS11 HC, AS16, AS19 and CS16 columns. The gradient conditions employed were: AS11 HC: KOH 6mM to 60mM in 36 min; AS16: KOH 6mM to 86mM in 20 min; AS19: KOH 9mM to 81mM in 24 min; and CS16: MSA 10mM to 94mM in 24 min

each new value of initial eluent strength. These are major limitations to the use of Equation 4.1 for predictive purposes.

There are two possible approaches to the evaluation of Equation 1.14 as a model for prediction of gradient retention data. In the first approach (designated GDGP, or *gradient data for gradient prediction*), data in the gradient database can be used to calculate values of a and b using a series of gradient separations in which gradient ramp and initial concentration are varied at a constant value of flow-rate. The gradient database contained 9 combinations of gradient ramps and initial concentrations for each analyte/column combination and these were used to solve Equation 1.14 to an acceptable level of accuracy.

The second approach (designated IDGP, or *isocratic data for gradient prediction*) involved determination of a and b from Equation 1.11 using the isocratic database (recognising that these data were obtained on different column batches and instruments) and using these values to predict retention data for a desired combination of gradient slope, start concentration and flow-rate. These two sets of a and b values generated from the GDGP and IDGP approaches were then used to predict retention on new columns under new gradient eluent conditions.

Table 4.2 shows observed retention data for a linear gradient (commencing at time zero) of 6-86 mM hydroxide over 20 min at 30 ^{o}C on an AS19 column; and 15-92 mM MSA at 40 ^{o}C on a CS16 column, together with retention data predicted from Equation 1.14 using the GDGP and IDGP approaches. It can be seen that close agreement between the experimental and predicted retention times was obtained for both GDGP (average error 2.7%) and IDGP (average error 1.4%) methods, with statistical analysis at the 95% confidence interval indicating that there was no significant difference between the two approaches. While both approaches gave satisfactory predictions of gradient retention data, the IDGP approach was preferred because only three experimental conditions were needed to derive a and b (from Equation 1.11), compared to a minimum of six experimental conditions for the GDGP approach (low, intermediate and high initial eluent concentration with two gradient ramps).

Table 4.2 Prediction of retention times using Equation 1.14 applied using the GDGP and IDGP approaches for anions on the AS19 column and for cations on the CS16 column. Conditions for anions: gradient 6 mM to 86 mM KOH in 20 min at 30°C. Conditions for cations: 10mM to 94 mM MSA in 24 min at 40°C

Analyte	Observed t_R (min)	Predicted t_R using GDGP approach		Predicted t_R using IDGP approach (min)	
		t_R (min)	|% Error|	t_R (min)	|% Error|
Anions					
Acetate	4.05	4.07	0.44	3.96	2.28
Bromate	4.90	4.98	1.59	4.81	1.82
Bromide	6.37	6.54	2.72	6.35	0.31
Carbonate	7.91	8.09	2.24	7.73	2.28
Chlorate	6.48	6.67	2.82	6.46	0.33
Chloride	5.08	5.15	1.28	4.98	2.03
Chlorite	4.48	4.55	1.59	4.39	1.95
Fluoride	4.01	3.98	0.71	3.90	2.59
Formate	4.24	4.25	0.30	4.15	2.21
Iodide	10.92	11.47	5.05	11.11	1.75
Molybdate	9.81	9.94	1.30	9.77	0.40
Nitrate	6.39	6.58	2.97	6.36	0.41
Nitrite	5.35	5.43	1.49	5.26	1.64
Oxalate	8.51	8.59	0.94	8.39	1.35
Perchlorate	16.28	17.38	6.78	16.72	2.71
Phosphate	11.02	10.65	3.31	10.95	0.61
Phthalate	10.51	10.45	0.52	10.45	0.52
Sulfate	8.18	8.24	0.70	8.04	1.74
Thiocyanate	14.34	15.23	6.21	14.65	2.17
Thiosulfate	10.38	10.57	1.88	10.37	0.04
Tungstate	9.38	9.49	1.17	9.30	0.82

Table 4.2 continues

Analyte	Observed t_R (min)	Predicted t_R using GDGP approach		Predicted t_R using IDGP approach (min)	
		t_R (min)	|% Error|	t_R (min)	|% Error|
Cations					
Ammonium	10.65	11.01	3.37	10.74	0.85
Barium	21.45	22.70	5.81	22.14	3.20
Calcium	16.45	17.11	3.99	16.58	0.78
Cesium	19.61	20.24	3.21	19.97	1.84
Ethylamine	11.46	11.97	4.43	11.60	1.24
Lithium	7.32	7.35	0.45	7.37	0.77
Magnesium	14.66	15.05	2.64	14.56	0.67
Manganese	15.03	15.43	2.64	14.92	0.76
Methylamine	11.34	11.79	3.97	11.48	1.23
Potassium	13.50	14.09	4.40	13.86	2.65
Rubidium	16.11	16.87	4.73	16.55	2.73
Sodium	9.16	9.38	2.38	9.22	0.64
Strontium	18.05	18.78	4.03	18.35	1.68

The generality of the IDGP approach was investigated further by using the isocratic database to predict gradient retention data for 24 anions under 5 different gradient conditions on 3 columns (AS11HC, AS16, AS19) and 13 cations under 5 different gradient conditions on 2 columns (CS12A and CS16) in Table 4.1. The set of test analytes was bolded and employed throughout in Chapters 4 and 5. All retention data were simulated using IDGP model and the predicted retention times were evaluated by comparing with the observed retention data, **Figure 4.2.**

It shows all predicted data *versus* all observed data and indicates the high correlation for both anions and cations. The average percentage difference between observed and predicted retention times was 3.73% for anions and cations. It should be noted again that the isocratic data used as a basis for calculation of gradient retention data were obtained on different column batches and chromatographic systems than those used for the

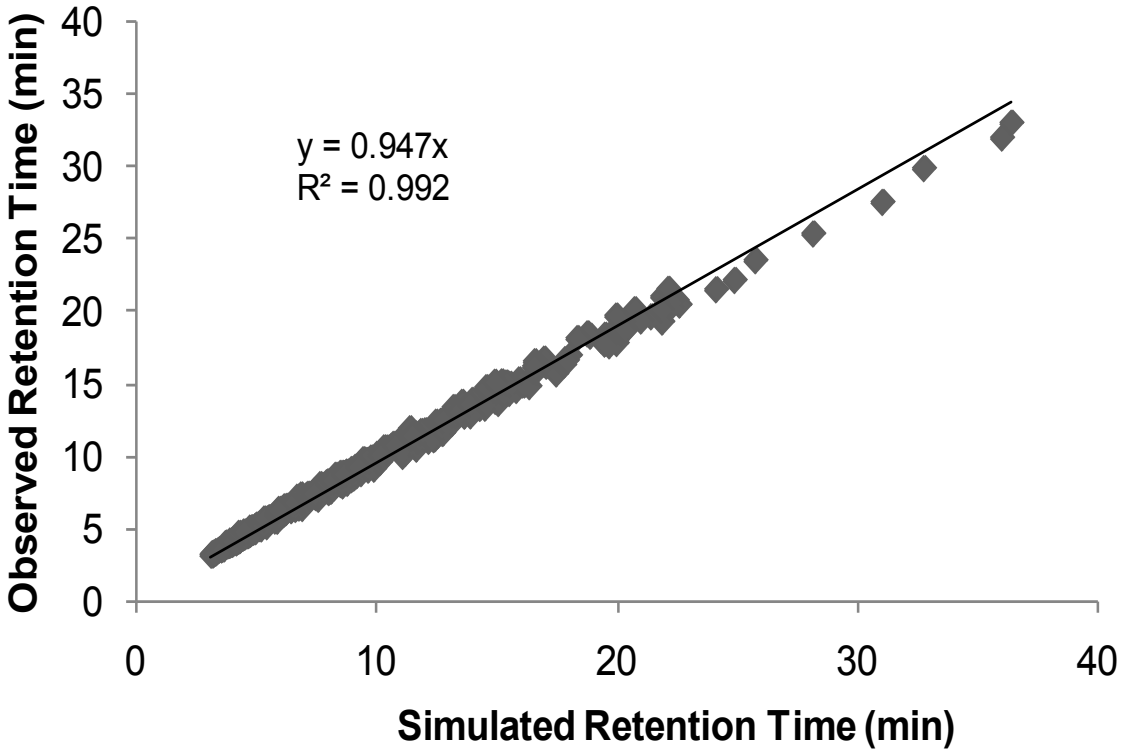

Figure 4.2 Observed retention times againsts gradient retention times predicted from isocratic data (i.e. IDGP approach) for 24 anions on the AS11 HC, AS16 and AS19 columns for 5 different gradient conditions at 30^{o}C and 13 cations on the CS12A and CS16 columns each for 5 different gradient conditions at 40^{o}C.

observed retention data. Under these circumstances, the degree of correlation shown in Figures 4.2 is remarkable.

4.4 Prediction of Peak Widths in Gradient Separations

In order to perform satisfactory simulations of IC retention behaviour under gradient conditions, knowledge of peak widths is required as well as the knowledge of retention times, so that resolution between peaks can be calculated. The simulation of peak width under gradient elution conditions is more complicated than for isocratic separations because the increasing ionic strength of the eluent results in a peak compression effect which to some extent counteracts the normal broadening experienced as the analyte peak travels down the column. This effect results in peaks from gradient elution being considerably narrower than those obtained under isocratic conditions. Two approaches to the prediction of peak width under gradient conditions were evaluated. The first, proposed by Snyder *et al.*[3] for reversed-phase liquid chromatography is based on a peak compression factor which is related to the slope of the gradient ramp. The second, proposed by Jandera and Churacek[9] is based on the column plate number under isocratic conditions and the instantaneous isocratic retention factor of the solute at the time the peak maximum leaves the column. Both approaches were applied to a limited set of analytes contained in the isocratic and gradient database and were found to severely underestimate the peak widths observed under gradient conditions.

An empirical approach was therefore proposed for the peak width simulation. Peak width is directly proportional to the compression observed in gradient elution. The plate height, H, was found to be constant of proportionality between the variance, σ equals approximately one quarter of the peak width, w, of the analyte band and the distance, L, it travelled in the column. This is illustrated by[21]:

$$H = \frac{\sigma^2}{L} \qquad \text{Equation 4.2}$$

The plate height can also be calculated from the following equation[21]:

$$H = \frac{2D_A}{u}$$ Equation 4.3

where D_A is the diffusion coefficient of the analyte. Equation 4.2 can be rearranged to be $\sigma^2 = HL$ where σ^2 can also be calculated from Equation 4.3 by multiplying t_R of the analyte on both sides of Equation 4.3, followed by rearranging u (analyte linear velocity) to the left hand side so that $\sigma^2 = HL = Hut_R = 2DAt_R$. On the other hand, σ^2 can also be expressed as a quarter of the peak width. Combining Equations 4.2 and 4.3, this gives rise to[21]:

$$\left(\frac{w}{4}\right)^2 = \sigma^2 = 2D_A t_R = Hut_R = HL$$ Equation 4.4

This implies that the width of the peak is proportional to the square root of the retention time. This means if the retention time of the analyte increases by a factor of four, the peak width will broaden by a factor of two. Therefore, by comparing an analyte's retention time, t_R, in gradient elution with the retention time, t_{Ri}, in isocratic elution at the same initial concentration, the compression factor can be determined and employed in peak width prediction, as shown in Equation 4.5

$$w = \frac{4t_R}{\sqrt{N}}\sqrt{\frac{t_R}{t_{R_i}}}$$ Equation 4.5

where t_R is the predicted retention time determined using the Equation 1.14, N is the plate count observed under the isocratic experimental conditions at the initial eluent concentration used, and the t_{Ri} is the isocratic retention time observed under isocratic conditions at gradient initial concentration.

The first part of Equation 4.5 expresses peak broadening and the second part of Equation 4.5 acts as a compression factor that was largely empirically derived, which only applies in gradient separations. Note that under isocratic conditions, t_R and t_{Ri} are equal and Equation 4.5 reverts to the customary isocratic equation for peak width.

Equation 4.5 was evaluated by comparing predicted and observed peak widths for gradient separations of anions or cations, **Figure 4.3** shows

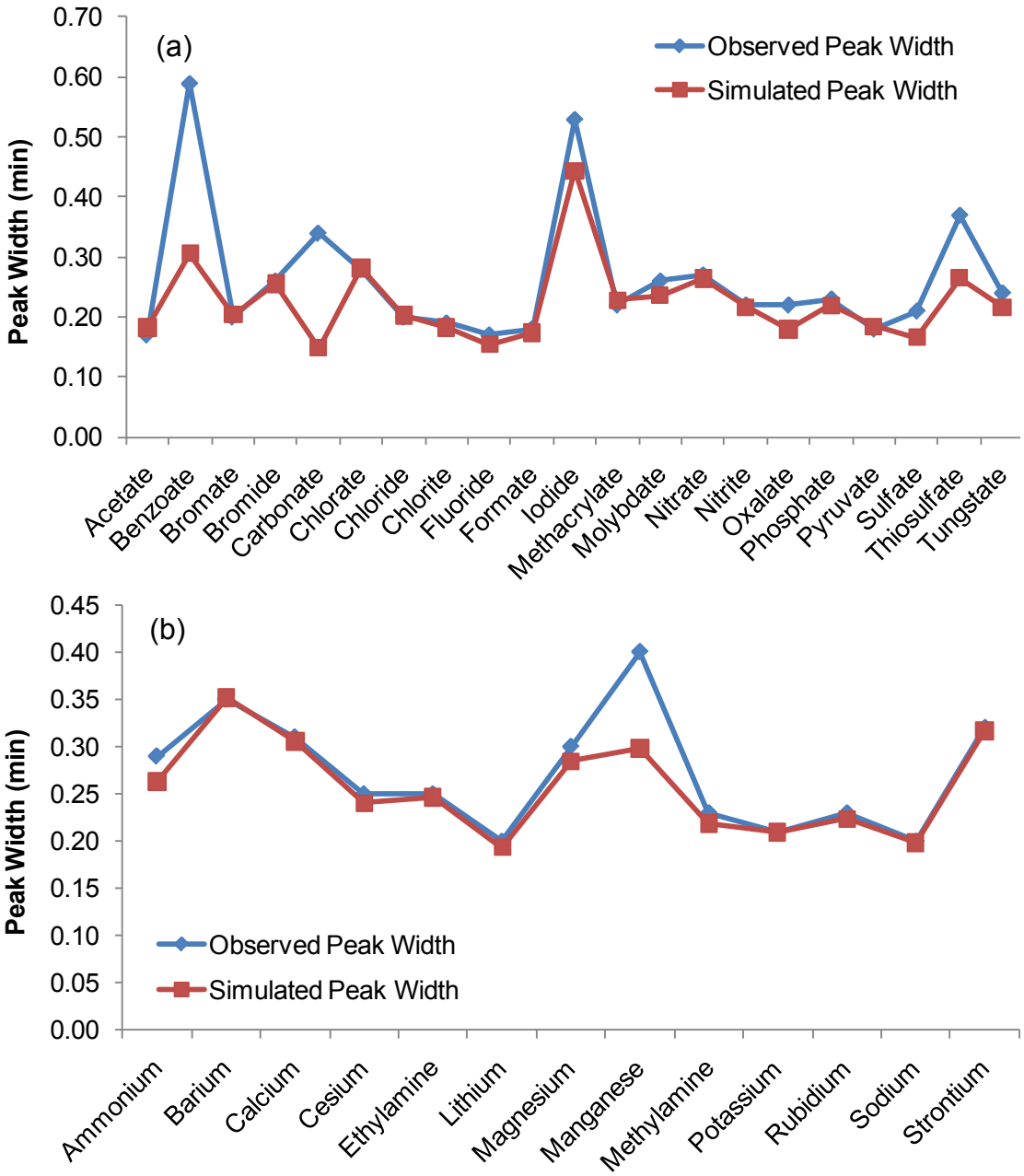

Figure 4.3 Peak width predictions for: (a) 21 anions on a Dionex AS11 HC column with a starting concentration of 15mM KOH and a linear gradient of 5mM/min at 30°C and (b) 13 cations on a Dionex CS12A column with a starting concentration of 8mM MSA and a linear gradient of 4.5mM/min at 40°C.

that predicted peak widths agreed generally well with the observed values, with the exception of two anions (carbonate and benzoate) and one cation (manganese). In these cases, the experimental peaks were considerably broader than those predicted from Equation 4.5. This discrepancy can be attributed to the behaviour of these analytes in a suppressed IC system. Carbonate and benzoate are weak acid anions which become partially protonated in the suppressor, and this leads to dispersion, creating broadened peaks. In the case of manganese, precipitation as the hydroxide salt may occur in the suppressor, again leading to band-broadening. This peak width model was initially employed to perform simulations on 2 anionic columns (Dionex AS11 HC and AS19) for 24 anions and the Dionex CS12A cationic column for 13 cations, all bolded in Table 4.1 over 5 gradient conditions on each column.

Figure 4.4 shows all observed peak width data *versus* all simulated peak width data and indicates the high correlation for both anions and cations. The average percentage difference between observed and predicted peak widths was 17% for both anions and cations. Despite its inapplicability to these specific analytes (benzoate, carbonate and manganese), Equation 4.5 was considered to be satisfactory for routine prediction of peak widths under both isocratic and gradient conditions.

4.5 Retention Time Predictions for Complex Elution Profiles (Method 1)

The availability of eluent generators and suppressors leads to the frequent use of complex elution profiles in which successive isocratic and gradient steps are combined to fine-tune the separation of complex mixtures. The results discussed thus far suggest that retention behaviour under both isocratic and gradient conditions can be simulated with good accuracy using Equations 1.11 and 1.14. However, there is a need to devise a way in which the isocratic and gradient calculations can be combined to enable them to be used for multi-step elution profiles.

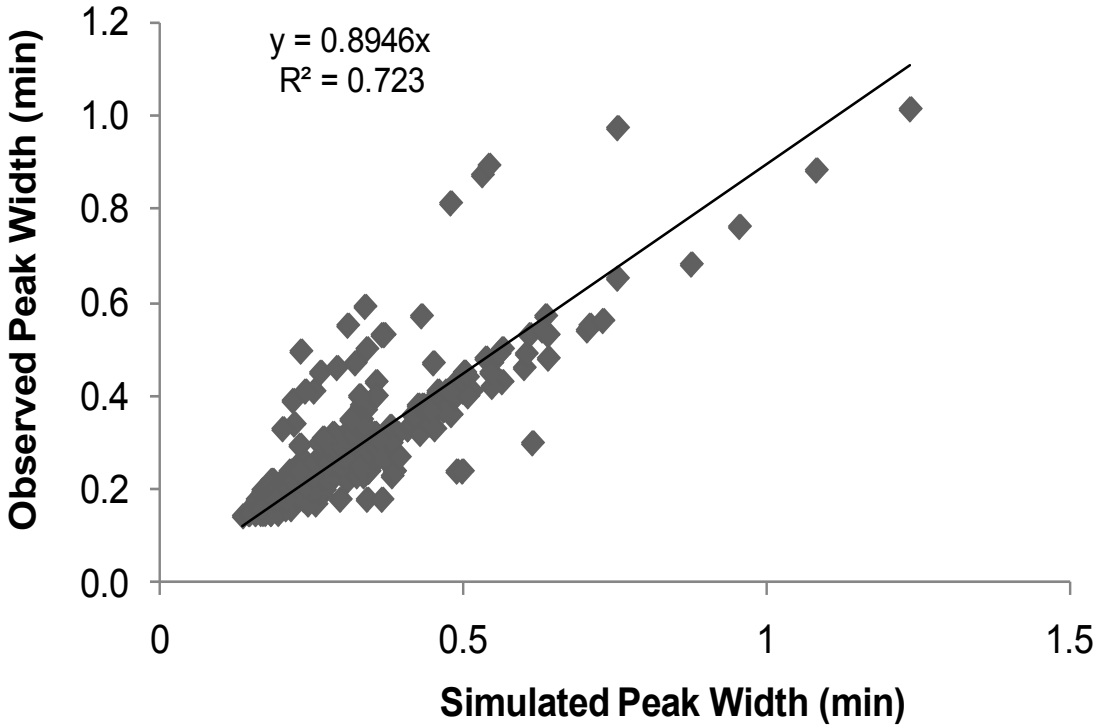

Figure 4.4 Experimental peak widths *versus* simulated peak widths of 24 anions and 13 cations bolded in Table 4.1 on the AS11 HC, AS19 and CS12A columns for 5 linear gradient gradient conditions at 30^{o}C for anion analysis and 40^{o}C for cation analysis

One approach to this task is to consider the separation column to be composed of a series of segments, each of which is under the control of only one step of the complex elution profile. This is represented schematically in **Figure 4.5** for a three-step elution profile comprising two linear gradient steps followed by an isocratic step. At the end of step 1 (i.e., after 10 minutes, see Figure 4.5 top section), the position of the analyte band on the column can be mapped using Equation 1.14 by setting t_R to be t_{step1} (10 minutes) and solving for the unknown (t_m), with an iterative tool (Goalseek, Microsoft Excel), and this position is shown as the first dotted box in Figure 4.5 (bottom section). The second gradient step (step 2) starts at 10 minutes after injection, but there will be a lag time before the start of the gradient reaches the position of the analyte band. During this lag time, the band will continue to move under the influence of the gradient eluent used in step 1 and can be mapped again using Equation 1.14 by solving for t_m (again employing Goalseek). The position of the analyte and when it is first influenced by the gradient in step 2 is shown by the solid box at a retention time of t_{step1} in Figure 4.5 (bottom section). The analyte position at the end of step 2 can be calculated from Equation 1.14, again after making allowance for the time needed for the new isocratic (step 3) to reach the position of the analyte on the column. This process is repeated for the final isocratic step (step 3) of the elution profile except Equation 1.11 is employed, and the analyte is considered to be eluted when it reaches the outlet of the column and passes through the suppressor to the detector. In the example illustrated in Figure 4.5, the analyte is eluted from the column during step 3, and the retention time is the sum of the times that the analyte moves under influence of each step of the elution profile. The retention time for a general elution profile is given in Equation 4.6,

$$t_R = t_{R_n} + \sum_{i=1}^{n-1} t_{step\ i} \qquad \text{Equation 4.6}$$

where the subscript i denotes the step number and Equation 4.7 shows the retention time for the specific example used in Figure 4.5.

$$t_R = t_{R_n} + t_{step\ 1} + t_{step\ 2} \qquad \text{Equation 4.7}$$

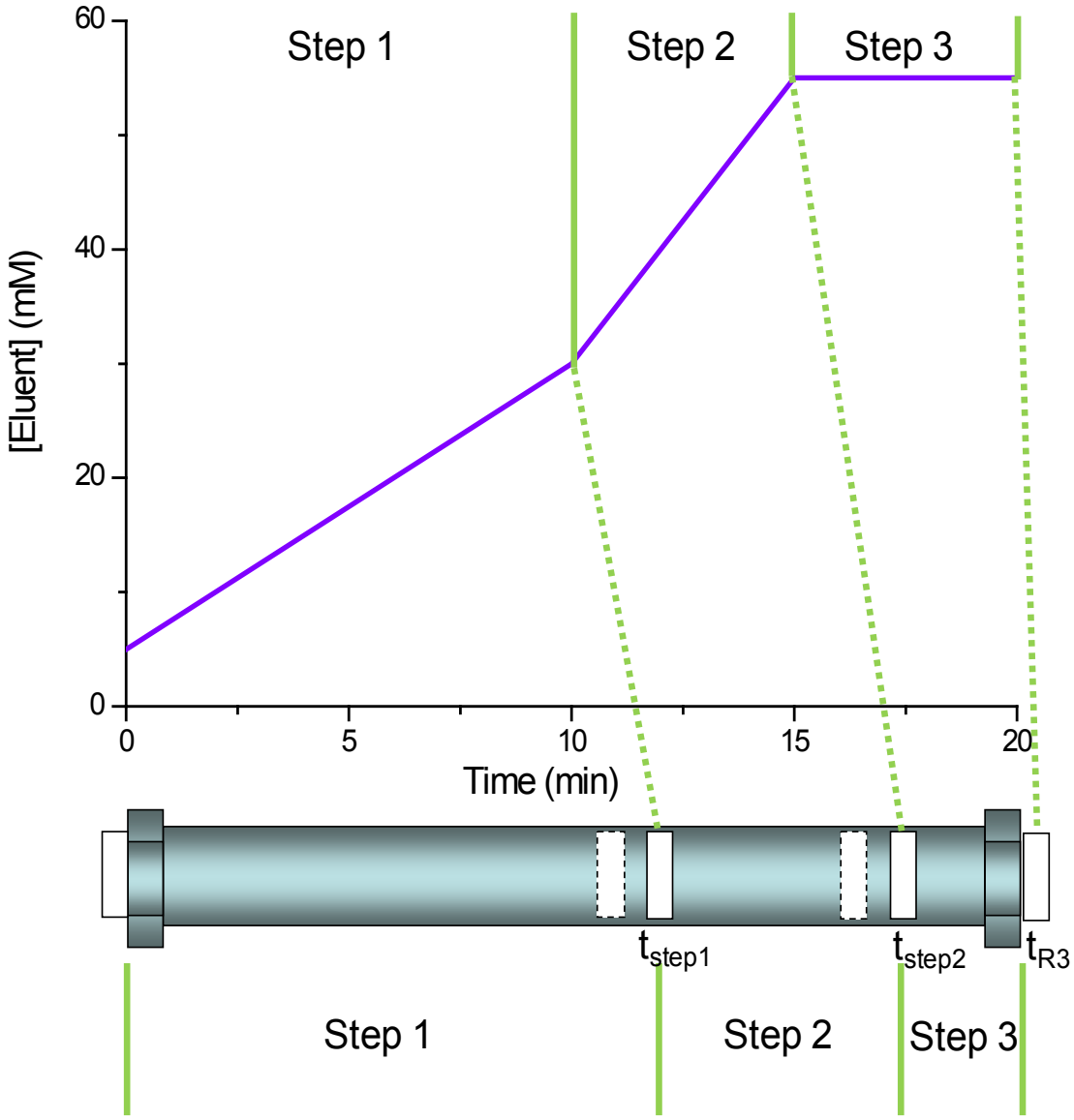

Figure 4.5 Schematic showing how retention under isocratic and gradient eluent steps can be joined together

The sequence was coined the "*linear analyte displacement approach*" and it was employed for predicting the retention time for an analyte eluted using a complex gradient is summarised in the flowchart in **Figure 4.6**. In the first step of the elution profile, the value of t_m is used as input data and the values of a and b are determined from the retention database using Equation 1.11. Equations 1.11 and 1.14 are also used to determine the position of the analyte band on the column (or its retention time if it has been eluted during the first step). The remaining length of the column can then be calculated, together with a new value for void time (t_{new}). The new void time is the product of the original void time (t_m) and the ratio of the remaining length of column relative to the full column length. After allowance is made for the lag time between the application of step 2 to the head of the column and the time that this new eluent actually reaches the analyte band, the process is continued for each eluent step until all analytes have been eluted.

A detailed evaluation was made of the accuracy of retention predictions under complex elution conditions, based on calculations using Equation 1.14 and isocratic data, together with combining isocratic and gradient steps using the approach described above. A total of 4 elution profiles on each column were programmed to validate this iterative predictive sequence, each comprising a combination of 5 separate isocratic and gradient steps, was initially applied to 24 analyte anions on the AS11 HC, AS16 and AS19 columns and 13 cations on the CS12A and CS16 columns as bolded in Table 4.1. The results of this evaluation are shown in **Figure 4.7**, from which it can be seen that excellent agreement was obtained between experimental and predicted retention times. The average percentage difference was 5.42%

4.5.1 Alternative Method for Complex Eluent Profiles (Method 2)

Notwithstanding the excellent performance of the linear analyte displacement approach described above, implementation of this algorithm to real time retention simulation will be problematic as the approach is dependent on an iterative solution to a complex equation. This complication arises because the retention models (Equations 1.11 and 1.14) are designed to estimate the retention time with a known void time where this void time correlates to the

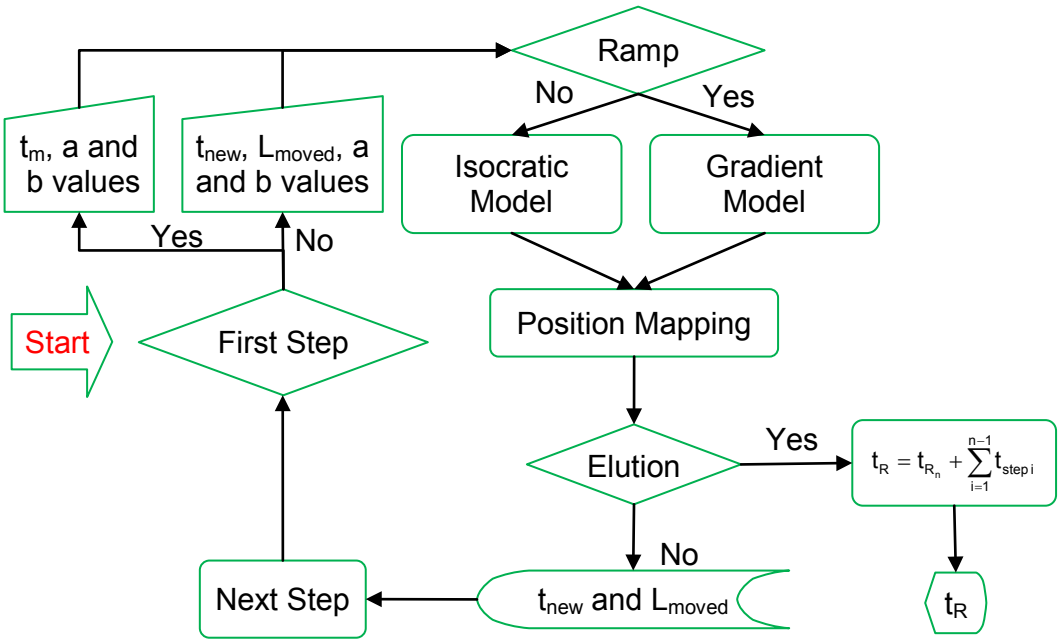

Figure 4.6 Flowchart summarising the overall procedure used for prediction of retention times for complex elution profiles

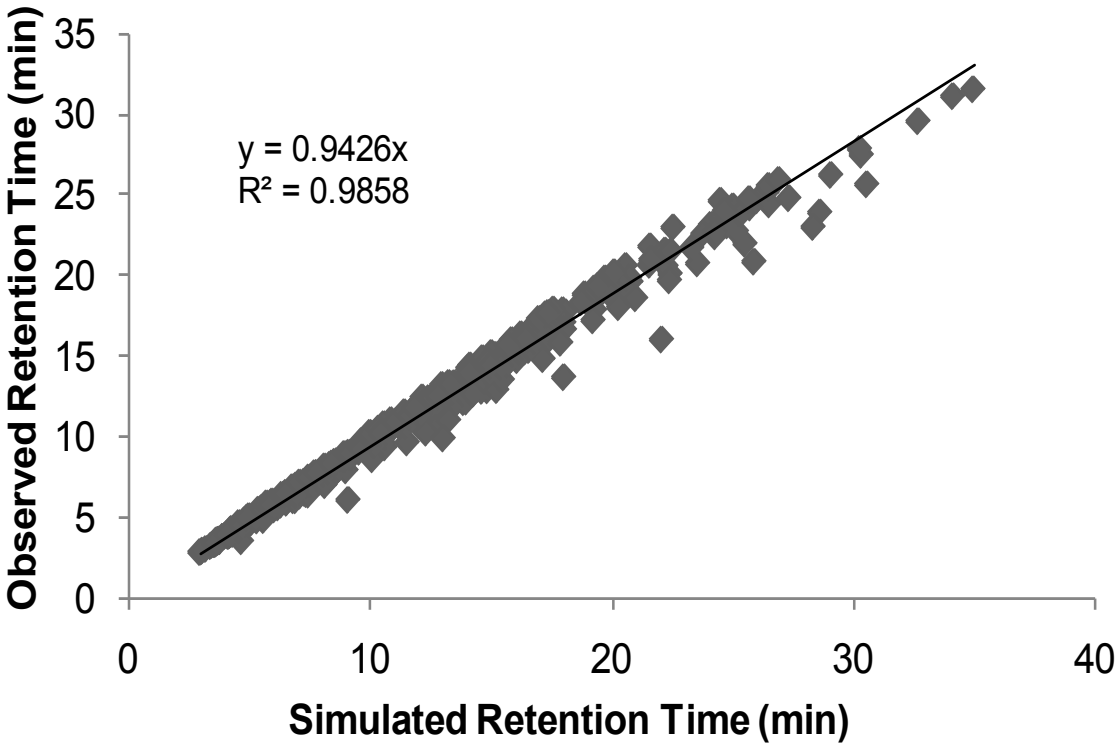

Figure 4.7 Observed *versus* predicted retention times for five-step elution profiles for 24 anions bolded in Table 4.1 on the Dionex AS11 HC, AS16 and AS19 columns at 30^{o}C and 13 cations on the Dionex CS12A and CS16 columns at 40^{o}C

length of a column (i.e. if a column is segmented into a number of shorter sub-columns, these sub-columns will have shorter void times and are defined as pseudo-columns). The LAD approach, however, uses the models (Equations 1.11 and 1.14) in the reverse direction. In normal use, void time and length of the column are known and the models (Equations 1.11 and 1.14) are used to estimate retention time. In the LAD approach, the step time is known and the models (Equations 1.11 and 1.14) are employed to estimate two unknowns, namely the void time and pseudo-column length in relation to the step time. This pseudo-column length reflects the distance travelled by analyte during the step time. Therefore, the analyte displacement during the step time is equal to the pseudo-column length, and can be obtained using the product of the average linear velocity (u) and the void time ($t_{m(step)}$) in relation to the step time. Since u is a constant, only one variable, $t_{m(step)}$, is required to calculate the displacement. Observation of Equation 1.11 reveals that it can be easily rearranged to solve for $t_{m(step)}$ in isocratic portions of the complex gradient. However Equation 1.14 is a highly complex gradient model where rearrangement is problematic, thus an iterative tool is used to solve for $t_{m(step)}$. The need to employ this iterative solution does not rule out an automated algorithm, indeed all calculations above were performed using a macro function in Microsoft Excel. However this method is calculation intensive thus an alternative approach was sought.

An alternative approach was applied to which modifies Equation 1.14 so that the analyte position can be monitored using the mathematical expression instead of relying on the iterative solution approach. This enabled the real time simulation. The detailed derivation of this algorithm is expressed as follows.

According to Section 4.2, isocratic separations can be predicted using the following expression:

$$t'_R\left(\left[E^-\right]\right) = a\left[E^-\right]^b \qquad \text{Equation 4.8}$$

where t'_R is the adjusted retention time with its operating concentration, $[E^-]$.

In gradient elution, Equation 4.8 is not valid as it does not take into account the change in solvent strength. Integration of Equation 4.8 is required to account for the increasing competing ion concentration in gradient elution. Since the gradient ramp employed is known, an expression for the hydroxide concentration with respect to time can be derived,

$$\left[E^-\right](t) = \left[E^-\right]_i + Bt \qquad \text{Equation 4.9}$$

where $[E^-]_i$ is the initial concentration, B is the gradient ramp in mM/min and t is the applied gradient time. Substituting Equation 4.9 into Equation 4.8 gives an expression for retention time in terms of time,

$$t_R'\left(\left[E^-\right]\right) = a\left(\left[E^-\right]_i + Bt\right)^b \qquad \text{Equation 4.10}$$

The velocity of the analyte, v(t), at any time along the column is then given by,

$$v(t) = \frac{L}{a\left(\left[E^-\right]_i + Bt\right)^b} \qquad \text{Equation 4.11}$$

where L is the length of the column. The displacement, L(t), of the analyte at any time is the integral of v(t),

$$L(t) = \int_0^{t_R - t_m} v(t)\,dt = \int_0^{t_R - t_m} \frac{L}{a\left(\left[E^-\right]_i + Bt\right)^b}\,dt \qquad \text{Equation 4.12}$$

where t_m is the void time of the IC system. Setting L(t) = l, the displacement at a given time before elution from the column, Equation 4.12 can be integrated to give rise to the following expression,

$$L(t) = \frac{L}{a\,B(1-b)}\left(\left\{\left[E^-\right]_i + B\left(t_R - t_m\right)\right\}^{1-b} - \left[E^-\right]_i^{1-b}\right) \qquad \text{Equation 4.13}$$

Since, this expression can be rearranged for $t_R(B)$ with respect to time, the retention time of an analyte in gradient elution can be determined using the following equation,

$$t_R = \frac{1}{B}\left\{\left[\frac{laB(1-b)}{L} + \left[E^-\right]_i^{1-b}\right]^{\frac{1}{1-b}} - \left[E^-\right]_i\right\} + t_m \qquad \text{Equation 4.14}$$

A complex elution system was presented in Figure 4.5, comprising two linear gradient steps followed by an isocratic step. At the end of step 1 (i.e., after 10 minutes, see Figure 4.5 top section), the position of the analyte band on the column can be mapped using Equation 4.13 and this position is shown as the first dotted box in Figure 4.5 (bottom section). The second gradient step (step 2) starts at 10 minutes after injection, but there will be a lag time, t_{lag}, before the start of the gradient reaches the position of the analyte band and the lag time is given by:

$$t_{lag} = \frac{L_{moved}}{L} t_m \qquad \text{Equation 4.15}$$

where L_{moved} is the displacement after the step and t_m is the void time.

During this lag time, the band will continue to move under the influence of the gradient eluent used in step 1 and can be mapped again using Equation 4.13. The solid box shows the position of the analyte and when it is first influenced by the gradient in step 2 at a retention time of t_{step1} in Figure 4.5 (bottom section). The analyte position at the end of step 2 can be calculated from Equation 4.13, again after making allowance for the time needed for the final step (step 3) to reach the position of the analyte on the column. This process is repeated for the final isocratic step (step 3) of the elution profile except Equation 4.8 is employed, and the analyte is eluted when it reaches the outlet of the column and passes through the suppressor to the detector. In the example illustrated in Figure 4.5, the analyte is eluted from the column during step 3, and the retention time is the sum of the times that the analyte moves under influence of each step of the elution profile. The retention time for a general elution profile is given in Equation 4.16 if the final step is isocratic,

$$t_R = a\left[E^-\right]_n^b + t_m + \sum_{i=1}^{n-1} t_{step\ i} \qquad \text{Equation 4.16}$$

where the subscript i denotes the step number and Equation 4.17 shows the retention time for the example if the final step is gradient.

$$t_R = \frac{1}{B}\left\{\left[\frac{IaB(1-b)}{L} + \left[E^-\right]_i^{1-b}\right]^{\frac{1}{1-b}} - \left[E^-\right]_i\right\} + t_m + \sum_{i=1}^{n-1} t_{step\ i} \qquad \text{Equation 4.17}$$

The entire sequence for predicting the retention time for an analyte eluted using a complex gradient is identical to the iterative algorithm summarised in the flowchart in Figure 4.6.

A detailed evaluation of the accuracy for prediction of retention times was made under complex elution conditions, based on this algorithm. A total of 4 elution profiles on each column were programmed to validate this iterative predictive sequence, each comprising a combination of 5 separate isocratic and gradient steps. These profiles were initially applied to 24 analyte anions on the AS11 HC, AS16 and AS19 columns and 13 cationic analytes on the CS12A and CS16 columns as shown in Table 4.1. The results of this evaluation are shown in **Figure 4.8**, from which it can be seen that excellent agreement was obtained between experimental and predicted retention times. The average percentage difference was 2.92 %.

4.6 Prediction of Peak Widths for Complex Eluent Profiles

The second part of Equation 4.5 acts as a compression factor that was largely empirically derived, which only applies in gradient separations. Likewise, an empirical weighting function is required to take into account the compression each step exhibited under complex eluent profiles, and the mathematical expression is given by:

$$w = \frac{4t_R}{\sqrt{N}}\sqrt{\sum_{i=1}^{n}\frac{t_R}{t_{R_i}} \times \left(\frac{L_{moved(stepi)}}{L}\right)^2} \qquad \text{Equation 4.18}$$

where subscript i denotes each step in the profile, L_{moved} represents the displacement travelled by analyte at the end of each step and L is the column length.

A total of 4 elution profiles on each column were utilised to validate this model, each comprising a combination of 5 separate isocratic and

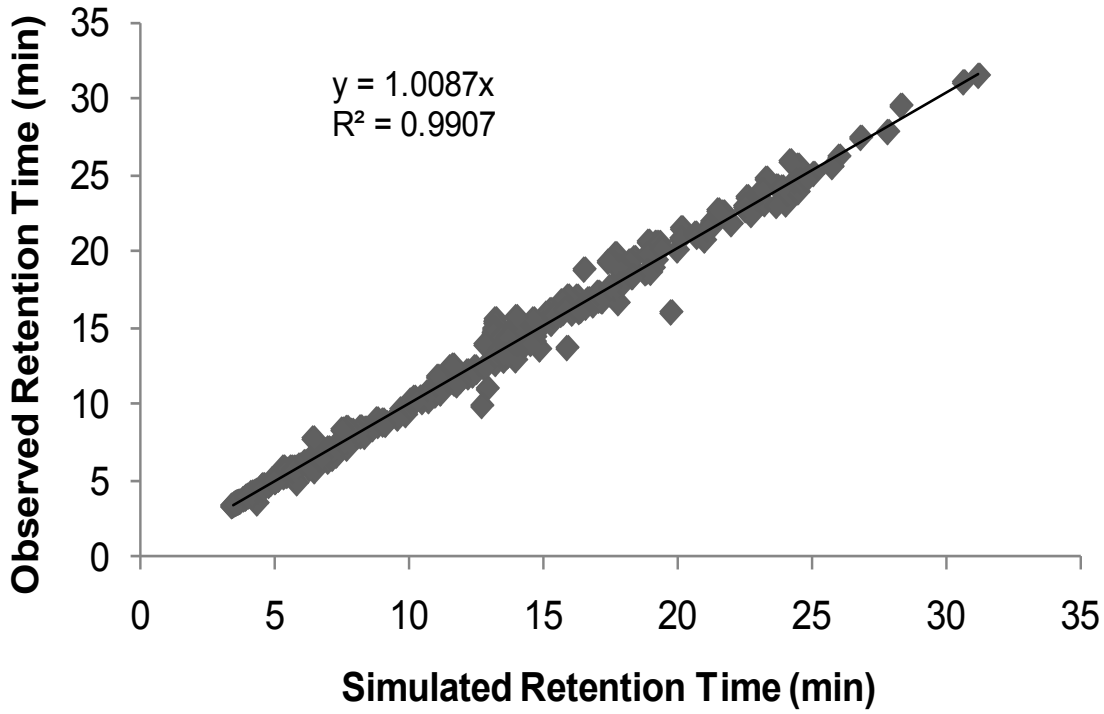

Figure 4.8 Experimental retention times *versus* simulated retention times of 24 anions and 13 cations bolded in Table 4.1 on the AS11 HC, AS16, AS19, CS12A and CS16 columns for 4 5-step complex eluent profiles at 30^{o}C for anion analysis and 40^{o}C for cation analysis

gradient steps, was applied to 24 analyte anions on the AS11 HC and AS19 columns and 13 cations listed on the CS12A column as shown in Table 4.1. The results of this evaluation are shown in **Figure 4.9**, from which it can be seen that satisfactory agreement was obtained between experimental and predicted peak widths. The average percentage difference was 19%. The peak width simulation of complex eluent profiles involved the prediction on multiple isocratic and gradient steps. The peak width predictions reported in Figure 4.9 contain cumulative errors from each individual step. Due to accumulation of error, a drop in accuracy and precision compared to Section 4.4 was expected, and this was strongly connected to the average error (19%) and R squared value observed in Figure 4.9 (0.6516) in which it had a poorer value when compared to the average error (17%) and R squared in Figure 4.4 (0.7230).

4.7 Optimisation

A series of sample mixtures containing 11 anions or 10 cations were employed for optimisation on the AS19 and CS16 columns, respectively. Two mixtures were optimised *in-silico* using the Microsoft Solver function to search the simulated optimal conditions. A 3-step profile consisting of 7 parameters ($[E^-]_i$, t_{step1}, B_1, t_{step2}, B_2, t_{step3} and B_3) was employed for optimising the anionic sample whilst a 5-step profile comprising 11 variables ($[E^-]_i$, t_{step1}, B_1, t_{step2}, B_2, t_{step3}, B_3, t_{step4}, B_4, , t_{step5}, and B_5) was implemented for optimising the cationic mixture. The *in-silico* optimisation process is described as follows. Initial inputs for all parameters were manually entered, the separation based on the initial input condition was then simulated using the algorithm described in Section 4.5.1, followed by assessing the resolution of the simulated separation. If the minimum resolution was less than 1.5, Solver would then randomly input a new set of numbers for all parameters followed by simulating the separation. The iterative process will be repeated until a minimum resolution of 1.5 for the separation is found. The optimum condition however might not be a global optimum. Multiple entries were therefore employed. The simulated chromatograms of the optimal condition were then compared with the experimental chromatograms.

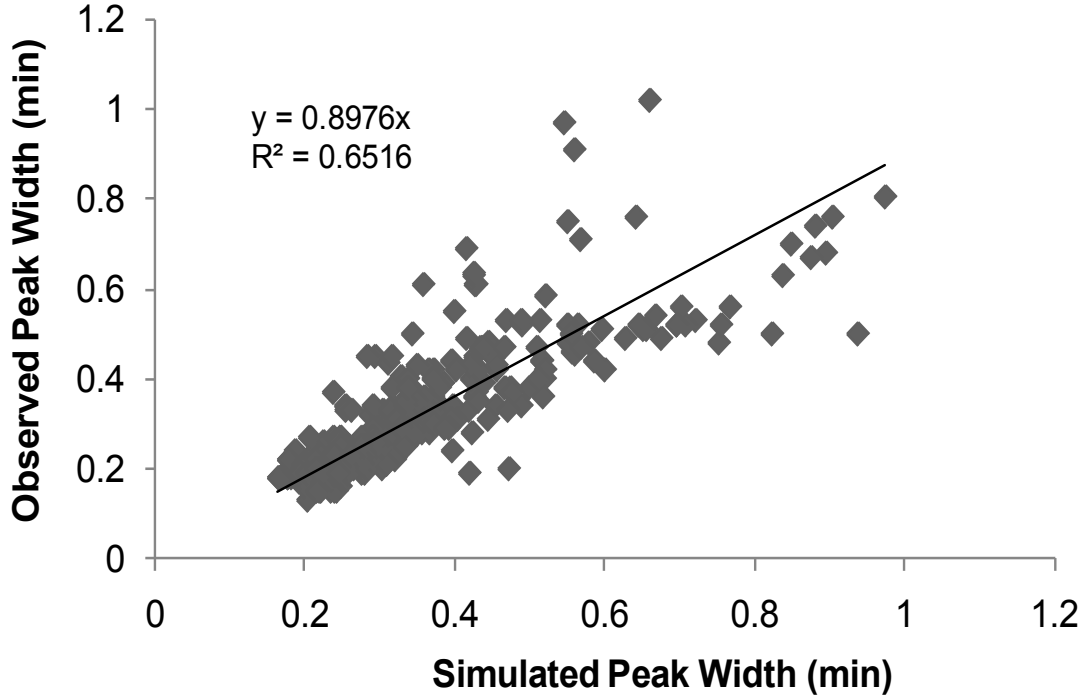

Figure 4.9 Experimental peak widths *versus* simulated peak widths for 24 anions and 13 cations bolded in Table 4.1 on the AS11 HC, AS16, AS19, CS12A and CS16 columns for 4 5-step complex eluent profiles at 30^{o}C for anion analysis and 40^{o}C for cation analysis

The accuracy of the proposed approach (using Method 1, iterative approach, Section 4.5) for retention times and peak widths can also be seen below. **Figure 4.10** shows the simulated and observed chromatograms of an 11-component mixture eluting in the order of 1-fluoride (5 ppm), 2-chlorite (5 ppm), 3-bromate (5 ppm), 4-chloride (5 ppm), 5-nitrite (5 ppm), 6-chlorate (10 ppm), 7-bromide (5 ppm), 8-nitrate (5 ppm), 9-carbonate (15 ppm), 10-sulfate (10 ppm) and 11-phosphate (15 ppm) using a 3-step sequential profile. **Figure 4.11** presents the simulated and observed chromatograms of a 10-component mixture eluting in the order of 1-lithium (I) (5 ppm), 2-sodium (I) (5 ppm), 3-ammonium (5 ppm), 4-ethylammonium (5 ppm), 5-potassium (I) (5 ppm), 6-magnesium (II) (10 ppm), 7-calcium (II) (10 ppm), 8-strontium (II) (10 ppm), 9-cesium (I) (15 ppm) and 10-barium (15 ppm) using a 5-step eluent profile. Figure 4.10 demonstrates excellent correlation for all anions between the simulated and the observed chromatograms whereas the predictions for a 10-component mixture (Figure 4.11) were slightly unsatisfactory. The first four predictions have excellent correlations comparing to the observed peaks while the final six predictions are not as good but the change of elution order does not emerge. Overall, the simulated chromatogram illustrates reasonable agreement with the experimental chromatogram.

Again the accuracy of the proposed approach (Method 2, real time simulator, Section 4.5.1) can be illustrated below. **Figure 4.12** shows the simulated and observed chromatograms of an 11-component mixture eluting in the identical order as in Figure 4.10 using the same 3-step eluent profile and **Figure 4.13** demonstrates the simulated and observed chromatograms of a 10-component mixture eluting in the identical order as in Figure 4.11 using the same 5-step eluent profile. Both sample mixtures demonstrate equally satisfactory agreements between the predicted and actual chromatograms.

4.8 Chapter Conclusion

This study has shown that a database of isocratic IC retention data can be used for the prediction of retention times for a wide range of anions and cations when separated under both isocratic and gradient conditions using

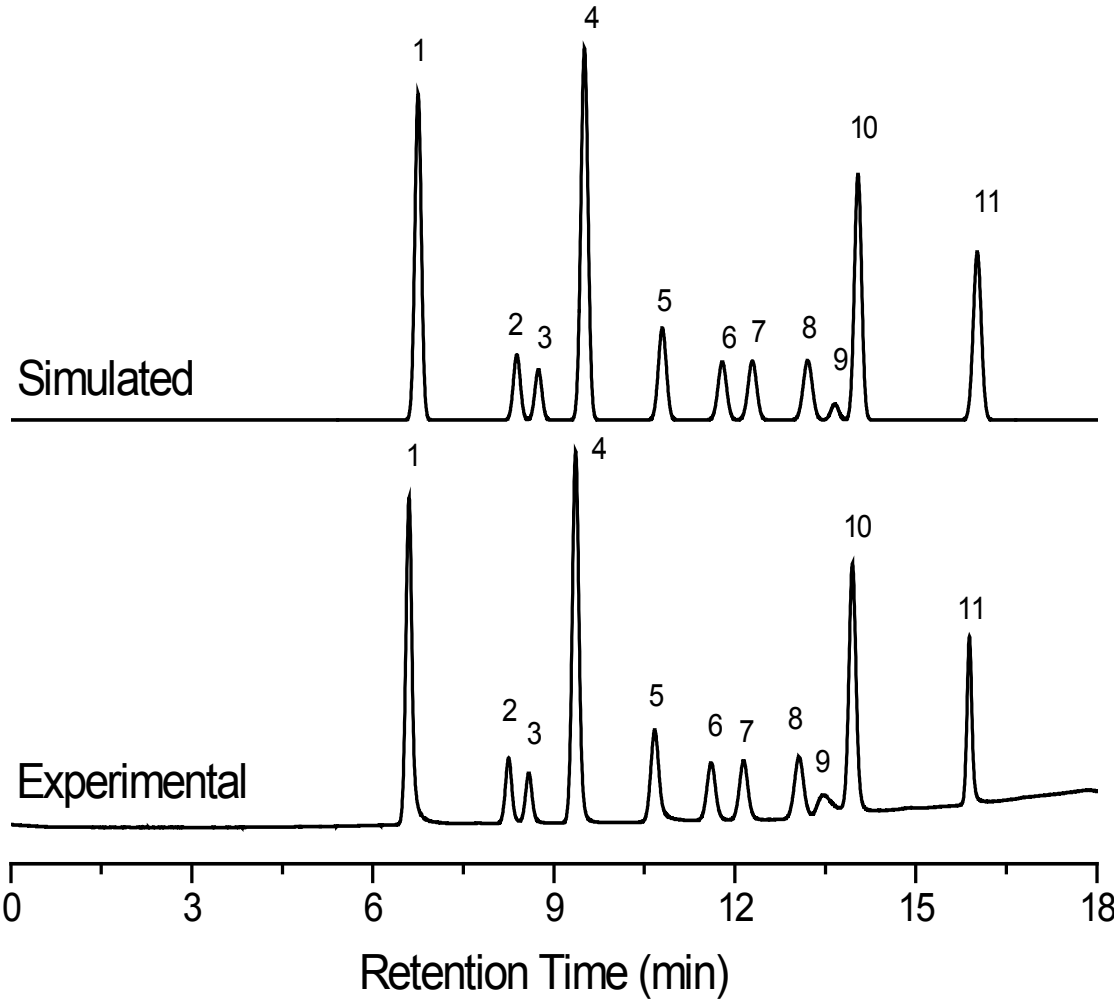

Figure 4.10 Simulated and experimental separations of 11 anions eluting in the order of 1-fluoride (5 ppm), 2-chlorite (5 ppm), 3-bromate (5 ppm), 4-chloride (5 ppm), 5-nitrite (5 ppm), 6-chlorate (10 ppm), 7-bromide (5 ppm), 8-nitrate (5 ppm), 9-carbonate (15 ppm), 10-sulfate (10 ppm) and 11-phosphate (15 ppm) on the Dionex AS19 column under a 3-step gradient profile consisting of: 3.75mM KOH for 0.8 min, 3.75 to 33.75mM KOH for 10 min followed by 33.75 to 99.75mM KOH for 4 min at 1mL/min at 30^{o}C where retention predictions rely on Method 1 (Section 4.5)

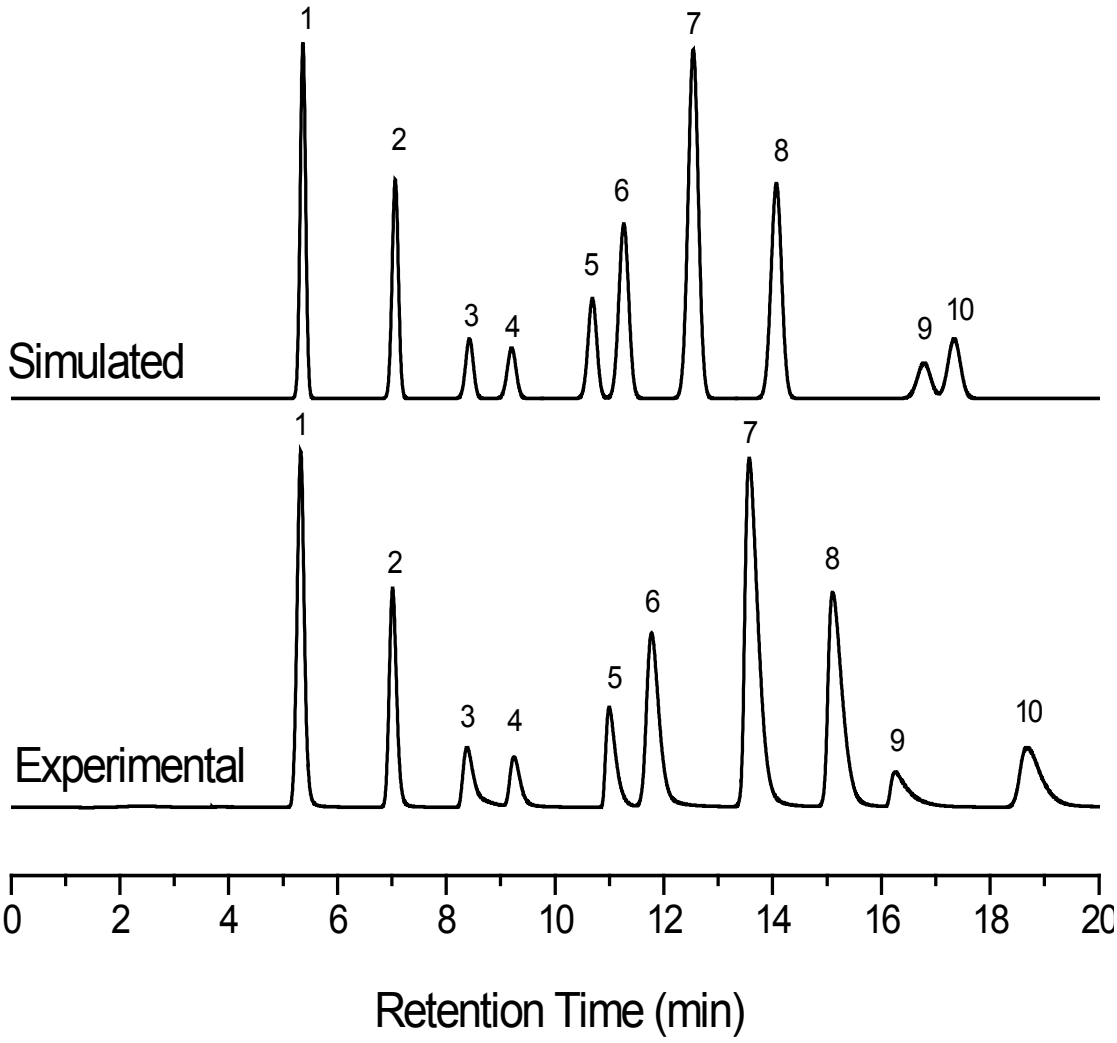

Figure 4.11 Simulated and experimental separations of 10 cations eluting in the order of 1-lithium (I) (5 ppm), 2-sodium (I) (5 ppm), 3-ammonium (5 ppm), 4-ethylammonium (5 ppm), 5-potassium (I) (5 ppm), 6-magnesium (II) (10 ppm), 7-calcium (II) (10 ppm), 8-strontium (II) (10 ppm), 9-cesium (I) (15 ppm) and 10-barium (15 ppm) on a Dionex CS16 column under a 5-step gradient profile consisting of: 30 to 35 mM for 3 min, 35 to 50 mM for 3 min, 50 to 60 mM for 3 min, 60 to 80 mM for 3 min followed by 80 to 95 mM for 12 min at 1mL/min, at 40^{o}C where retention predictions rely on Method 1 (Section 4.5)

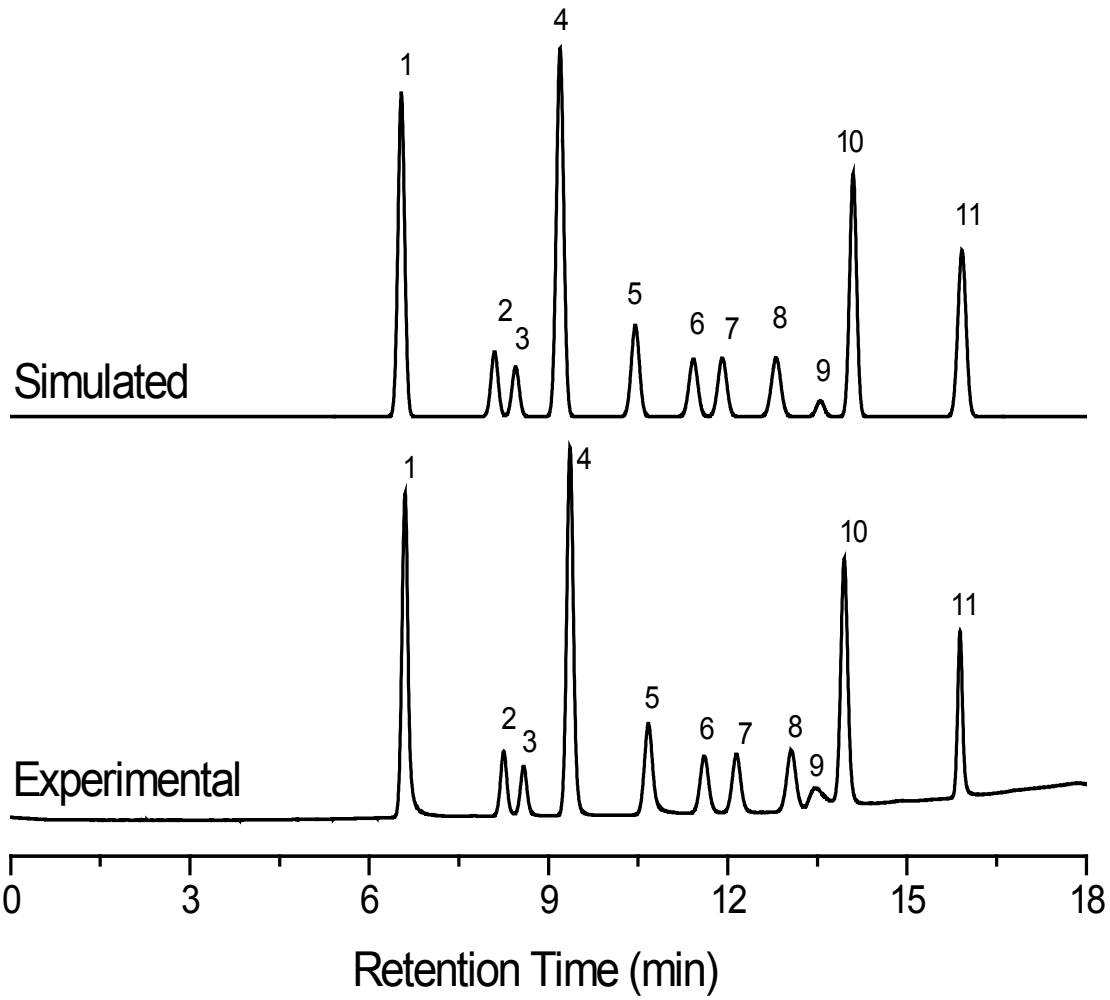

Figure 4.12 Simulated and experimental separations of 11 anions eluting in the identical order as in Figure 4.10 on the Dionex AS19 column under a 3-step gradient profile consisting of: 3.75mM KOH for 0.8 min, 3.75 to 33.75mM KOH for 10 min followed by 33.75 to 99.75mM KOH for 4 min at 1mL/min at 30^{o}C where retention predictions rely on Method 2 (Section 4.5.1)

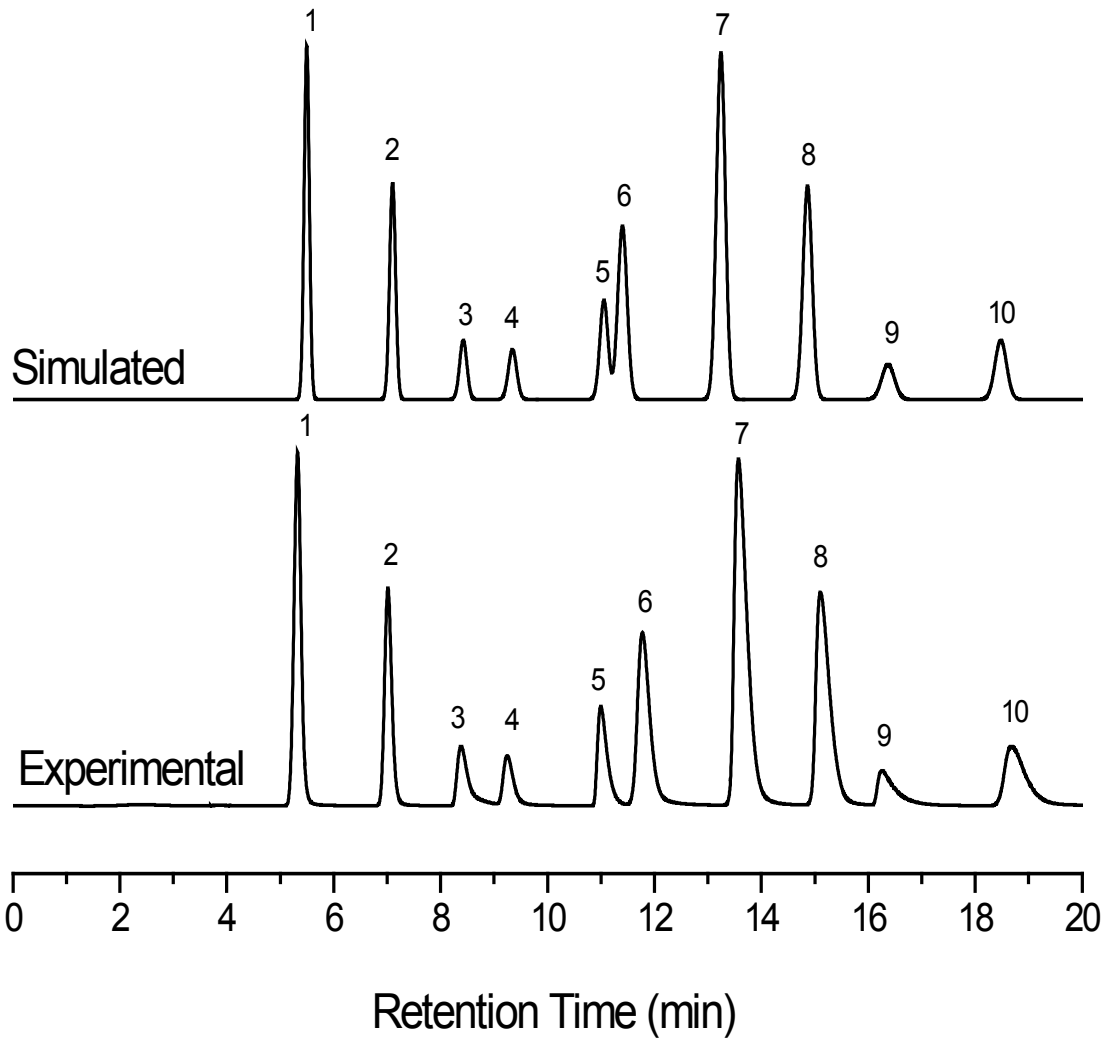

Figure 4.13 Simulated and experimental separations of 10 cations eluting in the identical order as in Figure 4.11 on a Dionex CS16 column under a 5-step gradient profile consisting of: 30 to 35 mM for 3 min, 35 to 50 mM for 3 min, 50 to 60 mM for 3 min, 60 to 80 mM for 3 min followed by 80 to 95 mM for 12 min at 1mL/min, at 40^{o}C where retention predictions rely on Method 2 (Section 4.5.1)

columns from different production batches than those used to generate the original retention data. Moreover, two approaches, namely Methods 1 and 2 were developed for the prediction of retention times for complex elution profiles comprising up to five sequential isocratic and gradient steps. Method 1 relies on iterative tool (Goalseek) to monitor the analyte position. The use of iterative tool (Goalseek) for Method 1 does not permit a real time simulation. In contrast, Method 2 uses a rearranged mathematical expression for position mapping, and therefore yields a very fast processing time. (i.e. a real time simulator) To this end, Method 2 is therefore a much better approach for *in-silico* optimisation.

By incorporation of an empirical algorithm for estimating peak width under complex elution conditions, chromatograms can be simulated with a high level of reliability. These methods described in this study can be used to assist method development in IC by simulating the effects of varying the elution conditions.

Chapter 5

Prediction of Retention Employing the Concept of Analyte Velocity

5.1 Introduction

It is known that isocratic and gradient elution regimes impart different effects on the movement of solutes in a chromatographic separation. Movement under isocratic conditions is dependent on the eluent concentration and analytes are thought to move at constant velocity. In contrast, the movement under gradient elution is thought to relate to both the velocity at the initial eluent concentration and the acceleration resulting from the applied gradient ramp. The motivation of this chapter was to study the elution behaviour based solely on the velocity and acceleration, and therefore introduce a new prediction algorithm without recourse to the mathematical retention models used earlier in Chapter 4.

5.2 Retention Time Modelling

5.2.1 Isocratic Elution Mode

The velocity of 38 analytes under isocratic conditions was evaluated as follows. Retention data were collected in triplicate and converted to adjusted retention times by subtracting the respective void times. Three retention times were measured for each analyte at three different eluent concentrations. Finally, the velocities of the analytes were obtained using the column length (L = 25.0 cm) and the adjusted retention times, using $v = L/t'_R$. The velocity of all analytes was assumed to be 0 at an eluent concentration of 0 mM. Therefore, a total of four velocities were obtained under isocratic concentrations for each analyte.

Following these isocratic analyses of 38 ion species (including singly, doubly and triply charged anions and cations), it was apparent that the relationship between eluent strength and analyte velocity is strongly dependent on the effective charge of the analyte.

In all, 25 monovalent ions were studied and a linear relationship between velocity and concentration for all singly charged species was observed. This relationship is illustrated in **Figure 5.1**(a) which provides a typical example of the linear relationship between velocity and concentration. This was perfectly fitted by a first order polynomial function (linear relationship, $v = 1.056\ [E^-]$ where $[E^-]$ is $[OH^-]$ in this specific case) and the first order relationship corresponds to the effective charge of chloride ion relative to the hydroxide competing ion. The plot of velocity *versus* concentration of sulfate is illustrated in Figure 5.1(b) where it was perfectly fitted by a second order polynomial function (quadratic relationship, $v = 0.017\ [E^-]^2 – 0.029\ [E^-]$). The second order relationship is consistent with the fact that the effective charge of sulfate is 2. In all, 12 divalent ions were studied and this observation was consistent across all doubly charged species investigated. Figure 5.1(c) shows the relationship between velocity and concentration for phosphate. Here, the relationship is closely fitted by a third order polynomial function (cubic relationship, $v = 0.0001\ [E^-]^3 + 0.0009\ [E^-]^2 + 0.0027\ [E^-]$). The cubic function is entirely consistent with the fact that the effective charge of phosphate is 3 at the high eluent pH used.

The relationships between velocities and competing ion concentrations of chloride, sulfate and phosphate are generalised in **Table 5.1**.

Table 5.1 Summary of the relationships between the velocities of singly (for example, chloride), doubly (for example, sulfate) and triply (for example, phosphate) charged analytes against the competing ion concentrations, where v denotes the velocity, and m, n and o denote cubic, quadratic and linear coefficients, respectively. The magnitudes of m, n and o describe the degree of interaction between the analytes and the stationary phases.

Effective Charge of Ion	Observational Relationship	Mathematical Expression
Singly	Linear	$v = o[E^-]$
Doubly	Quadratic	$v = n[E^-]^2 + o[E^-]$
Triply	Cubic	$v = m[E^-]^3 + N[E^-]^2 + o[E^-]$

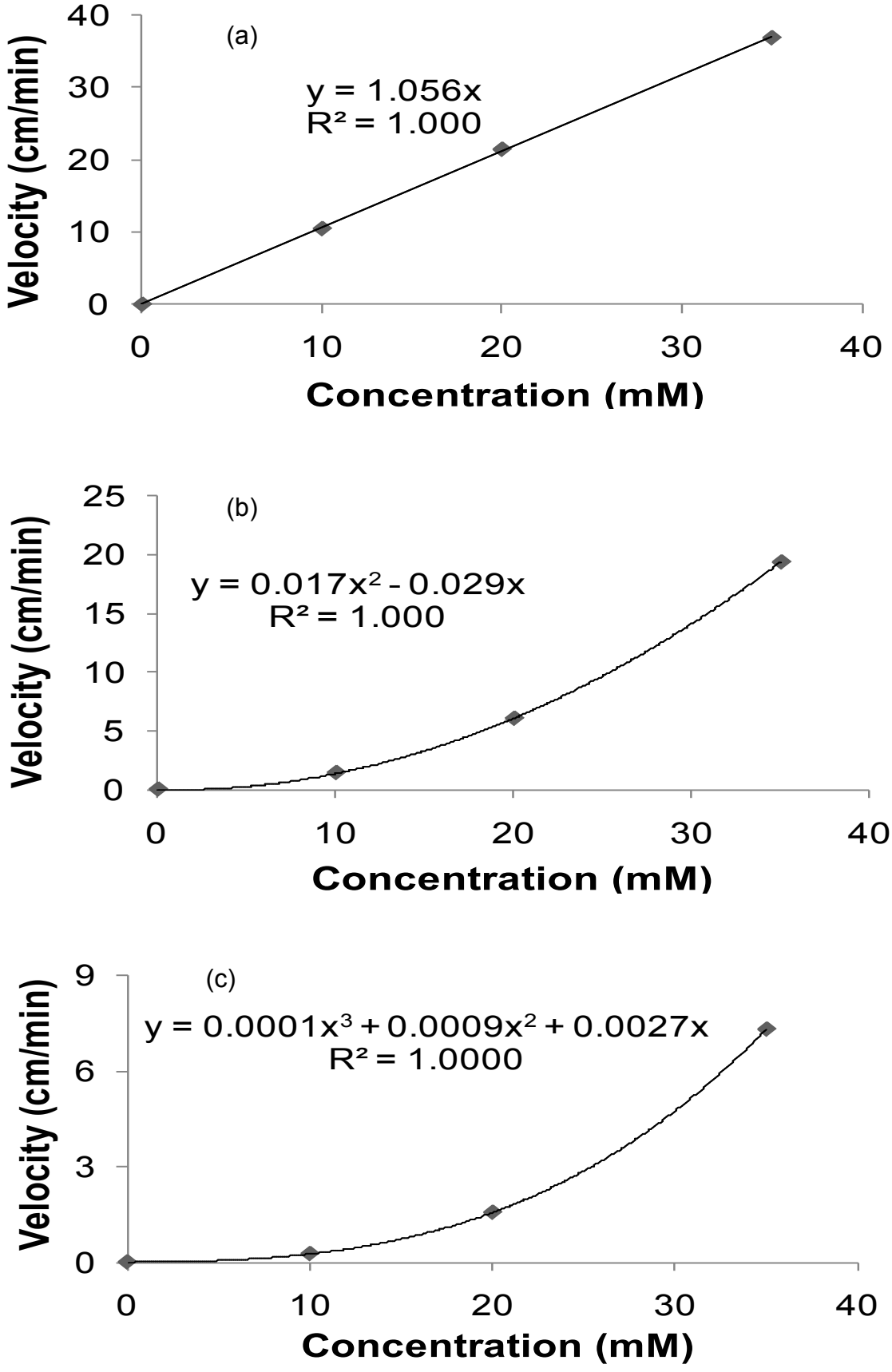

Figure 5.1 Velocities *versus* operating concentrations for (a) chloride, (b) sulfate and (c) phosphate at 0, 10, 20 and 35 mM on the AS16 column at 30°C

Using these general relationships it should be possible to simulate analyte retention under isocratic conditions, provided that the constants, m, n and o (where applicable) are known. This approach is discussed below.

The velocity of an analyte under isocratic conditions can be calculated using the following expression:

$$v(t) = m\left[E^-\right]_i^3 + n\left[E^-\right]_i^2 + o\left[E^-\right]_i \qquad \text{Equation 5.1}$$

while the retention time can be calculated using:

$$t_R = \frac{L}{v(t)} \qquad \text{Equation 5.2}$$

where L is the column length, which is normally 25 cm. From this, the retention of an analyte under isocratic conditions can be determined.

For instance, the retention time of iodide at 40mM can be easily predicted in the following manner. Iodide is a singly charged species, where m = 0, n = 0 and o = 0.133 (determined experimentally) meaning Equation 5.1 can be simplified to: $v = 0.133\ [E^-]$. Using this simplified Equation 5.1, the velocity of iodide can be mapped by entering $[E^-]$ to be 40. The retention time can be predicted using Equation 5.2. All the isocratic retention data were used for the calculation of coefficients (m, n and o) so no comparison between prediction and the observed data was possible at this stage. However the validity of this approach has been justified in Section 5.2.2.1.

5.2.2 Gradient Elution Mode

Investigation into the relationship between eluent profile and acceleration of analytes was based on the hypothesis that the retention in gradient separations relies on two components. The first is the initial velocity exhibited from the gradient starting concentration and the second is the acceleration exerted from the applied gradient slope. If a simple relationship between gradient conditions and analyte movement can be uncovered, then this relationship could be extended for predicting gradient separations. To this end, the retention behaviour of 38 analytes was investigated and a total of nine retention times were acquired for each analyte. These nine conditions

comprised three different concentration ramps and each beginning at one of three different starting competing ion concentrations. The retention data from the pre-existing data library was again converted to adjusted retention times by subtracting the system void time. The initial and final velocities of all analytes at the initial and final eluent concentrations were calculated using Equation 5.1. The average accelerations of the analytes were obtained from the difference between initial and final velocities over the adjusted retention times. It was assumed that there is no acceleration when the gradient ramp is 0 (that is under isocratic conditions). Therefore, there are a total of 12 acceleration data points corresponding to different gradient ramps and starting concentrations. **Figure 5.2** shows plots of the accelerations with respect to the gradient ramps. Different phenomena were observed for singly, doubly and triply charged species. The observed behaviour for uni-, di- and tri-valent analytes are comprehensively discussed below, using chloride, sulfate and phosphate as model analytes.

In all, 25 monovalent ions were studied and a linear relationship between acceleration and gradient slope was observed for all singly charged species. Figure 5.2(a) illustrates this observation using chloride as a case study. Notably, acceleration is directly proportional to the gradient ramp, as indicated by the straight lines. However, the three straight lines do not overlay with each other, which indicates that acceleration cannot be described by a simple function of gradient ramp. In addition to the slope of gradient, acceleration can also be seen to be strongly dependent on the eluent strength at the beginning of the applied gradient. Figure 5.2(b) illustrates the acceleration against gradient ramp for sulfate at three initial concentrations as a representative example for divalent ions. Acceleration is again observed to be related to the gradient ramp and this relationship can be represented by the quadratic curves. Acceleration of sulfate is again dependent on the initial eluent concentration at the start of the gradient, as well as on the effective charge. Likewise, Figure 5.2(c) demonstrates the acceleration data *versus* gradient slopes for phosphate at three different start

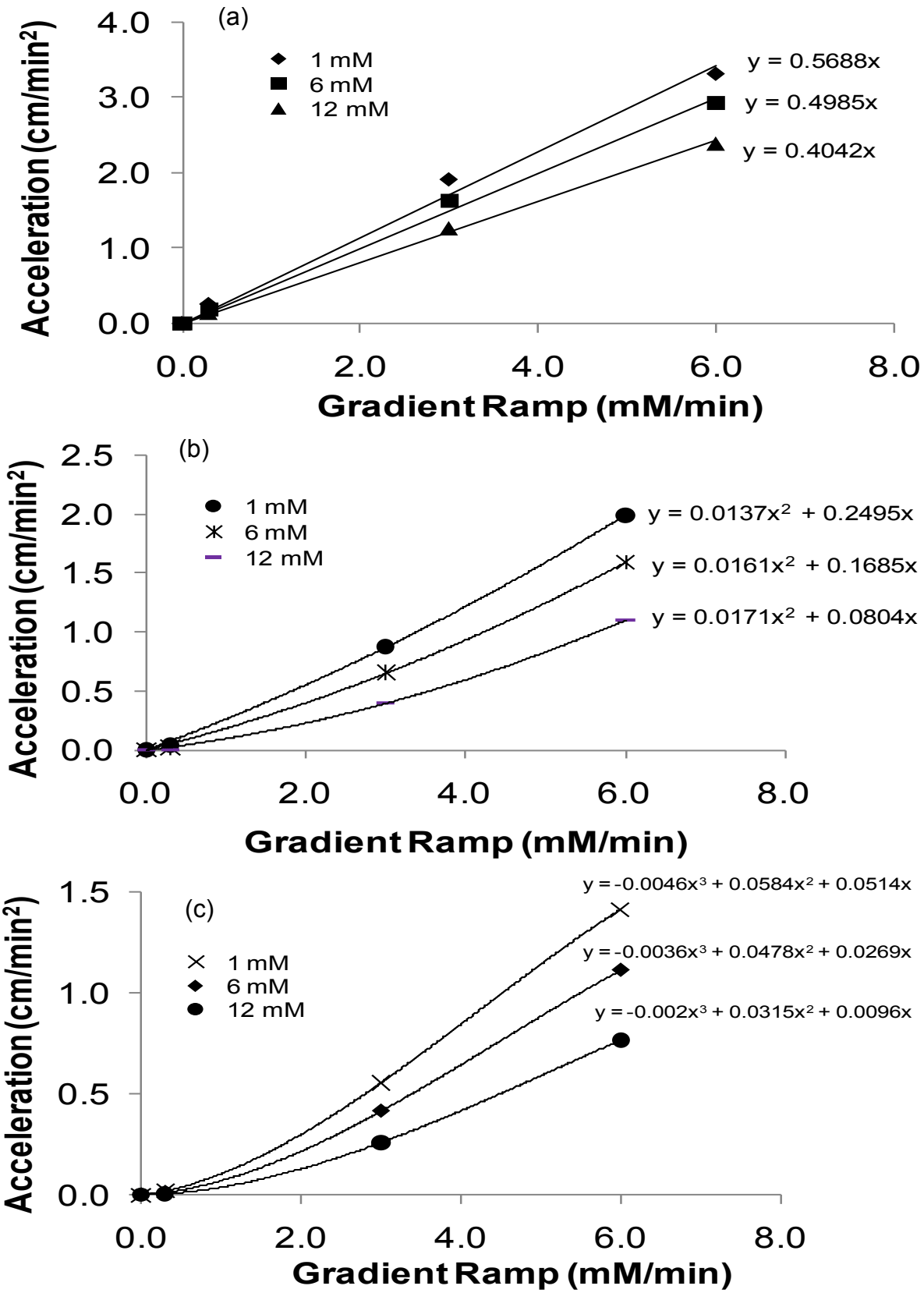

Figure 5.2 Accelerations against gradient ramps for (a) chloride, (b) sulfate and (c) phosphate at the starting concentrations of 1.0, 6.0 and 12.0 mM with three ramps of 0.3, 3.0 and 6.0 mM/min for each concentration on the AS16 column at 30^{o}C

concentrations. A cubic response relationship was observed but these are again dependent on the starting concentrations. The cubic curves are consistent with the fact that the effective charge for phosphate is 3 at the high pH of the eluent.

Further evaluation was carried out in an effort to ascertain the relationship between acceleration, initial concentration and gradient ramp. Typical results are presented in **Figure 5.3**. The observations for monovalent ions are represented in Figure 5.3(a), which shows that the acceleration is largely independent of the initial concentration at low gradient ramp of 0.3 mM/min while the magnitude of acceleration decreases as the initial concentration increases for greater gradient ramps at 3.0 mM/min and 6.0 mM/min. No consistent pattern was found and thus the relationship between the acceleration and the initial concentration remains elusive. Figure 5.3(b) and (c) show typical results for di- and tri-valent ions. Once again, a rugged and justifiable relationship could not be determined.

To this point, two important findings were noted from Figures 5.2 and 5.3 and these are summarised in **Table 5.2**. Firstly, the relationships of the acceleration *versus* the gradient slopes at each initial concentration for chloride, sulfate and phosphate were found to be linear, quadratic and cubic respectively, as observed for velocity under isocratic elution conditions.

Table 5.2 Summary of the relationships between the accelerations of singly (for example, chloride), doubly (for example, sulfate) and triply (for example, phosphate) against the applied gradient ramps

Effective Charge of Ion	Observational Relationship	Initial Concentration Effect
Singly	Linear	Positive
Doubly	Quadratic	Positive
Triply	Cubic	Positive

Secondly, none of the relationships of chloride, sulfate and phosphate were superimposable because of the strong influence of initial eluent concentration. This is also the limitation of Equation 4.1 (Rocklin *et al.*[57]) wherein the relationship between log k and log R is utilised to predict the

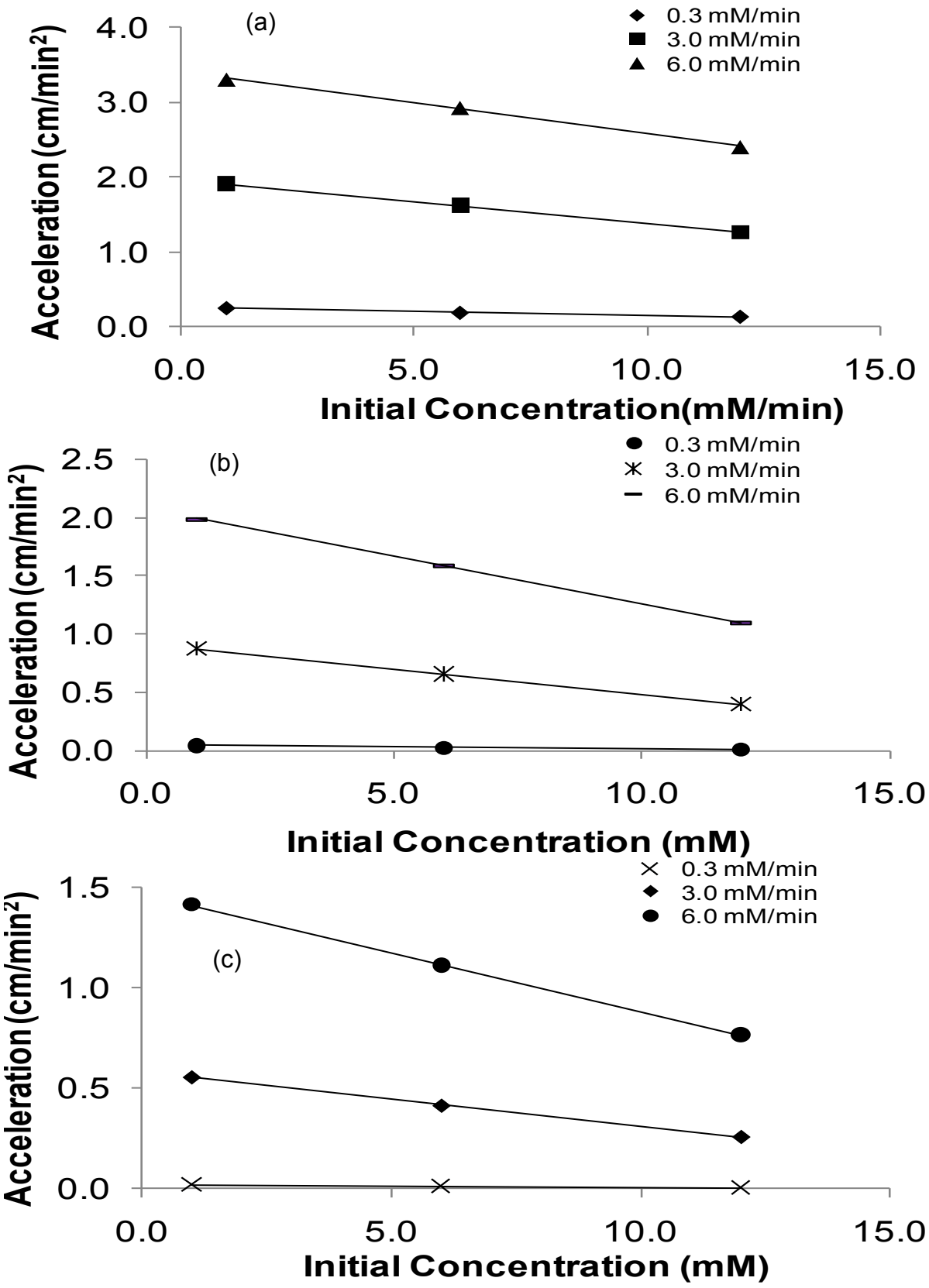

Figure 5.3 Accelerations against initial concentrations for (a) chloride, (b) sulfate and (c) phosphate at the gradient ramps of 0.3, 3.0 and 6.0 mM/min with three concentrations of 1.0, 6.0 and 12.0 mM for each ramp on the AS16 column at 30^{o}C

retention of ionic species in gradient elution. These analogous models are useful for predicting the retention in a gradient, but both suffer the same fundamental flaw. Since neither model can cope with the changes in initial eluent strength, neither of them provide the equivalent level of flexibility provided by Jandera's approach[9] (Equation 1.14) used in earlier phases of this work. Consequently, any further attempts to utilise acceleration in retention prediction were abandoned.

5.2.2.1 Solution for Retention Simulation of Gradient Conditions

Under gradient conditions the eluent profile involves an increase in competing ion concentration as time progresses. Therefore the gradient eluent profile can be segmented into very small sequential incremental isocratic steps. For example, the gradient eluent profile can be divided into 0.05 min segments and it can be assumed that the eluent concentration remains approximately isocratic within the 0.05 min increment, as shown in **Figure 5.4**. From this, the simulation of retention time can be calculated as follows:

First, the concentration, $[E^-]_j$, within this 0.05 min is given by:

$$\left[E^-\right]_j = \left[E^-\right]_i + Bt_j \qquad \text{Equation 5.3}$$

where $[E^-]_i$ denotes the initial concentration, B is the applied gradient ramp and subscript j denotes a single instantaneous step.

Equation 5.1 is employed to track the instantaneous velocity. The distance of the analyte moves within this 0.05 min segment can then be mapped using the following equation,

$$L_j = vt_j \qquad \text{Equation 5.4}$$

When the summation of L_j matches the column length, the final fraction of retention can be expressed as follows:

$$t_f = \frac{L_R}{v} \qquad \text{Equation 5.5}$$

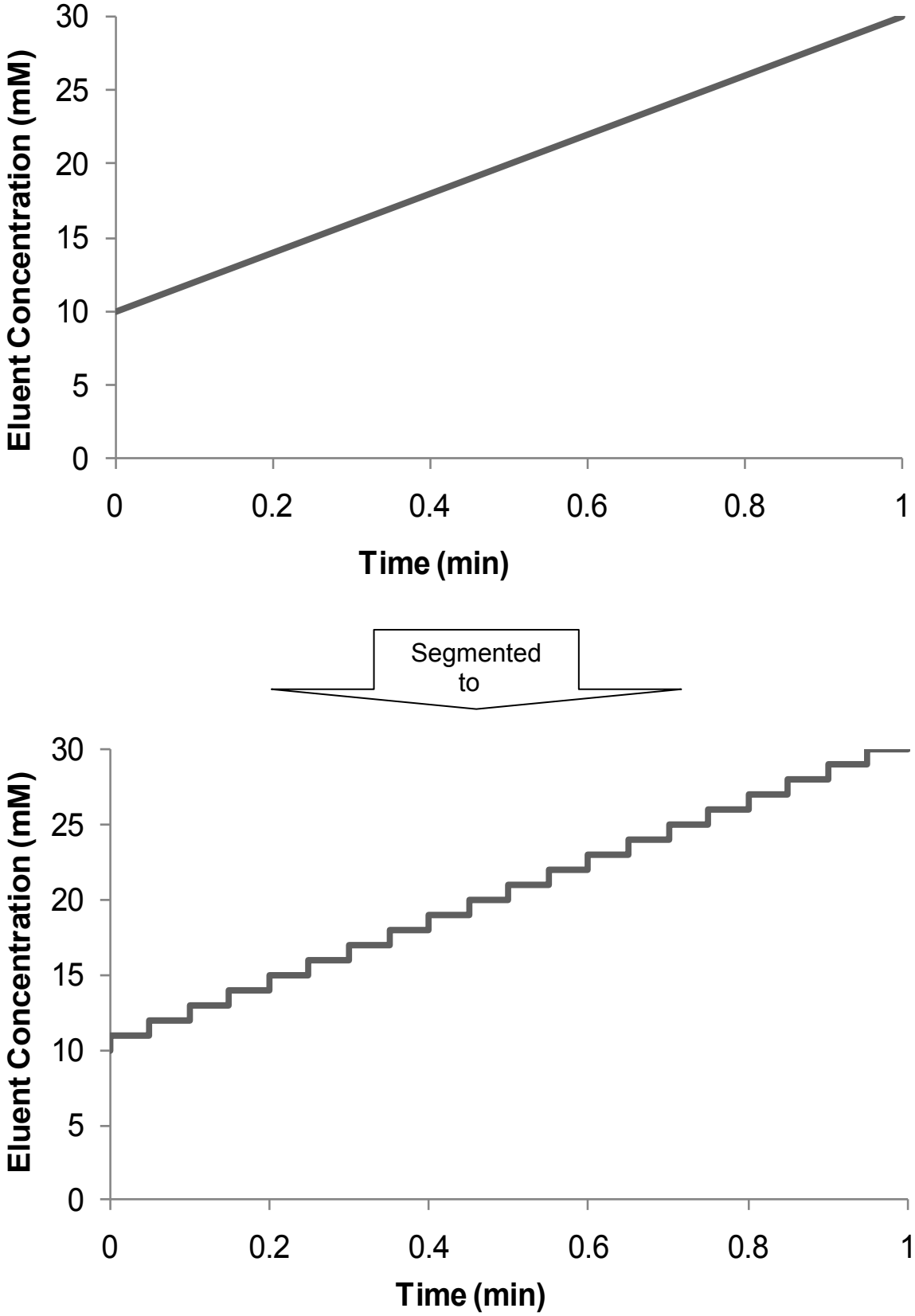

Figure 5.4 Schematic segmentation of a linear gradient eluent profile into a series of incremental isocratic steps to represent the overall eluent profile.

where t_f is the final fraction of retention which will be less than or equal to 0.05 min and L_R is the remaining distance to the end of the column. Summation of t_j, t_f and void time, t_m, will yield the retention time of the analyte.

$$t_R = t_f + t_m + \sum_{j=1}^{n-1} t_j \qquad \text{Equation 5.6}$$

Figure 5.5 illustrates the flow chart used to simulate a single-step, linear gradient eluent profile. The iteration will terminate when the distance travelled by the analyte matches the column length.

This new derived algorithm was initially employed to simulate the retention of 24 anions on 3 anionic columns (AS11 HC, AS16 and AS19) and 13 cations on 2 cationic columns (CS12A and CS16) over 5 gradient conditions on each column, which are bolded in Table 4.1.

All retention data were simulated using this algorithm and the predicted retention times were evaluated by comparing with the observed retention data. **Figure 5.6** shows all observed data *versus* all simulated data and indicates the high correlation for both anions and cations. The average percentage difference between observed and predicted retention times was 3.01% for both anions and cations. It should be noted again that the isocratic data used as a basis for calculation of gradient retention data were obtained on different column batches and chromatographic systems than those used for the observed retention data. Under these circumstances, the degree of correlation shown in Figures 5.6 is remarkable and this is highly promising for simulation of retention times under complex eluent profile conditions.

5.2.3 Complex Eluent Profiles (Method 3)

As indicated previously, the purpose of this chapter was to derive a simple predictive algorithm for multi-step gradient separations consisting of both isocratic and gradient steps. It is possible for the complex eluent profile to be segmented into incremental isocratic steps in the same manner as shown in Section 5.2.2.1. **Figure 5.7** shows a schematic illustration of a 3-step gradient profile with the linear gradient divided into incremental isocratic steps.

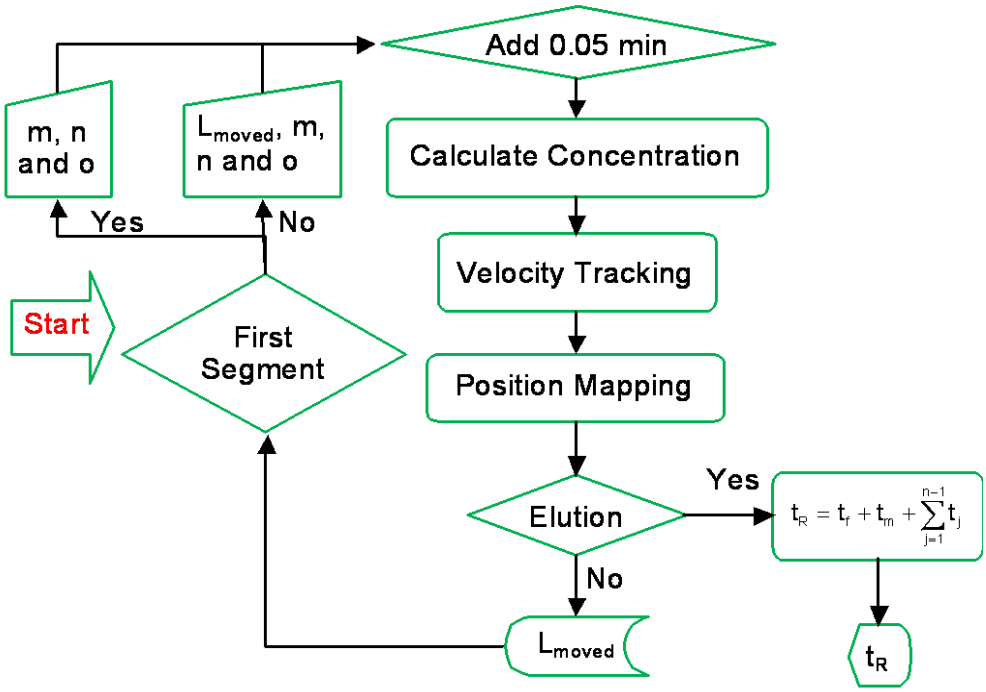

Figure 5.5 Flow chart for the predictive algorithm using the numerical incremental isocratic steps approach to represent a linear gradient.

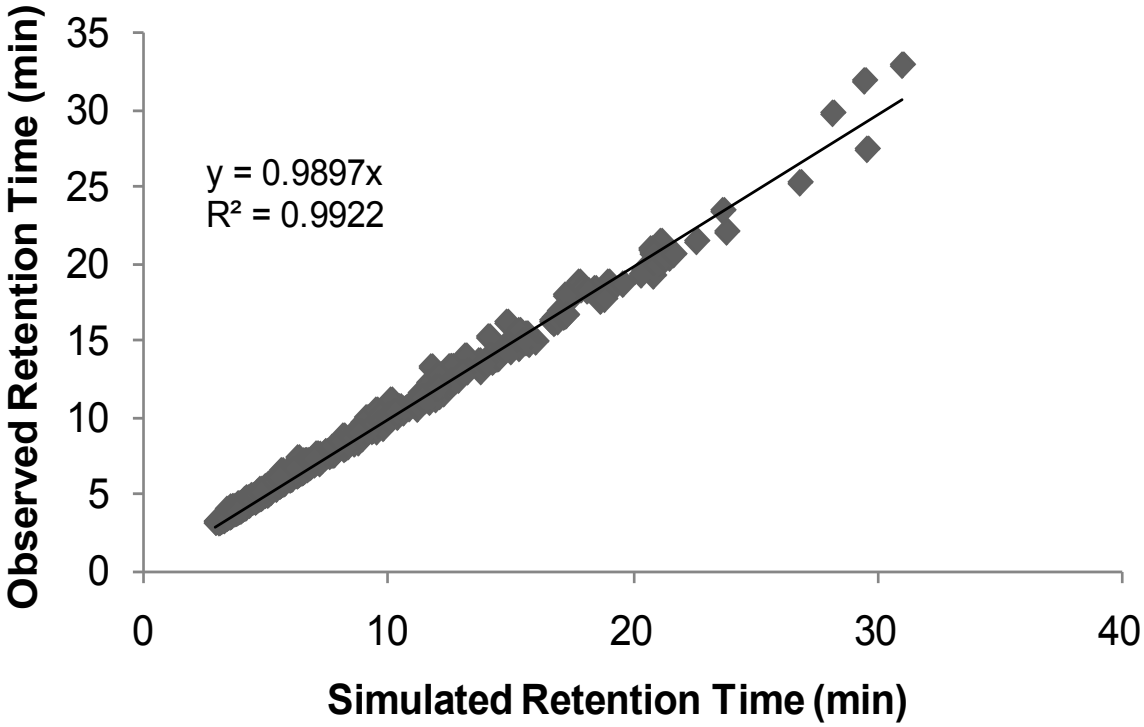

Figure 5.6 Experimental retention times *versus* simulated retention times of the 24 anions and 13 cations bolded in Table 4.1 on the Dionex AS11 HC, AS16, AS19, CS12A and CS16 columns for 5 linear gradient conditions at 30°C for anion analysis and 40°C for cation analysis.

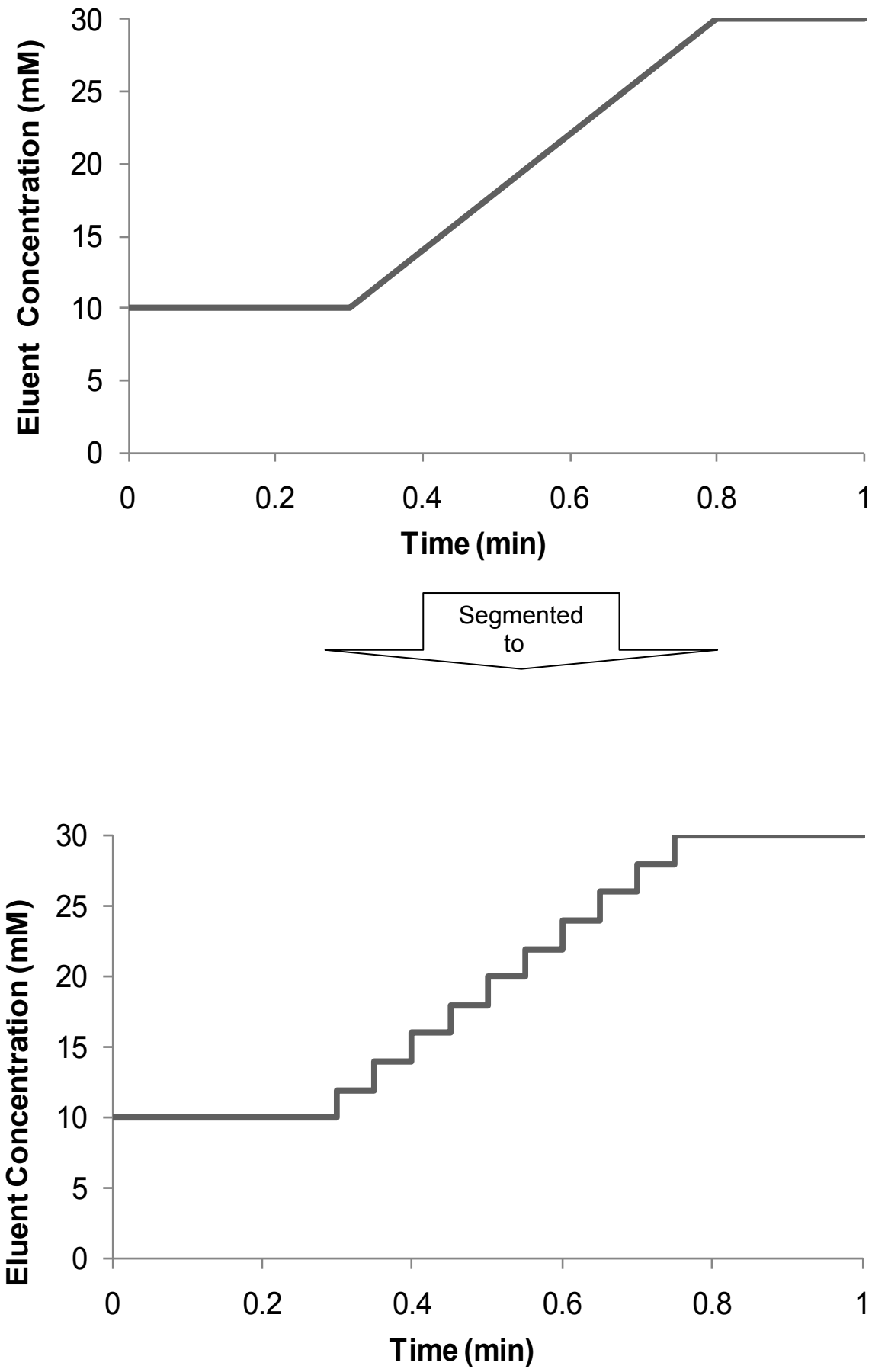

Figure 5.7 Schematic illustration of 3-step gradient profile into incremental isocratic profile

The simulation of a complex eluent profile was performed using the identical procedure for single step gradient profiles described previously in Section 5.2.2.1. The previous equations and flow chart were therefore applicable to monitor the retention times for complex eluent profiles. The algorithm was used to map the position of the analyte at the end of each instantaneous isocratic step. Since displacement and time are interchangeable, the retention time was easily determined.

A detailed evaluation was made of the accuracy of retention predictions under four elution conditions involving complex eluent profiles. The algorithm was initially applied to 24 anionic analytes on the Dionex AS11 HC, AS16 and AS19 columns and 13 cationic analytes on the Dionex CS12A and CS16 columns, as bolded in Table 4.1. The results of this evaluation are shown in **Figure 5.8**, from which it can be seen that excellent agreement was obtained between experimental and predicted retention times. The average percentage difference was 3.78%. As discussed, this error includes differences in the tubing combination and batch-to-batch variability, therefore the actual error should theoretically be less than the reported 3.78%.

5.2.4 Comparison of Predictive Algorithms for Complex Elution Systems

This study has resulted in the derivation of three predictive algorithms to simulate the retention of analytes under complex elution profiles, and as such a comparison of these three algorithms is warranted. **Table 5.3** details a qualitative comparison of all three algorithms. In this comparison, Methods 1 and 2 are the algorithms discussed in Chapter 4 (Sections 4.5 and 4.5.1) and Method 3 is the numerical incremental isocratic steps algorithm detailed in Section 5.2.2.1.

All methods were found to give approximately 4% error in predicting retention times for a total of 38 analytes on 5 columns over twenty 5-step eluent profiles with different complexity. From Section 3.4, it was determined that a typical 30 min separation window can only tolerate a 2.5% in difference between the prediction and the experimental data. This indicates that the

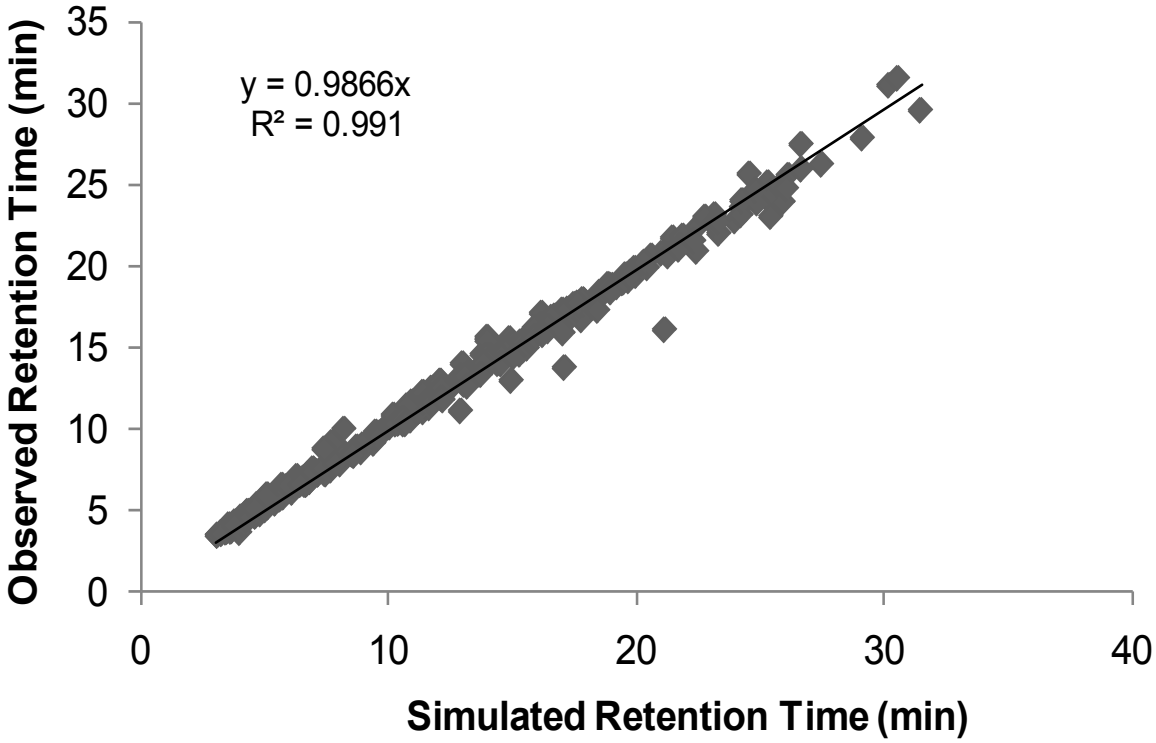

Figure 5.8 Experimental retention times *versus* simulated retention times for 24 anions and 13 cations bolded in Table 4.1 on the AS11 HC, AS16, AS19, CS12A and CS16 columns for 4 5-step complex eluent profiles at 30^{o}C for anion analysis and 40^{o}C for cation analysis

Table 5.3 Detailed comparison of Method 1, 2 and 3 in terms of percentage differences, velocity and displacement information, position mapping methods, calculations per analyte per profile and processing time per profile.

Description	Method 1	Method 2	Method 3
Reported percentage difference	5%	3%	4%
Velocity description	No	No	Yes
Displacement description	Yes	Yes	Yes
Position mapping method	Iterative tool (Goalseek on Excel)	Displacement incorporated equation (Equation 4.13)	Laws of motion (Equation 5.4)
Calculations per analyte per profile	35	25	6300
Processing Time per profile	Approximate 25 seconds per five step profile on Excel	Instantaneous on Excel	Less than 1 second on Excel

current approaches do not meet this expectation, but they are all very close to this requirement.

Method 1 involves sizeable iterations (see Table 5.3) per profile and this process generally takes an average of 25 seconds to calculate retention for a new set of conditions using a duo core processor desktop computer consisting of 1.8 GHz CPU processing power and 1 GB RAM. In addition, Method 1 relies solely on a mathematical descriptor to map the analyte position. Method 2 is largely identical to Method 1, except that it uses a direct solution for position mapping instead of the iterative approach, and therefore yields very fast processing times. Method 3 tracks both velocity and displacement, which involves a series of calculations to follow the movement of an analyte through the column. Methods 2 and 3 offer similar processing time of less than 1 second, i.e. they are “real time simulators”, while method 1 requires manual processing.

In terms of reliability of the simulation, Method 2 delivers the best accuracy and speed, however, it is greatly influenced by the void time of the system. A change of void time would lead to a dramatic decrease in the predictive accuracy and this factor makes this approach somewhat questionable. In comparison, Methods 1 and 3 take longer to simulate, but have greater reliability since they are not as susceptible to changes in the void time of the system. In conclusion, Methods 1 and 3 have much better predictive algorithms for simulation of retention times under complex eluent profiles.

5.3 Peak Width Modelling

In 2010, a collaboration was initiated with a research group in Slovenia. This group[1] have proposed an empirical peak width model which is highly similar to the width model proposed in 1974 by Jandera *et al.*[9]. Both models measure the gradient peak width based on the instantaneous isocratic retention factor of the solute at the time the peak maximum leaves the column.

This model found an observed linear relationship between the peak width, w, and the equivalent isocratic retention factor of the analyte, k_f, at the outlet of the column as the analyte is eluted. This empirical model is given by:

$$w = m + n k_f \qquad \text{Equation 5.7}$$

where m and n denote the parameters obtained from linear regression method. In practice, m and n are normally estimated on the basis of experiments in which the peak width is measured at a limited number of isocratic retention factors and the resultant data are fitted to Equation 5.7. The retention factor of the analyte, k_f, at the outlet of the column as it is eluted can be easily mapped using Equation 1.11.

This model was initially employed to simulate peak width on two anion-exchange columns (Dionex AS11 HC and AS19) for 24 anions and on the Dionex CS12A cation-exchange column for 13 cations as detailed in Table 4.1. This simulation was performed over five gradient conditions (**Figure 5.9**) and four complex elution profiles comprising a combination of five separate isocratic and gradient steps (**Figure 5.10**) on each column.

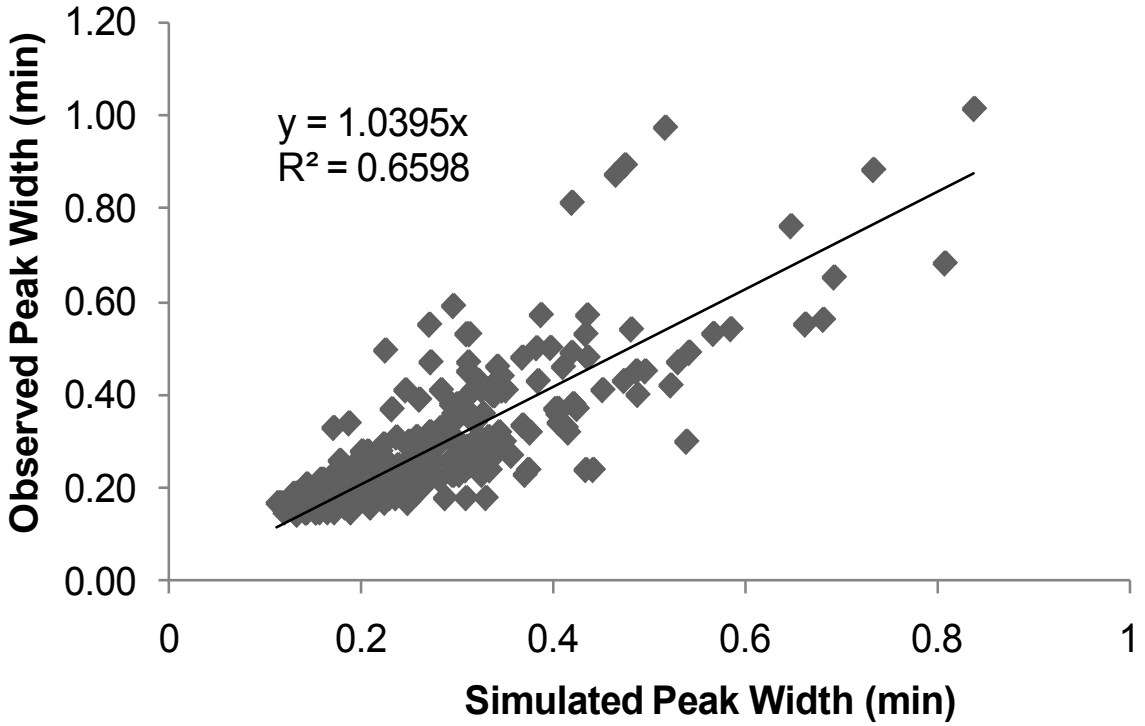

Figure 5.9 Experimental peak widths *versus* simulated peak widths of 24 anions and 13 cations bolded in Table 4.1 on the AS11 HC, AS19 and CS12A columns for 5 single step gradient conditions at 30°C for anion analysis and 40°C for cation analysis

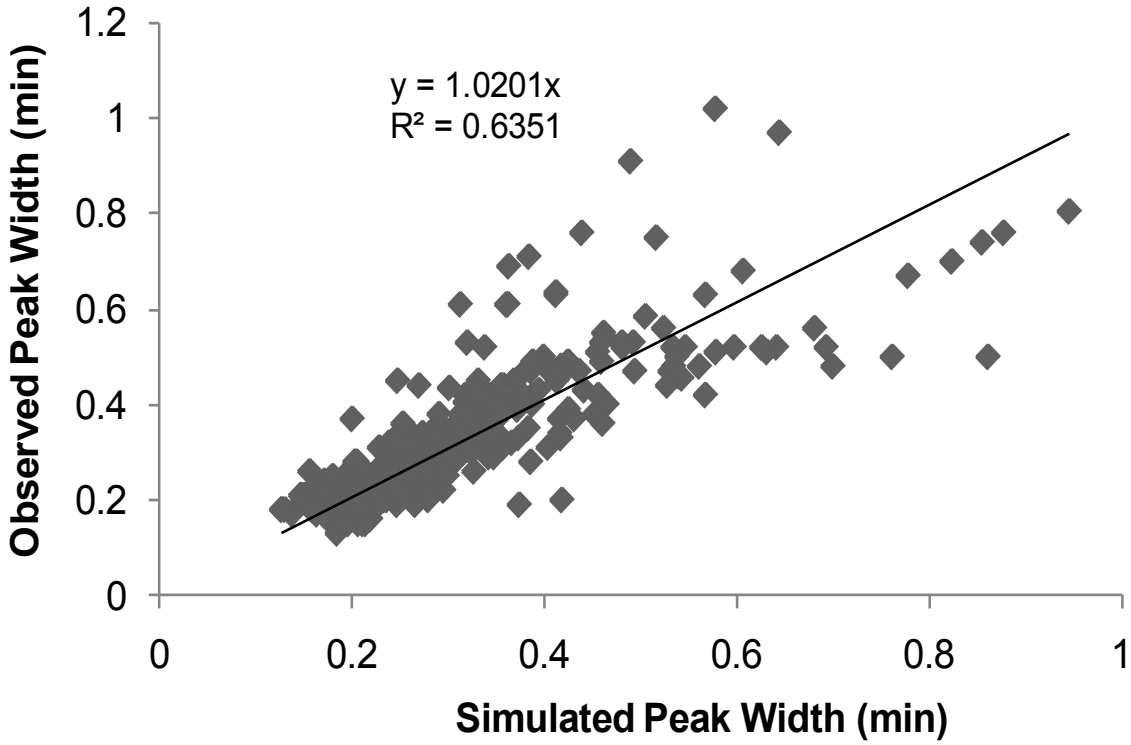

Figure 5.10 Experimental peak widths *versus* simulated peak widths for 24 anions and 13 cations bolded in Table 4.1 on the AS11 HC, AS16, AS19, CS12A and CS16 columns for 4 5-step complex eluent profiles at 30°C for anion analysis and 40°C for cation analysis

Figures 5.9 and 5.10 show all observed data *versus* all simulated data and these figures indicate the high correlation for both anions and cations. Here it can be seen that satisfactory agreement was obtained between experimental and predicted peak widths. The average percentage difference between observed and predicted peak widths for gradient conditions and complex elution method was found to be 17%.

The peak width prediction algorithm explained in Sections 4.4 and 4.6 relies on integrating the compression exerted from each individual step, hence it differs significantly from this model where the prediction of peak width incorporates the eluting retention factor of the analyte. Since this empirical model disregards the compression caused by the gradient, this potentially indicates that a decrease in the accuracy and precision of the peak width simulation may be seen. This is borne out in the lower R squared values observed in Figures 5.9 and 5.10 compared to Figures 4.4 and 4.9 indicating that the peak width prediction using this model has a lower precision. However, the predictive ability of this peak width model was found to be slightly superior to the peak width model discussed in Sections 4.4 and 4.6. This model was shown to have same predictive error of 17% for linear gradient separations as model employed in Section 4.4 while the peak width prediction for complex eluent profiles using this model (17%) was slightly superior to the model discussed in Section 4.6 (19%). The higher than expected accuracy of this model compared to that in Section 4.6 indicates that the compression prediction exhibited from each step is not as crucial as first thought, and also demonstrates that the elution retention factor is the only critical information required for accurate peak width prediction. Therefore, this peak width model is a more superior model due to its accuracy and simplicity.

According to Section 3.4, a percentage error of up to 35% is tolerable for peak width simulation, which means that both models (Sections 4.6 and 5.3) were deemed to achieve the goal of reliable peak width simulation.

5.4 Comparison of Simulated and Observed Chromatograms

The capability of Method 3 can be assessed using the observed separations of two sample mixtures containing 11 anions and 10 cations respectively (as described in Section 4.7). Simulated chromatograms of these two mixtures were predicted using Method 3, followed by comparison with experimental chromatograms to determine the accuracy of the prediction.

Figure 5.11 shows the simulated and observed chromatograms of the 11 component anion mixture eluting in the order of 1-fluoride (5 ppm), 2-chlorite (5 ppm), 3-bromate (5 ppm), 4-chloride (5 ppm), 5-nitrite (5 ppm), 6-chlorate (10 ppm), 7-bromide (5 ppm), 8-nitrate (5 ppm), 9-carbonate (15 ppm), 10-sulfate (10 ppm) and 11-phosphate (15 ppm) using a 3-step sequential profile.

Figure 5.12 presents the 10 component cation mixture which was found to elute in the order of 1-lithium (I) (5 ppm), 2-sodium (I) (5 ppm), 3-ammonium (5 ppm), 4-ethylammonium (5 ppm), 5-potassium (I) (5 ppm), 6-magnesium (II) (10 ppm), 7-calcium (II) (10 ppm), 8-strontium (II) (10 ppm), 9-cesium (I) (15 ppm) and 10-barium (15 ppm) using a 5-step eluent profile. Excellent agreement was observed between the actual and predictive chromatograms for the 11-component anion sample (Figure 5.11). Figure 5.12 illustrates excellent predictions for lithium, sodium, ammonium, ethylamine, calcium and strontium, while the predictions for potassium, magnesium, cesium and barium were reasonable. A co-elution problem was observed in the simulated chromatogram for potassium and magnesium whereas the predictions for barium and cesium were slightly out of place. Utilisation of finer increments (such as 0.01 min rather than the 0.05 min segments used, see Section 5.2.2.1) in profile segmentation might slightly improve the accuracy but this will also increase the processing time exponentially. Overall, Method 3 has a satisfactory accuracy in retention predictions.

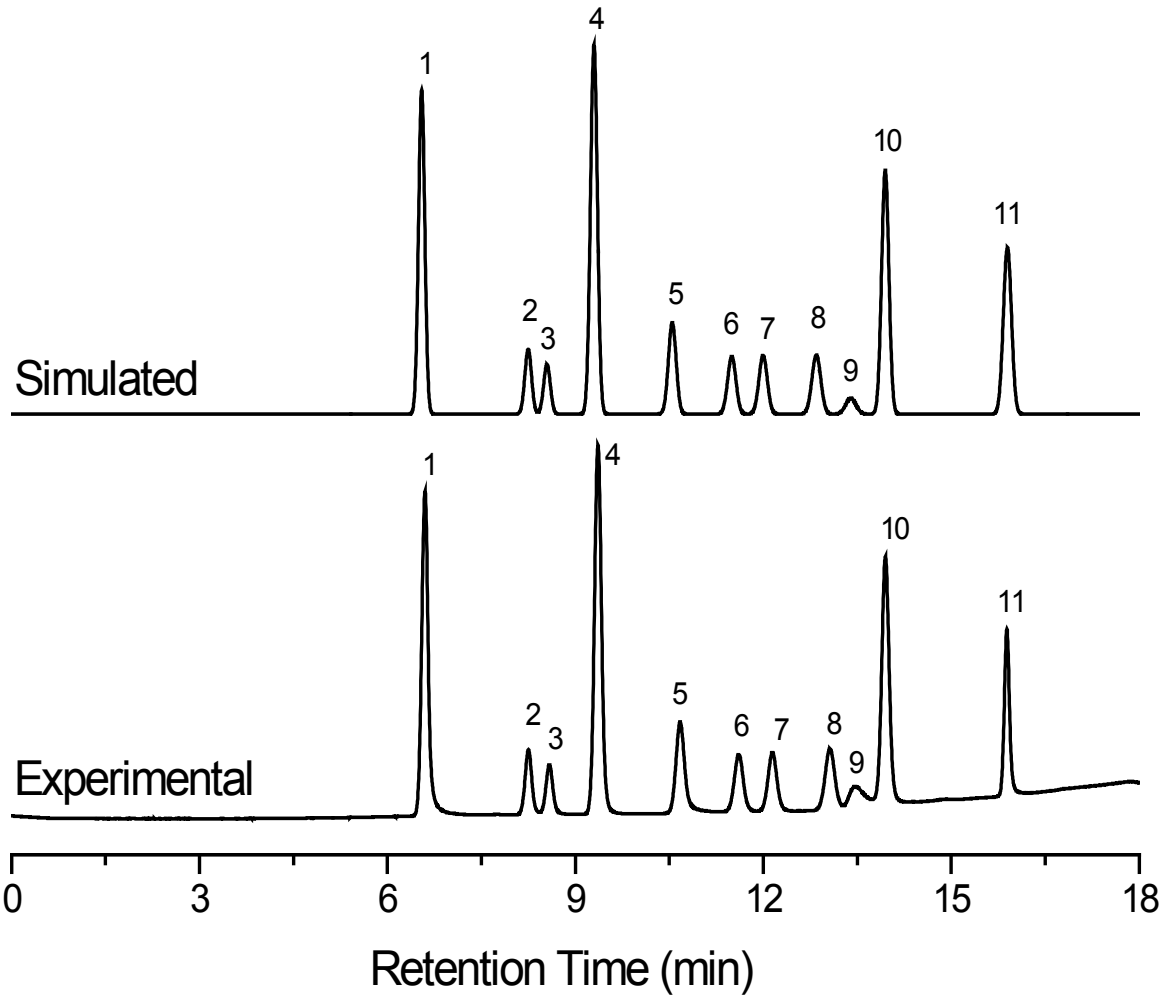

Figure 5.11 Simulated and experimental separations of 11 anions eluting in the order of 1-fluoride (5 ppm), 2-chlorite (5 ppm), 3-bromate (5 ppm), 4-chloride (5 ppm), 5-nitrite (5 ppm), 6-chlorate (10 ppm), 7-bromide (5 ppm), 8-nitrate (5 ppm), 9-carbonate (15 ppm), 10-sulfate (10 ppm) and 11-phosphate (15 ppm) on the Dionex AS19 column under a 3-step gradient profile consisting of: 3.75mM KOH for 0.8 min, 3.75 to 33.75mM KOH for 10 min followed by 33.75 to 99.75mM KOH for 4 min at 1mL/min at 30^{o}C where retention predictions rely on Method 3 (Section 5.2.2.1)

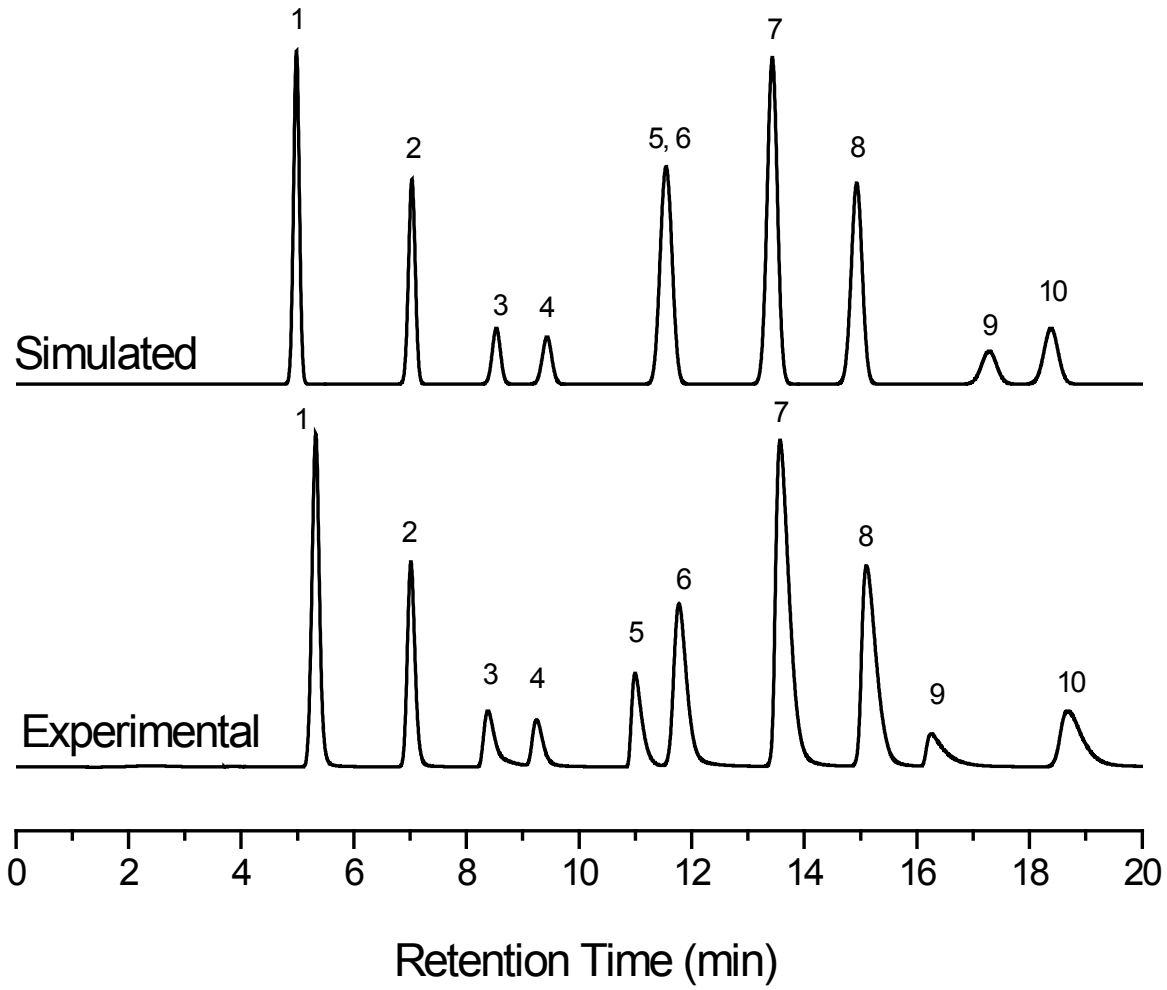

Figure 5.12 Simulated and experimental separations of 10 cations eluting in the order of 1-lithium (I) (5 ppm), 2-sodium (I) (5 ppm), 3-ammonium (5 ppm), 4-ethylammonium (5 ppm), 5-potassium (I) (5 ppm), 6-magnesium (II) (10 ppm), 7-calcium (II) (10 ppm), 8-strontium (II) (10 ppm), 9-cesium (I) (15 ppm) and 10-barium (15 ppm) on a Dionex CS16 column under a 5-step gradient profile consisting of: 30 to 35 mM for 3 min, 35 to 50 mM for 3 min, 50 to 60 mM for 3 min, 60 to 80 mM for 3 min followed by 80 to 95 mM for 12 min at 1mL/min, at 40^{o}C where retention predictions rely on Method 3 (Section 5.2.2.1)

5.5 Chapter Conclusions

In conclusion, this study demonstrates that an analyte moves at constant velocity under isocratic conditions and accelerates under gradient conditions, but this acceleration is dependent on the applied gradient ramp as well as the initial concentration. A different set of gradient constants will therefore be required for each initial eluent concentration used to start the gradient. This limitation is also evident in Equation 4.1.

A numerical incremental isocratic step algorithm for gradient elution profiles was then implemented to overcome the problems encountered with gradient conditions. This method was applied to the simulation of retention time for substantial sets of analytes and columns. The major finding of this chapter was that this algorithm had good predictive ability for both anionic and cationic samples using complex eluent profiles, although the predictive ability is similar to Method 2.

A detailed comparison for all methods was undertaken. The three algorithms possess different strengths and weaknesses. Overall, Method 3 is the most flexible algorithm due to its simplicity and accuracy. None of the tested models provides the level of accuracy for retention time prediction (error ≤ 2.5%) established as the target level in Chapter 3.

A peak width model proposed by Drgan *et al.*[1] was utilised for the simulation of peak widths of analytes separated under complex eluent profiles, and it was found to deliver an average percentage error of 17% when compared to observed data. This approach was slightly superior to the previous peak width model (average error of 19%) discussed in Sections 4.4 and 4.6. Both models provide accuracy which meets the threshold requirement of ≤ 35% for error.

Chapter 6

Methodology for porting retention prediction data from conventional-scale to miniaturised ion chromatographic systems

6.1 Introduction

In recent times there has been an increasing focus on research associated with the miniaturisation of liquid chromatography (LC) techniques. This impetus has been supported by the wider availability of smaller diameter columns from commercial vendors and has been driven in part by an increased awareness of enhancing detection limits, reducing running costs, maintaining continuous instrument operation, and minimising environmental pollution by solvents and chemicals. Importantly, the use of miniaturised systems often opens opportunities for achieving faster separations, and thus it supports a long-standing goal of research in separation science. In the simplest instance miniaturisation is achieved by using narrow-bore separation columns, leading to micro-, capillary-, and nano-scale chromatography. The use of narrow-bore columns is a recognisable intermediate technique between conventional LC and microchip separations [84] and the concepts that lead to narrow-bore LC will be useful in designing approaches for even smaller scare separations. In miniaturising any method, it is important to comprehend the effect that changing the column dimensions has on the integrity of the existing separation.

When scaling down from conventional scale to narrow-bore LC, it is often desirable to keep the separation selectivity constant, because a great deal of effort will have typically gone into optimising and validating the existing method. However, the goal of using the miniaturised separation system may also be to reduce the analysis time. Miniaturising the separation system can also result in changes in the overall peak distribution pattern of analytes if proper precautions are not taken. Several years ago Blumberg, and Klee described the concept of method translation for gas chromatography (GC) [85, 86], which permits the variation of components

(columns, carrier gases, detectors, etc) and method parameters (pressures, temperature program etc) without affecting the peak elution pattern. Recently, Guillarme *et al.* described an approach for method transfer in LC [87]. Although this approach works well for translation to shorter columns[87], if the column inner diameter or the diameter of the packing material is altered, then changes in overall separation selectivity will be observed. Guillarme *et al.* attributed this to dwell volume effects [87]. However, selectivity changes exist even if careful attention is paid to correcting dwell volume and such selectivity changes to changes in phase ratio. This rationale is consistent with the theory supporting method translation in GC, which clearly states that phase ratio is a non-translatable parameter [85, 86]. If the phase ratio in a liquid chromatography system cannot be maintained by careful scaling of both the column internal diameter and the stationary phase particle diameter, then method re-optimisation will usually be required to compensate for any selectivity changes introduced as a result of miniaturisation.

There have been significant interests in ion chromatography (IC) separations as well as in the miniaturisation of IC systems and during the last decade a number of strategies for retention prediction and the simulation and optimisation of IC that involve variations of the linear solvent strength retention equation were devised [5, 56, 88]. These strategies are based on a database of carefully measured isocratic and linear gradient retention data obtained for a wide range of analytes and IC columns, with these data being “embedded” into the software used to simulate separations. These data were acquired some years ago using conventional 4 mm diameter IC columns, and through the use of a range of mathematical algorithms these data permit the calculation of retention times for analytes on 4 mm diameter columns using eluent compositions which are isocratic, linear gradient, or multi-step elution profiles comprising a combination of the two. Rapid *in-silico* optimisation of IC separations can therefore be undertaken. The lifespan of the existing database remains questionable. This is because every column has a minor batch-to-batch variability despite the same packing material and procedure being employed. The variability causes each existing database to be

technically valid only for the particular column. Therefore each new column will need a recalibration in order to perform reliable retention prediction.

In the present study a method was devised to address the question of how the existing retention database can be implemented to permit prediction of retention times on new columns which may exhibit batch-to-batch variability, and also in miniaturised IC column formats using columns having diameters different to that which was used to acquire the original retention data. This procedure is described as "*porting*", wherein the retention database is recalibrated to account for the stationary phase and column differences. Porting leads to substantially improved accuracy of predicted retention times and hence more reliable *in-silico* optimisation of IC separations. It is important to note that there are two retention databases (existing and new databases) created for the each same column. The existing database is currently embedded in Virtual Column Separation Simulator, whilst the new database is freshly acquired from experiments in order to evaluate the difference between the two databases.

6.2 Effects of Altering Column Diameter

In principle, an isocratic separation method developed for a column of a particular diameter can be translated to a column of a different diameter by simply adjusting the eluent flow-rate in proportion to the square of the radius of the two columns. In the case of gradient separations or when using complex elution profiles which comprise both isocratic and gradient steps, it is also necessary to normalise the elution profile to account for the change in void volumes resulting from changing the column diameter. Thus, if the column diameter is halved, the flow-rate should be reduced by a factor of 4. However, this simple method translation is valid only when altering the column diameter causes no change in the fundamental parameters which govern the separation.

Before considering miniaturising an ion-exchange separation it is therefore pertinent to evaluate how modifying column dimensions might affect the separation. Retention in ion-exchange chromatography is described by the equation (Equation 1.10)[2]:

The total ion-exchange capacity of a column can be calculated from Q and w. However, altering the total ion-exchange capacity does not influence k provided that Q remains unaltered and the same isocratic or normalised eluent composition is used. This is illustrated in **Figure 6.1**, which shows the separation of a mixture of fluoride, chlorite, bromate, chloride, nitrite, nitrate, chlorate, carbonate, sulfate, and phosphate using a 250 mm x 4 mm i.d. IonPac AS11 analytical column (Figure 6.1(a)) or two IonPac AS11 analytical columns joined in series (Figure 6.1(b)). A three-step complex elution profile was used for each separation, with the eluent profile adjusted for the different void volumes of each separation system. The total ion-exchange capacity differs for each chromatogram but since the same stationary phase material has been used, retention factors and separation selectivities are identical.

Reducing column inner diameter will invariably lead to a small change in the ratio w/V_m (which is defined as the phase ratio) due to the increased influence of wall effects in packed columns of small diameter. In such situations simple method translation will not be possible. To illustrate this effect, chromatograms of suitable test solutes were collected using a Dionex 250 mm x 4 mm i.d. IonPac AS19 analytical column and a Dionex 250 mm x 2 mm i.d. IonPac AS19 analytical column. In this experiment both column formats (4 mm and 2 mm i.d.) were packed with identical 7.5 μm stationary phase material so the two column formats will have slightly different phase ratios due to wall effects. The retention factors for the two separations are shown in **Table 6.1** and clearly demonstrate non-equivalent separations.

Table 6.1 Retention factors for the IonPac AS19 4mm i.d. and 2 mm i.d. columns using 25 mM hydroxide as eluent. The void times were 2.785 min for the 4 mm i.d. column operating at 1 mL/min and 2.868 min for the 2 mm i.d. column operating at 0.25 mL/min.

Anion	k (4 mm i.d.)	k (2 mm i.d.)	k_{2mm} / k_{4mm}
Fluoride	0.28	0.30	1.06
Nitrate	1.53	1.25	0.82
Thiocyanate	5.95	4.53	0.76
Perchlorate	6.89	5.16	0.75

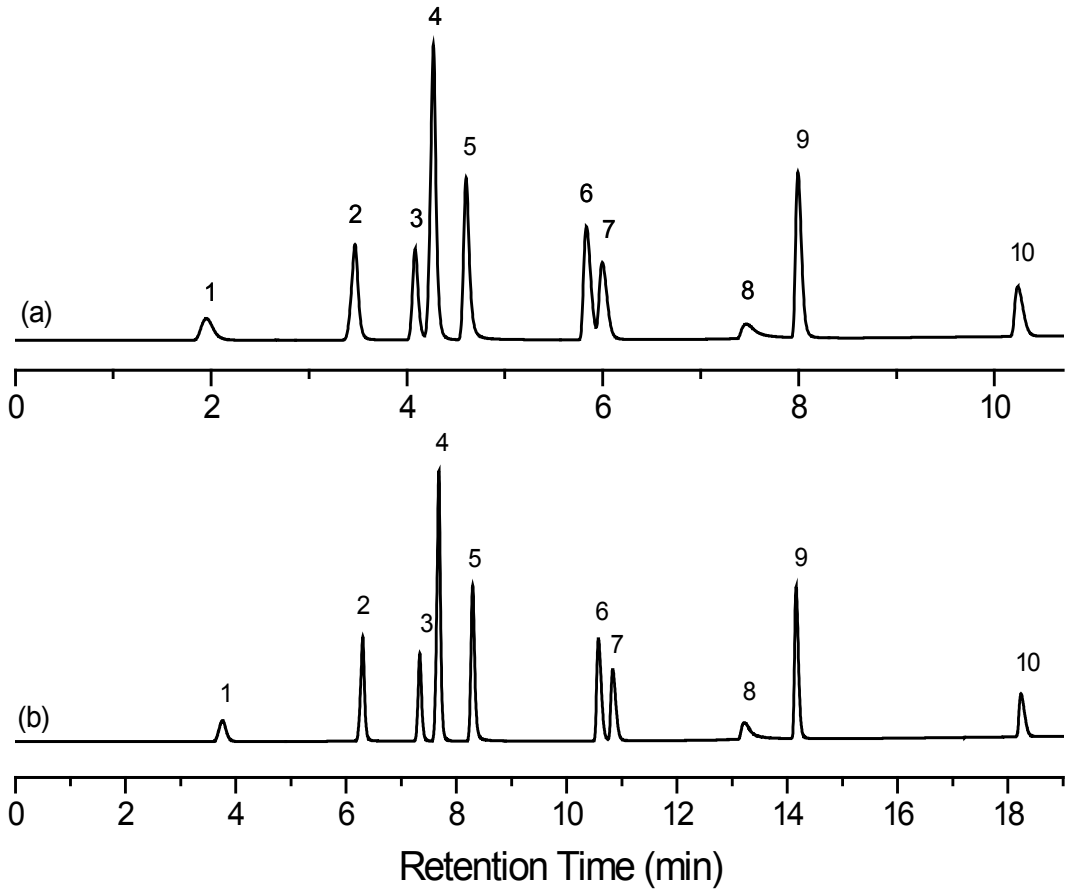

Figure 6.1 Comparison of the separation of inorganic anions using (a) a single 250 mm x 4 mm i.d. IonPac AS11 column and (b) two 250 mm x 4 mm i.d. IonPac AS11 columns connected in series. Solute identities: 1-fluoride, 2-chlorite, 3-bromate, 4-chloride, 5- nitrite, 6-nitrate, 7-chlorate, 8-carbonate, 9-sulfate and 10-phosphate where each component was prepared in 10 ppm using a complex eluent profile starting at 0.50 mM for 2 min, 0.50 mM to 5.00 mM over 5 min, 5.00 mM to 38.25 mM over 15 min at 2 mL/min and 30^{o}C on the AS11 4mm column.

These differences will be further exacerbated by the use of a multi-step gradient, and since such operation is common in IC, this is a serious consideration. The inability to achieve direct method translation from conventional scale to miniaturised IC is therefore the main reason to start this evaluation process. This inability to perform direct method translation also means that an eluent profile which has been optimised on a 4 mm column will generally require further optimisation when translated to a column of smaller diameter.

6.3 Effects of Column Variability

It was recently shown that it is possible to simulate IC gradient separations using a small number of isocratic retention data[5]. In this case, a database of retention factors for a particular stationary phase and eluent competing ion had been acquired previously and this database was used to predict gradient retention data. **Figure 6.2** illustrates the predictive capability of this approach for a three-step complex elution profile applied to the separation of inorganic cations. Figure 6.2(a) shows the experimentally-obtained separation, while Figure 6.2(b) shows the predicted separation. Comparison of the two chromatograms shows that correlation between experimental and predicted retention times was good for the first 5 analytes, but was less satisfactory for the later-eluted analytes. The simulation relies on two prediction coefficients (a_i and b_i) that are normally estimated on the basis of experiments in which the retention factor (k_i) of each analyte is measured at a limited number of isocratic eluent compositions and the resultant data fitted to Equation 1.11 (which is a simplification of Equation 1.10)[5].

The derived values of a_i and b_i can then be used to predict retention factors for any desired isocratic, gradient, or multi-step eluent composition[5]. The simulated chromatogram shown in Figure 6.2(b) was derived using this process by applying the isocratic retention database embedded in the Virtual Column Separation Simulator. These embedded data were acquired on columns which were manufactured more than 5 years ago and the observed differences between Figures 6.2(a) and 6.2(b) can therefore be attributed to batch-to-batch variability in column manufacture. Therefore, there is a clear need to either update the retention database to reflect changes in column

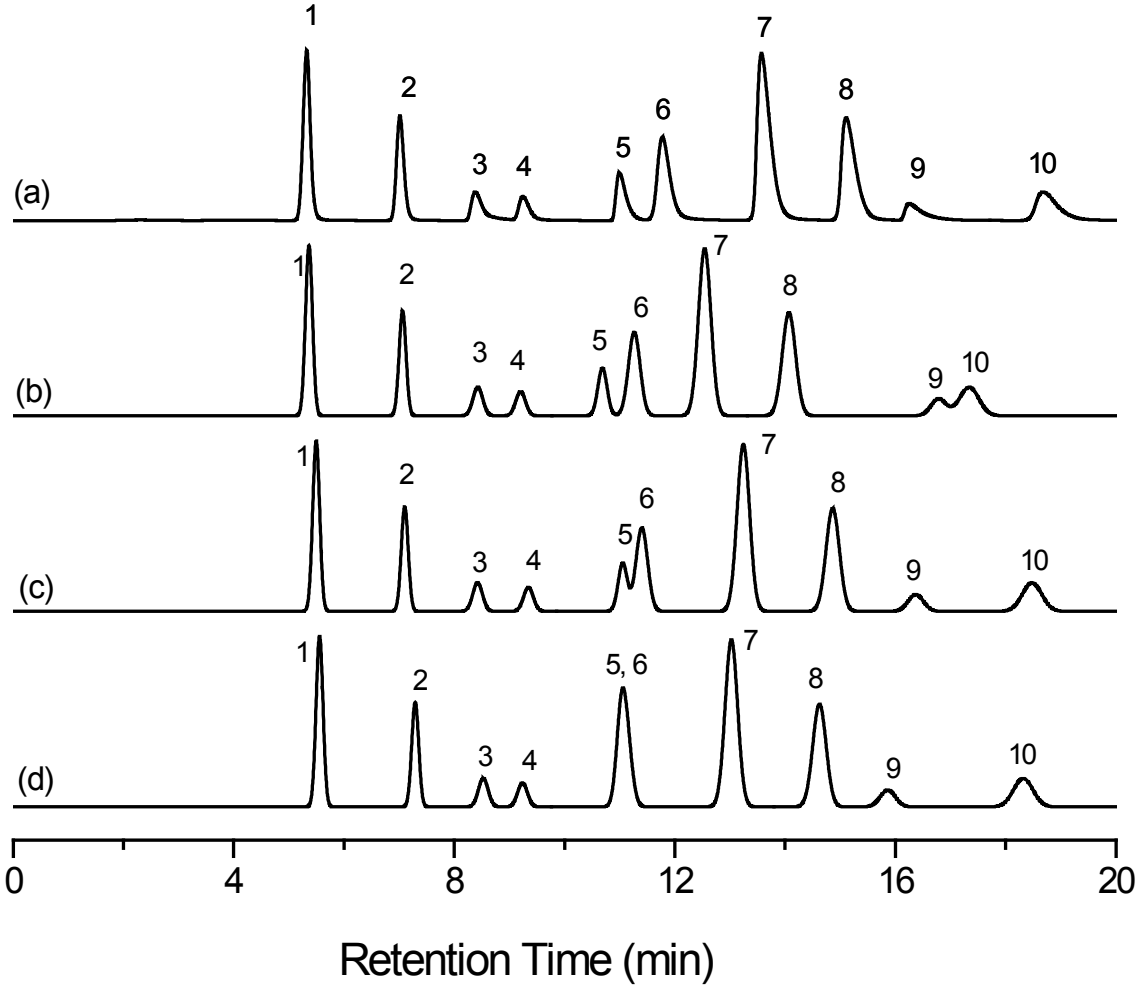

Figure 6.2 (a) Experimental chromatogram on a 5 mm CS16 column for a 10-component mixture consisting of 1-lithium (I) (5 ppm), 2-sodium (I) (5 ppm), 3-ammonium (5 ppm), 4-ethylammonium (5 ppm), 5-potassium (I) (5 ppm), 6-magnesium (II) (10 ppm), 7-calcium (II) (10 ppm), 8-strontium (II) (10 ppm), 9-cesium (I) (15 ppm) and 10-barium (15 ppm) using a complex eluent profile starting from 30 to 35 mM over 3 min, 35 to 50 mM over 3 min, 50 to 60 mM over 3 min, 60 to 80 mM over 3 min followed by 80 to 95 mM over 12 min at 1mL/min and 40^{o}C. (b) Simulated separation using embedded retention data obtained on a 5 mm CS16 column. (c) Simulated separation using new retention coefficients obtained on the same 5 mm CS16 column used in (a). (d) Simulated separation using retention coefficients ported from the embedded database after recalibration.

manufacture or to establish a means by which the existing retention data can be utilised for retention simulation on columns which have been manufactured more recently.

The chromatogram shown in Figure 6.2(c) was simulated using retention data obtained from a new series of isocratic experiments performed on the same column as used for Figure 6.2(a). These experiments involved the measurement of retention times for each analyte at three eluent concentrations, followed by derivation of new a_i and b_i values from Equation 1.11. This leads to a substantial improvement in the match between simulated and experimental results. Although the approach of using fresh retention data prior to each simulation clearly generates accurate prediction of retention times, implementation of this approach would require that considerable experimentation be performed prior to simulation and optimisation of separations. A more attractive option is to modify the existing retention database to enable it to be used for more accurate predictions. Essentially, this can be accomplished if the a_i and b_i values for each analyte in the database can be updated for each new column with minimal experimentation.

6.4 Recalibration of Retention Database

Retention data were measured experimentally using a new 5 mm CS16 column and 13 representative analyte cations (ammonium, barium (II), calcium (II), cesium (I), ethylammonium, lithium (I), magnesium (II), manganese (II), methylammonium, potassium (I), rubidium (I), sodium (I) and strontium (II)). a_i and b_i values were calculated for these analytes and compared with those for the same analytes in the Virtual Column Separation Simulator embedded retention database. The a_i and b_i values obtained by both approaches were found to be highly correlated, as follows:

$$a_{new} = 0.617\ a_{embedded}\ (R^2 = 0.9976) \qquad \text{Equation 6.1}$$

$$b_{new} = 0.923\ b_{embedded}\ (R^2 = 0.9984) \qquad \text{Equation 6.2}$$

Predictably, the *b*-coefficients, which reflect the ratio of the charge of the analyte to the charge of the competing ion in the eluent were found to be essentially unchanged between the new data and the embedded database

data. However, the *a*-coefficients, which reflect changes in $K_{A,E}$ and Q (since the particle size and column diameter are constant), showed considerable change between the two data sets, although most importantly all analytes showed essentially the same degree of change (as reflected by the high correlation coefficient for the plot of a_{new} vs $a_{embedded}$). This creates the possibility for recalibration of the entire suite of cations based on experimental data for a very limited number of analytes.

To this end, barium (II) and methylammonium were randomly selected as analytes for the recalibration experiments on the IonPac CS16 analytical column, although it is likely that the choice of cations is not particularly important. A mixture of these two analytes was analysed at three eluent strengths (25, 40, 62 mM MSA) and retention factors used to determine a_i and b_i values. These values were averaged and the ratio of new embedded values was used to recalibrate the a_i and b_i values for all analytes in the embedded retention database. The recalibration factors are shown in the first line of **Table 6.2** and are very similar to the factors in Equations 6.1 and 6.2 which were derived using all 13 analytes. A new separation was then simulated for the eluent conditions used in Figure 6.2, leading to the simulated chromatogram shown in Figure 6.2(d). Comparison of Figures 6.2(a) and 6.2(d) shows that this process provided a simulated chromatogram which matched closely with the experimental chromatogram, except for potassium and magnesium for which co-elution was predicted when in fact separation was achieved in practice. The co-elution could be due to the predictive error from using Method 1.

Since this recalibration approach potentially increases the portability of the original embedded Virtual Column Separation Simulator data, the word "*porting*" is used to describe this approach. The porting process was repeated for the separation of anions. A test set of analytes comprising acetate, bromate, bromide, carbonate, chlorate, chloride, chlorite, chromate, fluoride, formate, iodide, methanesulfonate, nitrate, nitrite, oxalate, phosphate, propionate, sulfate, thiocyanate and thiosulfate was separated on a new 4 mm AS19 column.

Table 6.2 Summary of porting equations used for CS16 cation-exchange and AS19 anion-exchange columns of various internal diameter. The equations for CS16 are used to update embedded retention data acquired using a 250 mm x 5 mm i.d. IonPac CS16 cation-exchange column. Those for AS19 are used to update embedded retention data acquired using a 250 mm x 4 mm i.d. IonPac AS19 anion-exchange column.

Column	Porting Equation (a)	Porting Equation (b)
5 mm CS16	$a_{new} = 0.624\ a_{embedded} + 16.102$	$b_{new} = 0.930\ b_{embedded} + 0.005$
3 mm CS16	$a_{3mm} = 0.634\ a_{embedded} + 2.976$	$b_{3mm} = 0.976\ b_{embedded} + 0.112$
4 mm AS19	$a_{new} = 0.830\ a_{embedded} + 2.796$	$b_{new} = 1.004\ b_{embedded} - 0.024$
2 mm AS19	$a_{2mm} = 0.567\ a_{embedded} + 4.884$	$b_{2mm} = 0.978\ b_{embedded} - 0.013$
0.4 mm AS19	$a_{0.4mm} = 0.687\ a_{embedded} + 4.034$	$b_{0.4mm} = 1.00\ b_{embedded} - 0.012$

The chromatogram obtained appears as **Figure 6.3**(a). The *a*- and *b*-coefficients were determined from the new retention data and were compared with the values for these coefficients in the embedded data set. A correlation plot of measured *a*- and *b*- coefficients for the new column *versus* the embedded *a*- and *b*- coefficients exhibited very strong correlation as shown below:

$a_{new} = 0.809\ a_{embedded}$ ($R^2 = 1.000$) Equation 6.3

$b_{new} = 0.994\ b_{embedded}$ ($R^2 = 0.9998$) Equation 6.4

Again, this process was repeated using only two representative anions (chloride and thiosulfate, randomly selected), with the result being shown in the third row of Table 6.2. The porting equations which use only two analytes for updating the embedded 4 mm AS19 retention data are again similar to Equations 6.3 and 6.4 which were based on 20 analytes.

Figure 6.3(b) shows the simulated chromatogram obtained using *a*- and *b*-coefficients from the embedded retention data, and Figure 6.3(c) shows the chromatogram simulated using the porting equations shown for the 4 mm AS19 column in Table 6.2. All three chromatograms in Figure 6.3

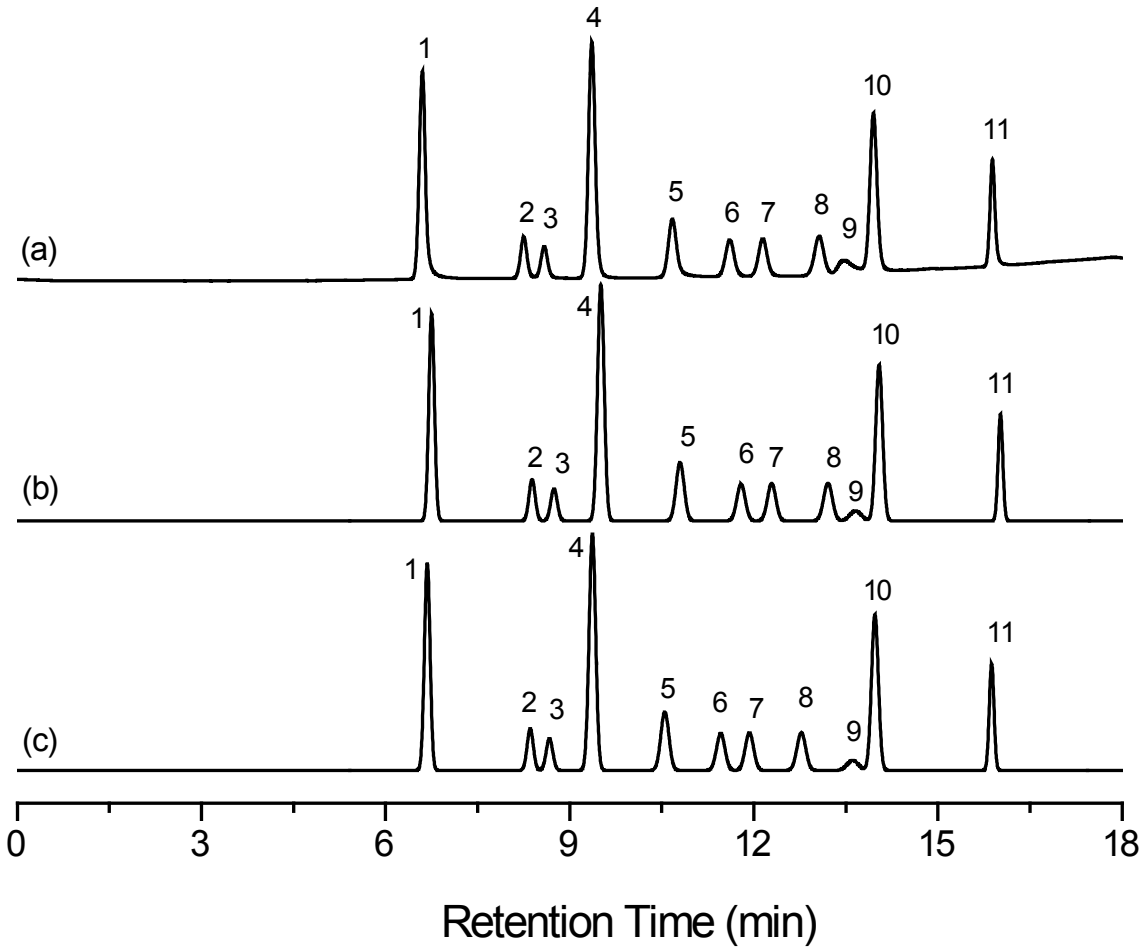

Figure 6.3 (a) Experimental chromatogram on a 4 mm AS19 column for an 11-component mixture comprising 1-fluoride (5 ppm), 2-chlorite (5 ppm), 3-bromate (5 ppm), 4-chloride (5 ppm), 5-nitrite (5 ppm), 6-chlorate (10 ppm), 7-bromide (5 ppm), 8-nitrate (5 ppm), 9-carbonate (15 ppm), 10-sulfate (10 ppm) and 11-phosphate (15 ppm) using a complex eluent profile starting at 3.75 mM for 0.8 min, 3.75 mM to 33.75 mM over 10 min, 33.75 mM to 99.75 mM over 4 min at 1 mL/min and 30^{o}C on the AS19 4mm column. (b) Simulated separation using embedded retention data obtained on a 4 mm AS19 column. (c) Simulated separation using retention coefficients ported from the embedded database after recalibration.

are quite similar, which indicates that there has been little change in the stationary phase characteristics for this column.

6.5 Prediction of Retention for Different Column Diameters

The above porting process compensates primarily for changes in the a_i term of Equation 1.11 and thereby addresses changes in $K_{A,E}$, Q, w, and V_m. Of these parameters, $K_{A,E}$ and Q can be expected to be related only to the stationary phase, while w and V_m can be expected to be related only to the column packing process, the particle diameter, and to the column diameter. Since all of the porting calculations performed thus far have been applied to columns of the same diameter, they relate only to changes in $K_{A,E}$ and Q. However, it should also be possible to apply the same procedure to recalibrate the retention database to simultaneously accommodate changes in both the characteristics of the stationary phase and the physical characteristics of the column.

In order to investigate the validity of porting retention data between columns of differing diameter, a set of *a*- and *b*- values was calculated from retention data acquired for a Dionex 3 mm i.d. IonPac CS16 column using ammonium, barium (II), calcium (II), cesium (I), ethylammonium, lithium (I), magnesium (II), manganese (II), methylammonium, potassium (I), rubidium (I), sodium (I) and strontium (II) as analytes. These data were compared with the 5 mm prediction coefficients for the same analytes. The hypothesis is that porting can be applied to different internal diameter columns, is supported by the strong correlation between both sets of coefficients:

$$a_{3mm} = 0.624\ a_{5mm}\ (R^2 = 0.9976) \qquad \text{Equation 6.5}$$

$$b_{3mm} = 0.899\ b_{5mm}\ (R^2 = 0.9909) \qquad \text{Equation 6.6}$$

Again the above relationships can be approximated using only two analytes (barium (II) and methylammonium) at three eluent strengths (25, 40, 62 mM MSA). The resultant porting equation is shown in the second row of Table 6.2. **Figure 6.4**(a) shows an experimental separation of 10 cations on the Dionex 3 mm CS16 column. A simulated separation using coefficients calculated from the embedded database of 5 mm CS16 retention data and a flow-rate adjusted to compensate for the changed column diameter is shown in

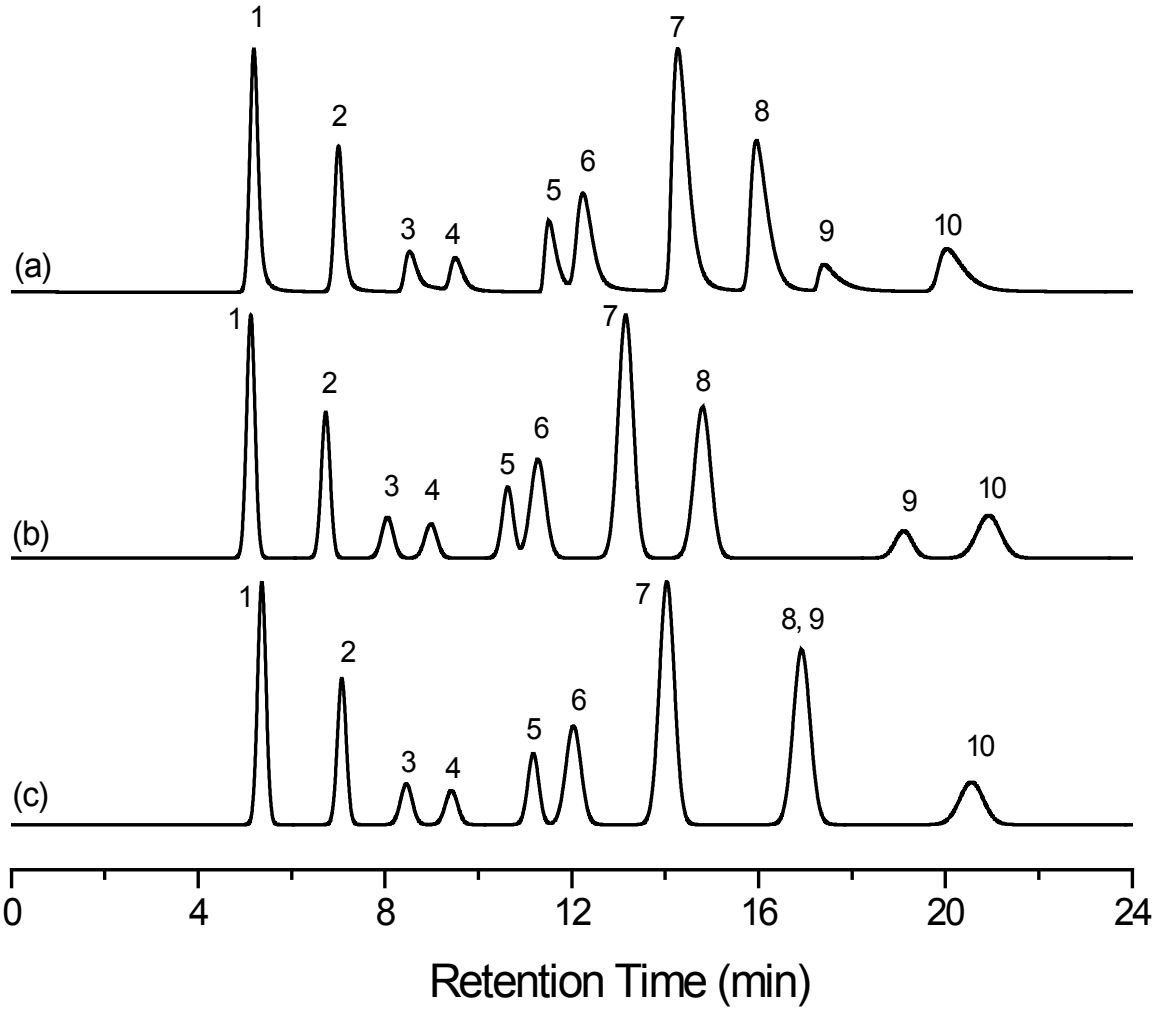

Figure 6.4 (a) Experimental chromatogram on a 3 mm CS16 column for a 10-component cation mixture of the same composition as in Figure 6.2 and using the same complex eluent profile at a flow-rate of 0.36 mL/min and 40^{o}C. (b) Simulated separation using embedded retention data obtained on a 5 mm CS16 column. (c) Simulated separation using retention coefficients ported from the embedded database after recalibration.

Figure 6.4(b). Comparison of this separation with Figure 6.4(b) reveals significant differences, which can be attributed to differences in the phase ratio for each column. Figure 6.4(c) shows the simulated separation obtained using the *a*- and *b*-coefficients calculated using the porting equation given in Table 6.2 where the different values between a_{new} and $a_{embedded}$ in Table 6.2 can be attributed to change in the phase ratio. The predicted retention times are now much closer to those in the experimental chromatogram, although co-elution of strontium (II) and cesium (I) is predicted erroneously. Again, the co-elution could be due to the predictive error from using Method 1.

Next, the applicability of porting to a different diameter anion-exchange column was explored. The Dionex IonPac AS19 stationary phase was selected for this purpose because it is available in a variety of **a**column diameters (4 mm i.d, 2 mm i.d and 0.4 mm i.d). Chloride and thiosulfate were used to provide retention data to generate the porting equations for 2 mm and 0.4 mm AS19 columns (Table 6.2). **Figure 6.5**(a) shows the experimental separation of 11 anions on a 2 mm AS19 column using a three step complex elution profile, while simulated separations calculated from the embedded 4 mm AS19 data (Figure 6.5(b)) and from the porting equation derived from retention measurements of chloride and thiosulfate (Figure 6.5(c)) are also shown.

Figure 6.6 shows chromatograms for experimental and simulated separations performed on a 0.4 mm AS19 column. In both figures, the simulated chromatograms obtained using the porting equations are a very close match for the experimental chromatograms. Finally an extended series of separation conditions was employed to further validate the porting procedure and the results are presented in **Figure 6.7**. These separations include retention simulations of 20 anions with three different column diameters and four different five-step elution profiles, together with 13 cations using two different column diameters over four different five-step elution profiles. A total of 344 retention data points are included in Figure 6.7 and there is a high correspondence between predicted and observed retention times. The porting procedure delivers an average of 3% error for simulating

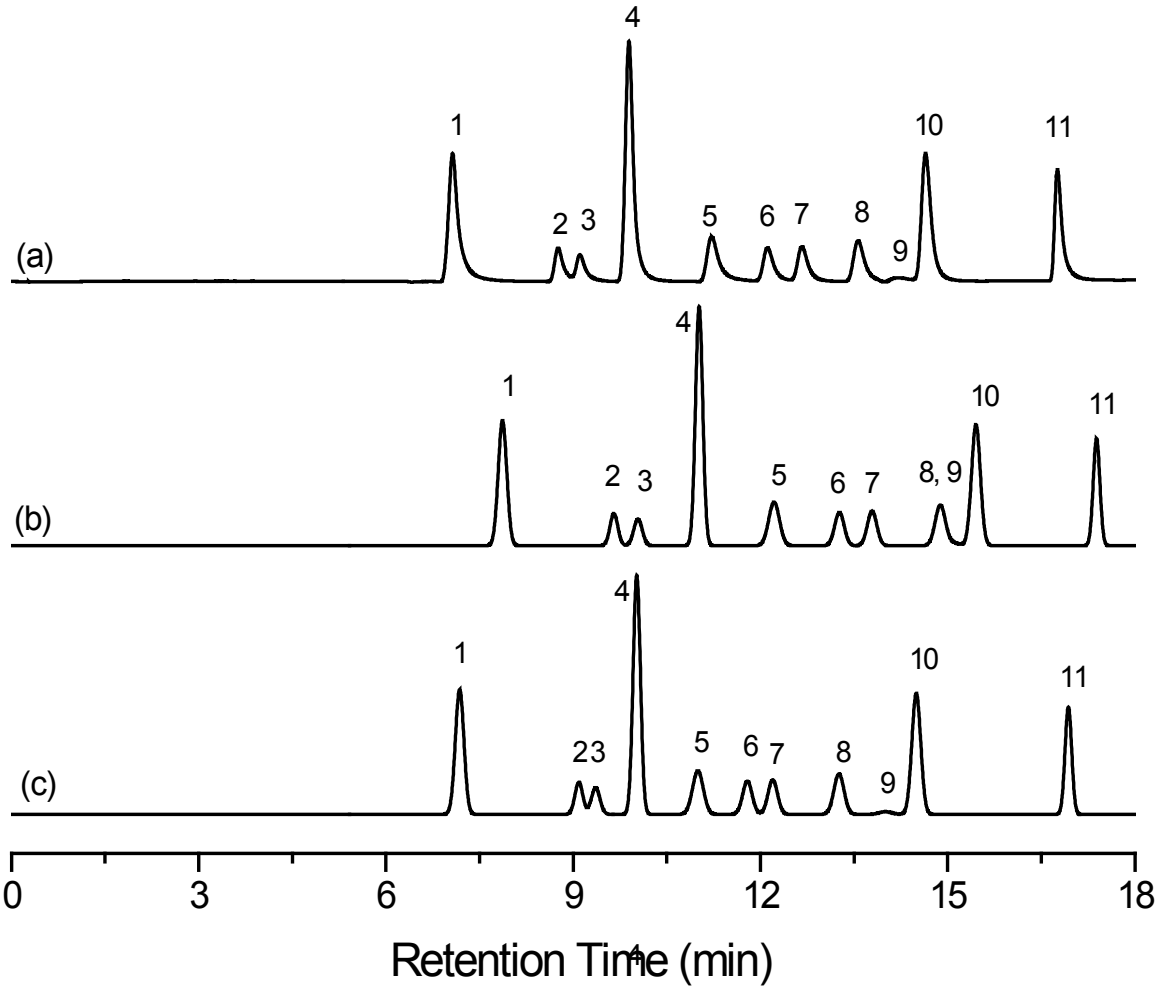

Figure 6.5 (a) Experimental chromatogram on a 2 mm AS19 column for an 11-component anion mixture of the same composition as in Figure 6.3 and using the same complex eluent profile at a flow-rate of 0.25 mL/min and 30^{o}C. (b) Simulated separation using embedded retention data obtained on a 4 mm AS19 column. (c) Simulated separation using retention coefficients ported from the 4 mm AS19 embedded database after recalibration.

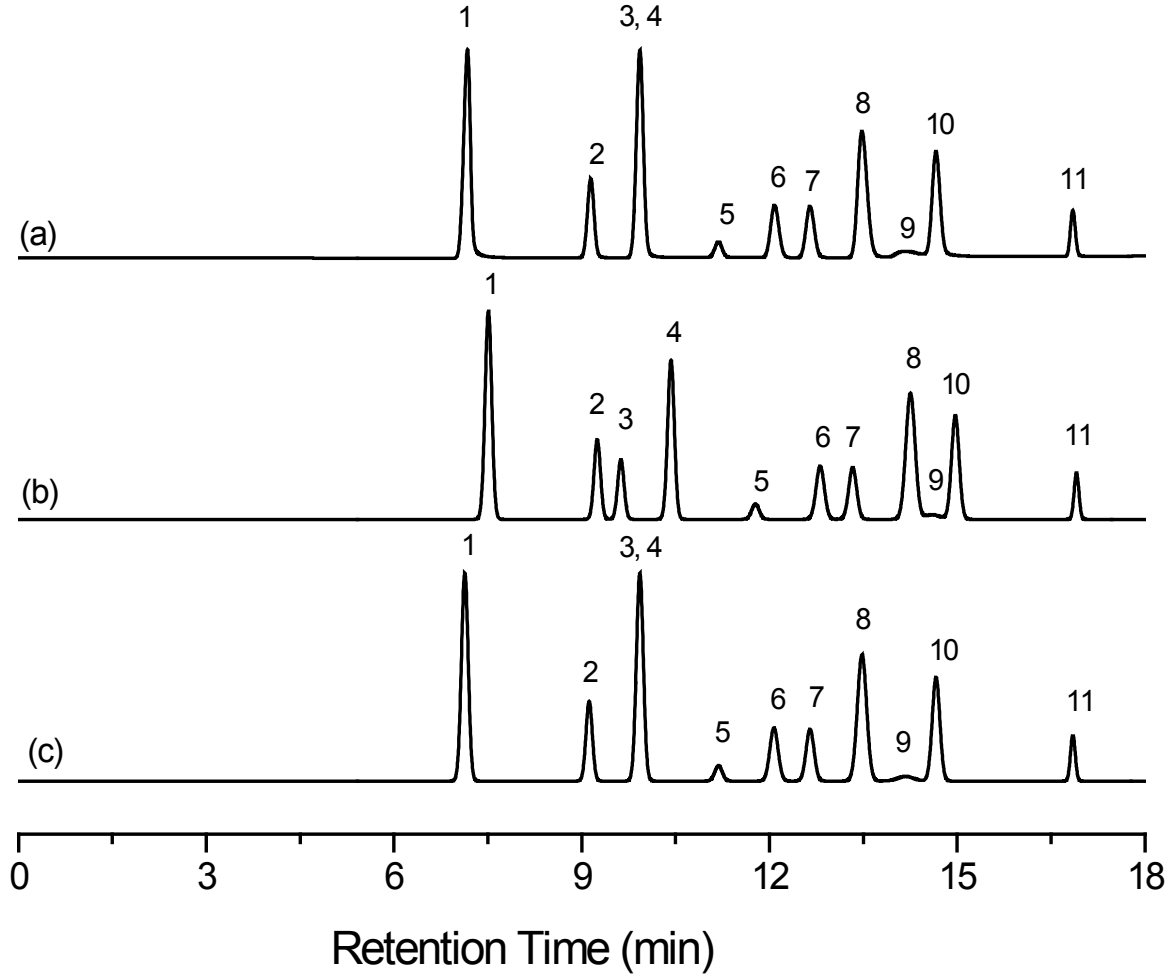

Figure 6.6 (a) Experimental chromatogram on a 0.4 mm AS19 column for an 11-component anion mixture of the same composition as in Figure 6.3 and using the same complex eluent profile at a flow-rate of 0.01 mL/min and 30^{o}C. (b) Simulated separation using embedded retention data obtained on a 4 mm AS19 column. (c) Simulated separation using retention coefficients ported from the 4 mm AS19 embedded database after recalibration.

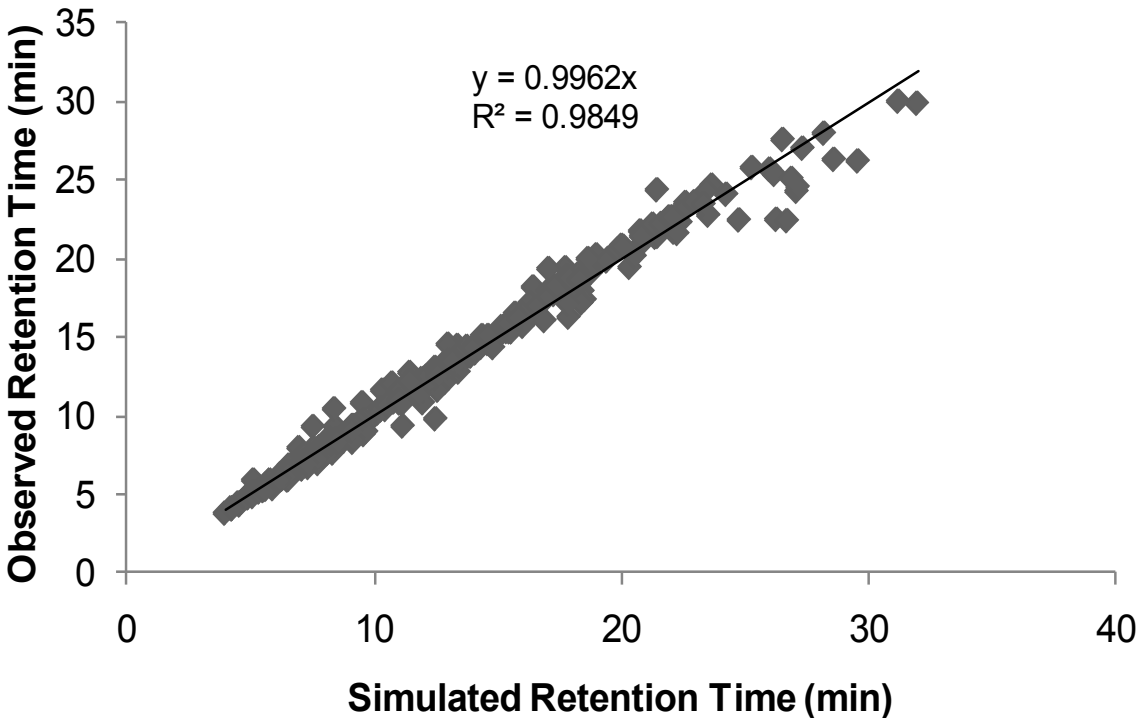

Figure 6.7 Observed retention times *versus* simulated retention times of 20 anions (acetate, bromate, bromide, carbonate, chlorate, chloride, chlorite, chromate, fluoride, formate, iodide, methanesulfonate, nitrate, nitrite, oxalate, phosphate, propionate, sulfate, thiocyanate and thiosulfate) and 13 cations (ammonium, barium, calcium, cesium, ethylammonium, lithium, magnesium, manganese, methylammonium, potassium, rubidium, sodium and strontium) using 8 different complex elution conditions on five different internal diameter columns at four different flow-rates and two operating temperatures. A total of 344 data points are included on the graph

the retention behaviours of an extensive set of analytes and columns. It substantially improves the prediction accuracy of simulated separations in IC.

The entire porting project relies on empirical model where it does not have any real in-built physical or chemical meaning. It is however believed that there is embedded chemical explanation to account for the difference between existing and new databases. Overall, it proves porting method can address the systematic difference using only two probe analytes.

6.6 Chapter Conclusions

In this study an extensive database of IC retention data obtained more than 5 years ago has been demonstrated for the use in accurate prediction of retention times under complex elution conditions, using new columns. With minimal experimental data obtained on a desired column using just two analytes, the embedded retention data for all analytes on that particular column can be recalibrated to account for changes in selectivity coefficient and ion-exchange capacity. Moreover, the same process can be used to recalibrate embedded retention data so that it can be used for accurate simulation of separations on columns having different diameters to those used to compile the original database.

These processes permit accurate simulations of separations on a wide range of stationary phases and varying column diameters to be performed with minimal experimentation. In this way, method development in IC can be undertaken systematically and rapid.

Chapter 7

General Conclusions and Future Directions

The Virtual Column Separation Simulator is an effective commercial software package for simulating and optimising IC separations. It has however a number of limitations, such as its inability to simulate a separation in which the eluent profile consists of multiple isocratic and gradient steps. The overarching objective of this project was to develop new prediction and optimisation approaches for ion chromatography that overcome these liabilities.

This study firstly evaluated the maximum tolerances on errors associated with predicted retention time and peak width needed for an accurate *in-silico* optimisation. A series of 15 chromatograms containing different components, separation times and elution methods were selected for statistical analysis. Each chromatogram was analysed by generating random errors in retention time and peak width (to a defined average error) using the random number generation function in Microsoft Excel. It was found that an average error of 0.7% in retention time can be tolerated before the quality of the chromatogram (as measured by numerical criteria) shows a statistically significant change. However the target error range for peak width remained ambiguous. Further investigation was conducted based on the first and final peaks in a typical 30-min separation. It was found that the thresholds of peak width were far more flexible than for retention time. Based on the typical 30 minute separation window, the acceptable average error limits for accurately predicting the retention time and peak width were determined to be 2.5% and 35% respectively.

Three retention time algorithms and two peak width models were introduced in this study for modelling the IC separations. Retention time prediction of analytes under the influence of a complex eluent profile using these methods relies on monitoring the analyte displacement through the chromatographic column. These three algorithms were devised by mapping the analyte position in different ways. The first method (Chapter 4) tracks the

displacement via mathematical iteration, Method 2 (Chapter 4) maps the analyte position using an integrated displacement approach, while the third algorithm (Chapter 5) relies on numerical segmented incremental isocratic steps to monitor the position of the analyte. Substantial sets of analytes (38 ion species) and columns (5 Dionex IonPac columns) were employed for validation and it was found that Methods 1, 2 and 3 delivered similar errors of 5%, 3% and 4%, respectively. Meanwhile, two empirical peak width models were found to be suitable for peak width simulation under the influence of complex eluent profiles with satisfactory agreement. Peak width prediction using the first model relies on integrating the compression exhibited from each individual step, and this model delivered a predictive error of 19% when predicting the peak width for analytes under the complex eluent profiles. On the other hand, peak width prediction employing the second model, which focuses solely on the eluting retention factor of the analyte, yielded predictive errors of 17% on average. Therefore, the second peak width model was slightly superior.

This study indicates that the average percentage errors for retention time and peak width prediction are 4% and 17%, compared to the target error thresholds of 2.5% and 35% for a typical 30-min separation window. The predictive capabilities of retention models were slightly outside of the target but considered as adequate for prediction purposes, while the peak width models were deemed to achieve the goal of reliable peak width simulation.

Retention prediction in the Virtual Column Separation Simulator relies heavily on the pre-existing data library which is known as the embedded data. This embedded data provides information on the unique characteristics of each analyte. However this pre-existing data library is now more than 5 years old, and to use this embedded data to predict the retention for newer columns could be problematic due to the variability in column manufacture and tubing configuration. This problem becomes more obvious when this older embedded data, acquired originally on 4 mm i.d columns, was employed to predict separations on the new microbore (2 mm) and capillary (0.4 mm) IC columns. This results because of changes in column internal diameter which leads to changes in parameters such as wall effects, phase

ratio and total ion-exchange capacity. These changes will somewhat alter the selectivity of the original separation. A method, which was termed "*porting*", was developed to calibrate the pre-existing data library with minimal data acquisition. This process allowed the data to be "refreshed" for newer columns, along with those of different internal dimensions, to address all the changes involved allowing retention time and peak width simulation to be reliably performed. By incorporation of this porting methodology for calibration and the *linear analyte displacement model* for retention prediction, a predictive error of 3% was observed for these newer column formats while employing data collected on older column formats.

Further research is required in the following areas:

1. The development of retention time and peak width modeling enables *in-silico* optimisation for complex eluent profiles. This optimisation approach should provide a comprehensive searching method for the optimal separation condition for the desired set of analytes. The development of an optimisation tool involves two process, namely modeling and optimum search. Modeling of retention time and peak width has been completed so this optimisation tool should incorporate the best algorithms for retention time and peak width simulations that have arisen from this thesis. The research should continue to work on the optimum search where two methods are proposed to be feasible, manual and automatic modes. In manual mode, user could closely monitor the optimisation by stepwise adjustment of conditions. For example, to optimise a 10-component mixture using a 3-step profile, user could employ first step of the profile to optimise first four peaks (early eluters) in the mixture by manually adjusting the profile on the optimisation tool. Likewise, user could then focus on separating the medium and later eluters in the second and third steps in the same manner. In contrast, if the user has no knowledge in method development, an automatic mode can be utilised where it relies entirely on the computing algorithm (Monte Carlo method) for optimum search. For example, if the user is a beginner in method development, this mode will be a good option. To optimise the same 10-component mixture using a 3-step profile, the user is only

required to input the desired set of analytes followed by selecting the automatic mode and choosing a criterion function (such as the minimum resolution must be no less than 1.5). As the optimisation of a 3-step profile involves 7 variables, the software will rely on the Monte Carlo method to randomly generate a large set of different 3-step profiles where each 3-step profile has 7 different values to account for the variables. The separations for all conditions will be predicted using the devised models. All simulated separations will then be assessed using the criterion function selected by user followed by selecting the optimal elution profile yielding a separation which meets the desired criterion function (for example the chromatogram achieves a minimum resolution of 1.5) within the shortest possible time.

2. The development of all models and algorithms in this study were only validated for their predictive ability with a limited set of analytes (38 ions species) and columns (5 columns). The validation was conducted at two constant flow-rates and temperatures. There are over 150 analytes, 20 different columns, other flow-rates and temperatures which are yet to be tested. Validation of these models and algorithms should therefore be expanded extensively to other ions (including inorganic, organic, polarisable and polyvalent), columns (including CarboPac columns) at other constant flow-rates and temperatures. The validation could then be incorporated into data library of the Virtual Column Separation Simulator to enhance its predictive capability. All the validation were completed using Dionex IonPac columns, so IC columns from other manufacturers should also be considered;
3. Separations employing complex eluent profiles were the primary focus of this project as eluent concentration gradients possess the greatest influence on analyte retention. The prime reason for using complex eluent profiles is the enhanced peak capacity available for separating problematic mixtures. Optimisation of a complex eluent profile however can be considerably difficult due to the numerous variables involved. In such case, a simple non-linear gradient elution might be a more promising alternative to achieve the optimal separation. This alternative involves only two parameters, namely initial concentration and the curvature of the

non-linear gradient ramp. Therefore retention time and peak width prediction should be enabled for this gradient mode in the optimisation tool. The highly useful gradient model proposed by Jandera *et al.* in 1974[9, 58] contains a parameter, x, which describes the curvature of a gradient ramp which can be modified for these non-linear eluent profiles. Therefore this model may be suitable to predict the retention for non-linear gradient separations. A validation process is required to prove the validity of Jandera's approach for retention time simulation under these non-linear gradients.

References

[1] V. Drgan, Modeling of Retention Processes and Structure-Retention Relationships in Ion Chromatography, University of Ljubljana, Ljubljana, 2010.

[2] P.R. Haddad, P.E. Jackson, Ion Chromatography Principles and Applications, Elsevier Science Publishers B. V., Amsterdam, 1990.

[3] L.R. Snyder, J.W. Dolan, J.R. Gant, J. Chromatogr., 165 (1979) 3.

[4] M. Gilar, H. Xie, A. Jaworski, Anal. Chem., 82 (2010) 265.

[5] R.A. Shellie, B.K. Ng, G.W. Dicinoski, S.D.H. Poynter, J.W. O'Reilly, C.A. Pohl, P.R. Haddad, Anal. Chem., 80 (2008) 2474.

[6] P. Nikitas, A. Pappa-Louisi, P. Agrafiotou, J. Chromatogr. A, 1120 (2006) 299.

[7] Dionex Reference Library, CD-ROM, April 2007. Sunnyvale, 2005.

[8] Y. Baba, J. Chromatogr. A, 485 (1989) 143.

[9] P. Jandera, J. Churacek, J. Chromatogr., 91 (1974) 223.

[10] D.D. Christianson, J.W. Paulis, J.S. Wall, Anal. Biochem., 22 (1968) 35.

[11] P. Jandera, Adv. Chromatogr., 43 (2005) 1.

[12] L. Barron, P.N. Nesterenko, B. Paull, J. Chromatogr. A, 1072 (2005) 207.

[13] R. Dybczynski, K. Kulisa, Chromatographia, 61 (2005) 573.

[14] A. Pappa-Louisi, S. Sotiropoulos, P. Balkatzopoulou, J. Liq. Chromatogr. Related Technol., 31 (2008) 1434.

[15] Y. Yokoyama, S. Tsuji, H. Sato, J. Chromatogr. A, 1085 (2005) 110.

[16] P. Nikitas, A. Pappa-Louisi, P. Balkatzopoulou, Anal. Chem., 78 (2006) 5774.

[17] P. Nikitas, A. Pappa-Louisi, P. Papachristos, C. Zisi, Anal. Chem., 80 (2008) 5508.

[18] A. Pappa-Louisi, P. Nikitas, P. Balkatzopoulou, G. Louizis, Anal. Chem., 79 (2007) 3888.

[19] A. Paci, A.-M. Caire-Maurisier, A. Rieutord, F. Brion, P. Clair, J. Pharm. Biomed. Anal., 27 (2002) 1.

[20] Y. Yukio, T. Sachiyo, S. Hisakuni, J. Chromatogr. A, 1085 (2005) 110.

[21] D.C. Harris, *Quantitative Chemical Analysis,6th Edition,* Freeman, New York, USA, 2007.

[22] T. Bolanca, S. Cerjan-Stefanovic, M. Novic, Chromatographia, 61 (2005) 181.

[23] T. Bolanca, S. Cerjan-Stefanovic, M. Lusa, M. Rogosic, S. Ukic, J. Chromatogr. A, 1121 (2006) 228.

[24] T. Bolanca, S. Cerjan-Stefanovic, M. Regelja, H. Regelja, S. Loncaric, J. Sep. Sci., 28 (2005) 1427.

[25] T. Bolanca, S. Cerjan-Stefanovic, M. Regelja, H. Regelja, S. Loncaric, J. Chromatogr. A, 1085 (2005) 74.

[26] T. Bolanca, S. Cerjan-Stefanovic, G. Srecnik, Z. Debeljak, M. Novic, Sep. Sci. Technol., 40 (2005) 1333.

[27] T. Bolanca, S. Cerjan-Stefanovic, G. Srecnik, Z. Debeljak, M. Novic, K. Lazaric, Z. Gumhalter-Lulic, Croat. Chem. Acta 75 (2002) 713.

[28] S. Cerjan-Stefanovic, T. Bolanca, L. Curkovic, J. Liq. Chromatogr. Related Technol., 23 (2000) 2169.
[29] J. Havel, J.E. Madden, P.R. Haddad, Chromatographia, 49 (1999) 481.
[30] J.E. Madden, N. Avdalovic, P.R. Haddad, J. Chromatogr. A, 910 (2001) 173.
[31] C.B. Mazza, C.E. Whitehead, C.M. Breneman, S.M. Cramar, Chromatographia, 56 (2002) 147.
[32] K. Héberger, J. Chromatogr. A, 1158 (2007) 273.
[33] C. Mazza, C. Whitehead, C. Breneman, S. Cramer, Chromatographia, 56 (2002) 147.
[34] F. Tian, L. Yang, F. Lv, P. Zhou, J. Sep. Sci., 32 (2009) 2159.
[35] J.G. Dorsey, K.A. Dill, Chem. Rev., 89 (1989) 331.
[36] C. Poole, T. Kollie, S. Poole, Chromatographia, 34 (1992) 281.
[37] L. Buydens, D.L. Massart, Anal. Chem., 53 (1981) 1990.
[38] C. Vendeuvre, F. Bertoncini, D. Thiébaut, M. Martin, M. C. Hennion, J. Sep. Sci., 28 (2005) 1129.
[39] B. Girard, J. Chromatogr. A, 721 (1996) 279.
[40] M.R. Schure, A.M. Lenhoff, Anal. Chem., 65 (1993) 3024.
[41] K.L. Ng, B. Paull, P.R. Haddad, K. Tanaka, J. Chromatogr. A, 850 (1999) 17.
[42] Y. Baba, J. Chromatogr. B, 618 (1993) 41.
[43] C. Quang, M.G. Khaledi, J. Chromatogr. A, 659 (1994) 459.
[44] M. Sugimoto, S. Kikuchi, M. Arita, T. Soga, T. Nishioka, M. Tomita, Anal. Chem., 77 (2004) 78.
[45] W. Kiridena, C.F. Poole, J. Chromatogr. A, 802 (1998) 335.
[46] M. Gilar, K.J. Fountain, Y. Budman, U.D. Neue, K.R. Yardley, P.D. Rainville, R.J. Russell Ii, J.C. Gebler, J. Chromatogr. A, 958 (2002) 167.
[47] J.E. Madden, P.R. Haddad, J. Chromatogr. A, 829 (1998) 65.
[48] J.E. Madden, P.R. Haddad, J. Chromatogr. A, 850 (1998) 29.
[49] D.T. Gjerde, J.S. Fritz, G. Schmuckler, J. Chromatogr., 187 (1980) 35.
[50] T.B. Hoover, Sep. Sci. Technol., 17 (1982) 295.
[51] D. Jenke, G.K. Pagenkopf, Anal. Chem., 56 (1984) 85.
[52] D. Jenke, G.K. Pagenkopf., Anal. Chem., 56 (1984) 88.
[53] M. Maruo, N. Hirayama, T. Kuwamoto, J. Chromatogr. , 481 (1989) 315.
[54] D.R. Jenke, Anal. Chem., 66 (1994) 4466.
[55] P. Hajos, O. Horvath, V. Denke, Anal. Chem., 67 (1995) 434.
[56] J.E. Madden, M.J. Shaw, G.W. Dicinoski, N. Avdalovic, P.R. Haddad, Anal. Chem., 74 (2002) 6023.
[57] R.D. Rocklin, C.A. Pohl, J.A. Schibler, J. Chromatogr., 411 (1987) 73.
[58] P. Jandera, J. Churacek, J. Chromatogr., 91 (1974) 207.
[59] Y. Baba, M. Fukuda, M. Yoza, J. Chromatogr. A, 458 (1988) 385.
[60] Y. Baba, N. Yoza, S. Ohashi, J. Chromatogr. A, 350 (1985) 461.
[61] L.R. Snyder, D.L. Saunders, J. Chromatogr. Sci., 7 (1969) 195.
[62] V. Drgan, M. Novic, M. Novic, J. Chromatogr. A, 1216 (2009) 6502.
[63] S.R. Gallant, A. Kundu, S.M. Cramer, J. Chromatogr. A, 702 (1995) 125.

[64] R.S. Hodges, J.M.R. Parker, C.T. Mant, R.R. Sharma, J. Chromatogr. A, 458 (1988) 147.
[65] C.A. Orellana, C. Shene, J.A. Asenjo, Biotechnol. Bioeng., 104 (2009) 572.
[66] S. Yamamoto, K. Nakanishi, R. Matsuno, T. Kamikubo, Biotechnol. Bioeng., 25 (1983) 1465.
[67] S. Yamamoto, K. Nakanishi, R. Matsuno, T. Kamikubo, Biotechnol. Bioeng., 25 (1983) 1373.
[68] P. Jandera, J. Liq. Chromatogr., 12 (1989) 117.
[69] M. Martin, J. Liq. Chromatogr., 11 (1988) 1809.
[70] T. Bolanca, S.C. Stefanovic, S. Ukic, M. Rogosic, J. Liq. Chromatogr. Related Technol., 32 (2009) 2765.
[71] U.D. Neue, J. Chromatogr. A, 1079 (2005) 153.
[72] U.D. Neue, D.H. Marchand, L.R. Snyder, J. Chromatogr. A, 1111 (2006) 32.
[73] T. Bolanca, S. Cerjan-Stefanovic, S. Ukic, M. Rogosic, M. Lusa, J. Liq. Chromatogr. Related Technol., 32 (2009) 1373.
[74] P. Jandera, J. Churacek, L. Svoboda, J. Chromatogr., 174 (1979) 35.
[75] J.E. Madden, Comparison of Retention Models for Optimisation of IC, University of Tasmania, Hobart, 1998.
[76] T. Bolanca, S. Cerjan-Stefanovic, J. Liq. Chromatogr. Related Technol., 30 (2007) 791.
[77] V.M. Morris, J.G. Hughes, P.J. Marriott, J. Chromatogr. A, 755 (1996) 235.
[78] S.V. Galushko, A.A. Kamenchuk, LC-GC Int. Mag., 8 (1995) 581.
[79] S. Galushko, V. Tanchuk, I. Shishkina, O. Pylypchenko, W.D. Beinert, A Practical Handbook for Optimisation, Wiley, Weinheim, 2008.
[80] G. Srecnik, Z. Debeljak, S.C. Stefanovic, T. Bolanca, M. Novic, K. Lazaric, Z. Gumhalter-Lulic, Croat. Chem. Acta, 75 (2002) 713.
[81] D. R. Jenke, Anal. Chem., 64 (1994) 4466.
[82] Y. Baba, N. Yoza, S. Ohashi, J. Chromatogr. A, 348 (1985) 27.
[83] Y. Baba, N. Yoza, S. Ohashi, J. Chromatogr. A, 350 (1985) 119.
[84] Y. Saito, K. Jinno, T. Greibrokk, J. Sep. Sci., 27 (2004) 1379.
[85] L.M. Blumberg, M.S. Klee, Anal. Chem., 70 (1998) 3828.
[86] M.S. Klee, L.M. Blumberg, J. Chromatogr. Sci., 40 (2002) 234.
[87] D. Guillarme, D. Nguyen, S. Rudaz, J.L. Veuthey, Eur. J. Pharm. Biopharm., 68 (2008) 430.
[88] P. Zakaria, G.W. Dicinoski, B.K. Ng, R.A. Shellie, M. Hanna-Brown, P.R. Haddad, J. Chromatogr. A, 1216 (2009) 6600.